...NTATION PAGE

Form Approved
OMB No. 0704-0188

AD-A247 326

...ORT DATE	3. REPORT TYPE AND DATES COVERED
...mber 1991	Annual Tech. Rpt. 3/15/90-3/15/91

4. TITLE AND SUBTITLE
Laser Physics and Laser Techniques

5. FUNDING NUMBERS
F49620-90-C-0004

6. AUTHOR(S)
A.E. Siegman

7. PERFORMING ORGANIZATION NAME(S) AND ADDRESS(ES)
Stanford University
Edward L. Ginzton Laboratory
Stanford, California 94305-4085

8. PERFORMING ORGANIZATION REPORT NUMBER
AFOSR-TR- 92 0006

9. SPONSORING / MONITORING AGENCY NAME(S) AND ADDRESS(ES)
Air Force Office of Scientific Research
Directorate of Physical and Geophysical Sciences
Bolling AFB, DC 20032

10. SPONSORING / MONITORING AGENCY REPORT NUMBER
3501/A1

11. SUPPLEMENTARY NOTES

12a. DISTRIBUTION / AVAILABILITY STATEMENT
Unlimited

12b. DISTRIBUTION CODE

13. ABSTRACT (Maximum 200 words)

Progress in AFOSR-supported research on laser physics and laser techniques for the period 15 March 1990-15 March 1991 is summarized, including work on laser resonators and laser resonator and optical beam software; new techniques for laser beam characterization and laser beam quality measurement; the generation of ultrashort optical pulses in the infrared; and measurement of a fundamental excess quantum noise effect in ultrastable laser oscillators.

14. SUBJECT TERMS	15. NUMBER OF PAGES
Subpicosecnod optical measurements, subpicosecond photodetector spontaneous emission, laser oscillator, diffraction limited diode lasers, laser beam quality	14+reprints
	16. PRICE CODE

17. SECURITY CLASSIFICATION OF REPORT	18. SECURITY CLASSIFICATION OF THIS PAGE	19 SECURITY CLASSIFICATION OF ABSTRACT	20. LIMITATION OF ABSTRACT
Unclassified	Unclassified	Unclassified	Unlimited

LASER PHYSICS AND LASER TECHNIQUES

Annual Technical Report

to the

AIR FORCE OFFICE OF SCIENTIFIC RESEARCH

under

Contract No. F49620-89-K-0004

for the period

15 March 1990–15 March 1991

Principal Investigator:

Professor A. E. Siegman

Professor of Electrical Engineering

Stanford University

Edward L. Ginzton Laboratory

Stanford University

Stanford CA 94305-4085

November 1991

ABSTRACT

Progress in AFOSR-supported research on laser physics and laser techniques for the period 15 March 1990–15 March 1991 is summarized, including work on laser resonators and laser resonator and optical beam software; new techniques for laser beam characterization and laser beam quality measurement; the generation of ultrashort optical pulses in the infrared; and measurement of a fundamental excess quantum noise effect in ultrastable laser oscillators.

Table of Contents

I. INTRODUCTION

This is the annual report and summary of accomplishments for the second year of a three-year program of research on laser physics and laser techniques carried out in the research group of Professor A. E. Siegman at Stanford University and supported by AFOSR Contract No. F49620-89-K-0004, covering the period from 15 March 1990 to 15 March 1991.

This report briefly summarizes results on laser resonators and laser resonator and optical beam software; new techniques for laser beam characterization and laser beam quality measurement; the generation of ultrashort optical pulses in the infrared; and the measurement of a fundamental excess quantum noise effect in ultrastable laser oscillators. Accomplishments in each of the areas of research covered by this program are described in more detail in the following sections, and in various reprints or preprints attached as Appendices

II. RAY-PULSE MATRIX ANALYSIS

A very useful ray-pulse matrix approach to optical pulse propagation was developed earlier under this program by Dr. A. Kostenbauder, as described in last year's annual report. This analysis appeared in print during the current period in the journal article:

> A. G. Kostenbauder, "Ray-pulse matrices: A rational treatment for dispersive optical systems," *IEEE J. Quantum Electron.* **QE–26**, 1148–1157 (June 1990).

This particular project is now completed; and a reprint of this publication is attached as Appendix A.

III. OPTICAL BEAM AND RESONATOR CALCULATIONS

Our group has made many contributions in previous years to optical resonator concepts, and has also done much work on fundamental methods for the analysis of optical beam propagation and the calculation of laser resonator modes; and these topics continue to be a productive area of work in the group.

In particular during the current reporting period we have completed the development of an integrated package of software programs with which optics engineers and laser researchers can carry out optical beam propagation and resonator mode calculations in real time on personal desktop computers. This package, which we have named PARAXIA because of its basic dependence on the paraxial wave approximation, includes:

- o An ABCD program for carrying out complex-valued ABCD matrix calculations, including two-transverse-dimension or astigmatic systems. This program is particularly useful in both stable and unstable optical resonator evaluation and in optical system design.
- o A program FRESNEL which carries out accurate optical beam propagation and diffraction calculations in rectangular or radial coordinates using fast transform algorithms. This program also includes scripting, iteration, and external function capabilities for doing iterative Fox-and-Li resonator mode calculations.
- o A program VSOURCE which implements the fast and efficient virtual source algorithm for calculating the modes of rectangular and circular unstable laser resonators, including both lowest and higher-order modes.
- o A VRM program for designing and evaluating the mode properties of gaussian variable-reflectivity-mirror resonators.

This software package was initially made available to other university, industrial and government laser laboratories through the Stanford Software Distribution Center, and at least several dozen copies were distributed to other laser researchers in this fashion, including site licenses to several large laser firms. A brochure describing this package and its capabilities is attached as Appendix B. We have received very favorable comments concerning the usefulness of this software from a number of university and industrial users. The package has now been licensed to Genesee Optics Software, Inc., of Rochester, NY, a widely known vendor of lens design and optics software packages

for the Macintosh, with the expectation that it will receive still wider distribution and use in the future through this channel.

These programs were initially written primarily for our internal use on this project, and we have made extensive use of this software ourselves in our own resonator design and laser beam quality research, as described in later sections of this report. Two such projects which were carried out using this software and which are now essentially complete, although the results are still being prepared for submission, are:

> K. Yasui, P. Mussche, J-L Doumont, and A. E. Siegman, "Off-axis one-sided positive and negative branch unstable resonators," *Appl. Optics*, in preparation (1991).
>
> K. Yasui, P. Mussche, J-L Doumont, and A. E. Siegman, "Comparison of misalignment sensitivities for positive and negative branch strip confocal unstable resonators," *Appl. Optics*, in preparation (1991).

A PhD dissertation reporting on the development of these programs and some of their applications was also essentially completed during the current period and will be submitted early in the coming period:

> Jean-luc Doumont, *Laser Beam and Resonator Calculations on Desktop Computers*, Ph.D. Dissertation, Department of Applied Physics, Stanford University, to be submitted (June 1991).

The abstract of this forthcoming dissertation is attached as Appendix C.

As a secondary effort in resonator theory, we also carried out during this reporting period a slightly extended analysis and evaluation of the so-called self-filtering unstable resonator (SFUR) design concept, leading to a pending journal article:

> A. E. Siegman, "Performance limitations of the self-filtering unstable resonator," *Optics Commun.*, accepted for publication (1991).

A preprint of this communication is attached as Appendix D. The primary point to this brief communication is that the SFUR concept, which has been widely discussed by others, does offer very good mode properties for laser systems with low Fresnel numbers; but it is not a useful solution for the more difficult (and generally more realistic) case of large-Fresnel-number laser resonators. The reason is that as the Fresnel number increases much above a few times unity, the output coupling of the SFUR design inherently must become very large, or the effective reflectivity of the

output mirror becomes very small, and so this type of resonator cannot be used with any normal gain medium.

An overall survey of advances in laser resonators and resonator theory over the past two decades, including a review of current and expected future developments in this field, was also prepared and presented as an invited lecture at the 1990 CLEO/QELS meeting:

> A. E. Siegman, "Laser Resonators: Retrospective and Prospective", R.V. Pole Memorial Lecture, CLEO/QELS '90, Anaheim, CA (21 May 1990).

An outline of this lecture and associated transparencies is attached as Appendix E to this report.

IV. LASER BEAM QUALITY DEFINITION AND MEASUREMENT

A major new area of research in our group during the present and the immediately preceding reporting periods has been the general topic of laser beam quality definition and measurement. This topic is a major new effort in our group, although it grows directly out of our earlier research interests in optical beams and resonators; and we believe it may have a substantial impact on the development and improvement of many types of lasers.

By way of background, since the earliest days of the laser there has been great interest in the transverse mode properties of lasers, and much effort has been devoted to obtaining laser output beams that were "diffraction limited" in character, since this characteristic of a laser beam has a critical impact on the usefulness of a laser beam, e.g., on its propagation and beam-spread properties for laser radars, or on the focusing properties of a laser beam for laser materials processing. Despite the importance of laser beam quality, however, there has been very little work in the past either on rigorous and meaningful definitions of laser beam quality, or on practical tools for accurate measurement of these laser beam characteristics.

In work under this program during the preceding reporting period our group first developed a very meaningful and widely useful, but also precise and universal definition for laser beam quality. This work produced a rigorous definition for the so-called "M^2 factor" of a laser beam, based on the spatial and angular second moments or standard deviations of a laser beam and their space-beamwidth product. Our analysis, which

was based on the so-called "moments method" for laser beam propagation, in fact gave a complete description of the propagation properties of any arbitrary real, distorted, multimode, or astigmatic laser beam in terms of only six easily measurable parameters: the real-beam waist size, the real-beam waist location, and the real-beam quality factor M^2 in each transverse coordinate. The motivation behind this work was to provide quantitative, measureable, and widely useful measures both of "beam quality" and of beam propagation parameters in the form of a few numbers which can be attached to a given optical beam and be valid at any point along the beam, rather than merely stating some quantitative measure of performance such as far-field brightness in watts per steradian or focused spot size in microns for a specific laser device under specific operating conditions.

This earlier analysis focused on the axial variation of the intensity profile of an arbitrary real beam. As one extension of this analysis, during the current period we were able to extend this analysis to define an effective spherical radius of curvature for an arbitrary laser beam, even one with an arbitrarily distorted or wrinkled phase front. This result has now been published as:

> A. E. Siegman, "Defining the effective radius of curvature for a nonideal optical beam," *IEEE J. Quantum Electron.* **QE-27**, 1146–1148 (May 1991).

This new result has proven to be extremely useful in evaluating the effects on beam quality of, for example, phasefront distortion by spherical aberration or other phase aberration effects. A reprint of this publication is attached as Appendix F.

In parallel with and partly based on these theoretical developments, at least one commercial firm (Coherent, Inc.) has developed over the past two years a comparatively simple and practical instrument for measuring laser beam quality and beam propagation parameters in real time. For simplicity this particular instrument measures beam diameter in terms of a knife-edge clip width, rather than a direct evaluation of the second moment. The approximations involved in this design compromise are evaluated in a joint publication from our two laboratories:

> A. E. Siegman, M. W. Sasnett, and T. F. Johnston, Jr., "Choice of clip levels for beam width measurements using knife-edge techniques", *IEEE J. Quantum Electron.* **QE–27**, 1098–1104 (April 1991).

a reprint of which is attached as Appendix G. Our group has also been using one of the Coherent instruments for various laser beam evaluations as described below.

In addition, since the Coherent instrument operates only with cw beams, while the beam parameters of pulsed lasers are also of substantial interest, during the past period we assembled and tested in our laboratory a single-shot pulsed beam quality and beam propagation measurement system using CCD-camera arrays and computer frame-grabber boards. This approach permits detailed evaluation of the measured beam profiles and evaluation of the beam quality using various algorithms in software. This work is described in:

> J. A. Ruff and A. E. Siegman, "Single pulse laser beam quality measurements using a CCD camera system," *Appl. Optics*, accepted for publication (1991).

A preprint of this publication is attached as Appendix H. An improved version of this approach is expected to be very useful for several types of pulsed lasers, such as Q-switched solid-state lasers and pulsed excimer lasers.

As one particularly interesting example of the utility of beam quality measurements, we have very recently begun a series of measurements of the laser beam quality and beam propagation factors in both transverse directions simultaneously for a variety of semiconductor diode lasers, including both narrow-stripe single-mode and wide-stripe multimode diode lasers. These measurements are being made using both the Coherent beam quality measuring instrument and our own CCD-camera-based beam quality meter. Preliminary indications are that measurements of this type can bring out very interesting new information concerning the modal properties and oscillation behavior of diode lasers, including correlations between the "kink" phenomena that are often observed in such diode lasers and discontinuities in the beam quality parameters. In preliminary tests of this concept we have also discovered that the beam quality and other beam properties of wide-stripe diode lasers can be measured even in the sub-threshold ASE region, and the variation in all of the beam parameters followed continuously through the threshold region. Continued work in this area is presently being carried out.

V. MEASUREMENT OF EXCESS QUANTUM NOISE EFFECTS

By way of background for this section, in 1979 K. Petermann in Germany published a theoretical analysis predicting the existence of an "excess spontaneous emission factor" or excess quantum noise emission effect in gain-guided semiconductor diode lasers. In 1989 under earlier AFOSR support we then published several theoretical analyses showing that this kind of excess emission would also occur and would lead to a sizable enhancement of the fundamental quantum noise fluctuations in any kind of laser oscillator using an unstable optical resonator. Our analysis, aided by theoretical calculations using the PARAXIA software described in Section III, showed that the excess noise factors in a typical unstable resonator laser design could range from several hundred to several thousand, according to our calculations.

These quantum fluctuations in turn will represent the ultimate lower limit on the amplitude and frequency stability of any laser device using such a resonator. Environmental or technical noise is usually predominant over quantum noise effects in practical laser devices. Current developments in laser technology, however, are leading to new laser devices with extremely small noise fluctuations and spectral widths, approaching the quantum limit; and such ultrastable laser devices are now becoming of practical importance in ultrahigh-performance coherent optical communications systems, in laser radars, and potentially also in gravity wave experiments. It becomes important, therefore, to verify experimentally the existence of this excess noise emission and the correctness of our theoretical predictions, not only for their fundamental interest as an unusual consequence of quantum electronics, but also in order to set the ultimate quantum limits on the performance of ultrastable laser devices.

We have therefore been carrying out as part of our current work a project to make a careful and definitive measurement of this excess noise factor in an unstable-resonator laser. During the previous and current reporting periods we designed a miniaturized monolithic diode-pumped Nd:YAG laser system, employing diode pumping for pump stability; a monolithic rod structure for mechanical and acoustic stability; and nitrogen cooling of the miniature YAG rod to narrow the laser linewidth and thus obtain the increased gain needed for the unstable cavity. During the current reporting period we have now built and operated this laser system, using a 100 mW single-mode diode laser pump and a 3-mm long Nd:YAG rod which is enclosed inside a liquid nitrogen cryogenic refrigerator. The unstable resonator is ground directly onto the monolithic

rod, and the diameter of the unstable mode is controlled in this initial experiment by the inverted region created by the focused diode laser pump beam. Much of the experimental work up to this point is summarized in the conference proceedings:

> P. L Mussche and A. E. Siegman, "Enhanced Schawlow-Townes linewidth in lasers with nonorthogonal transverse eigenmodes" in *Laser Noise*, Rajarshi Roy, ed., *Proc. SPIE* **1376** (November 1990). [Proceedings of SPIE Symposium on Laser Noise, OPTCON 90, November 1990.]

A reprint of this report is attached as Appendix I. Since then we have also designed and assembled a Pound-Drever cavity stabilization system which is used to measure the quantum frequency fluctuations of our experimental laser. In this system a slow feedback loop is used to lock the reference cavity to the laser frequency, so that the Pound-Drever system tracks slow drifts in the laser frequency. At the same time, faster fluctuations which are above the cutoff frequency of the feedback system are measured in the Pound-Drever output signal and used to determine the quantum noise spectrum of the laser output. This system is now in operation and working well. The shot noise in the measurement system has been established using a stable-cavity diode-pumped YAG laser with a much lower Schawlow-Townes noise level, and the enhanced noise in our unstable laser then measured with respect to this.

With the present system we have at this point been able to obtain a tentative confirmation of the expected excess noise level in our unstable laser; and the excess noise results we have obtained to date on this configuration appear to be in reasonable agreement with theory. We are attempting now to fabricate several similar monolithic unstable-resonator YAG lasers with conventional hard-edged mirrors which will represent a wider range of unstable-resonator parameters, in order to make careful and definitive measurements of the excess noise factors in these rods and thereby confirm in a definitive fashion the excess noise figures we have predicted. These results should then provide a firm foundation for future design and evaluation of ultrastable or ultraquiet laser oscillator and laser system designs, as well as confirming the unusual quantum aspects of the predicted excess spontaneous emission.

VI. ULTRASHORT PULSES IN THE INFRARED

Finally, in previous work under this contract we have summarized the potential advantages and capabilities of synch-pumped and mode-locked optical parametric oscillators (OPOs) pumped by mode-locked Nd:YAG lasers. Mode-locked OPOs provide a promising method for generating very short pulses in the infrared; and if these OPOs can be pumped by diode-pumped Nd:YAG lasers, one has the potential for a comparatively efficient all-solid-state system for IR pulse generation.

In our work during the current period we have constructed and operated two such synch-pumped and mode-locked OPO systems, making use in the first case of a $LiNbO_3$ crystal pumped at the doubled-YAG wavelength of 532 nm and oscillating at signal and idler wavelengths of ~880 nm and ~1350 nm, and in the second case of a KTP crystal pumped at the fundamental 1064 nm YAG wavelength with signal and idler at ~1.5 microns and ~3.5 microns. Both of these systems can now be operated reliably well above threshold with the YAG pump laser operating in a mode-locked plus repetitively Q-switched mode (at a 1 kHz repetition rate); and both are clearly mode-locking and generating short IR pulses. We are now proceeding with efforts to measure the exact pulsewidths and other detailed behavior of these systems.

Our future objectives on this project will include making better and more detailed measurements of the operation of these mode-locked OPOs in the repetitive Q-switched mode, including determination of pulse width at the IR frequencies, especially for the KTP oscillator in the middle IR. In addition, we will attempt to optimize the performance and operation of these OPOs, including reducing the pump threshold and increasing our Nd:YAG laser performance so that one or both of these OPOs—with the KTP version again taking precedence—can be operated as a reliable CW mode-locked system.

We are also considering an effort to take advantage of a combination of self phase modulation together with the newly emerging concept of "Kerr lens mode locking", to obtain significant pulse-shortening in our mode-locked Nd:YAG pump laser, both for its utility in our mode-locked OPO experiments, and as a potentially simple and inexpensive way of retrofitting a large number of existing YAG lasers to obtain substantially shorter mode-locked pulses.

VII. HONORS AND AWARDS

During the current reporting period Professor Siegman presented the R.V. Pole Memorial Lecture, "Laser Resonators: Retrospective and Prospective", at the 1990 CLEO/QELS Meeting in Anaheim, CA, May 21, 1990.

Professor Siegman also presented a George Eastman Invited Lecture on "Defining and Measuring Laser Beam Quality," to the Optical Society of America, Washington DC, April 18, 1990.

In November of this year Professor Siegman will receive the 1991 Schawlow Award of the Laser Institute of America and will be the Honored Speaker at the LIA's Annual ICALEO Meeting in San Jose.

APPENDICES

A. Reprint: "Ray-pulse matrices: A rational treatment for dispersive optical systems," *IEEE JQE* (June 1990).

B. Brochure for the PARAXIA Resonator Software Package

C. Abstract: *Laser Beam and Resonator Calculations on Desktop Computers*. PhD dissertation, J-L Doumont (June 1991).

D. Preprint: " Performance limitations of the self-filtering unstable resonator." *Opt. Commun.* accepted for publication (1991).

E. Outline: "Laser Resonators: Retrospective and Prospective", R.V. Pole Memorial Lecture, CLEO/QELS, (May 1990).

F. Reprint: "Defining the effective radius of curvature for a nonideal optical beam," *IEEE J. Quantum Electron.* (May 1991).

G. Reprint: "Choice of clip levels for beam width measurements using knife-edge techniques", *IEEE J. Quantum Electron.* (April 1991).

H. Preprint: "Single pulse laser beam quality measurements using a CCD camera system," *Appl. Optics*, accepted for publication (1991).

I. Reprint: "Enhanced Schawlow-Townes linewidth in lasers with nonorthogonal transverse eigenmodes", published in *Laser Noise*, Proc. SPIE **1376** (November 1990).

A

Ray-Pulse Matrices: A Rational Treatment for Dispersive Optical Systems

A. G. Kostenbauder

Reprinted from
IEEE JOURNAL OF QUANTUM ELECTRONICS
Vol. 26, No. 6, June 1990

Ray-Pulse Matrices: A Rational Treatment for Dispersive Optical Systems

A. G. KOSTENBAUDER

Abstract—**We present a new formalism to describe beam propagation in paraxial optical systems with dispersive elements, including both spatial and temporal variations in the propagating signal. This new formalism makes use of 4 × 4 "ray-pulse" matrices which take account of dispersive effects up to quadratic phases in both spatial coordinates (as in the usual paraxial *ABCD* matrix approach) and in the temporal domain. We show how to use these matrices to write a space-time integral analogous to a generalized Huygens integral, and derive propagation laws for Gaussian ray pulses which are space- and time-varying analogs of the conventional results for Gaussian beams. This new formalism should be very useful in analyzing dispersive optical systems such as prism beam expanders, femtosecond pulse compression systems, and dispersive mode-locked laser cavities.**

I. Introduction

MARTÍNEZ [1], [2] has recently discussed the use of 3 × 3 matrices to model polychromatic beam propagation through paraxial optical systems with dispersive elements. His treatment starts by defining an optical axis as the path a midband reference ray takes through the system. He then constructs 3 × 3 matrices of the same form given in Siegman [3] which model the path of slightly displaced and slightly detuned rays. In particular, the E and F elements of the matrix are frequency dependent, allowing different wavelengths to traverse different paths through the system.

Several aspects of this treatment can be improved by expanding the formalism. First, the Martinez formulation has ray matrix elements which depend upon the frequency of the incident wave, whereas one would like the vector that describes the ray to carry all of the information about the light and the matrix that represents the optical system to have no dependence on the ray. Second, the properties of the optical system are not fully described by the 3 × 3 matrix, since several additional phases must be carried along to get a complete description of the optical system.

In this paper, we show how a formalism making use of 4 × 4 matrices can be used to model time- and space-varying wave propagation in dispersive paraxial systems in a canonical way that overcomes these difficulties. In particular, the optical system is completely modeled by its ray-pulse matrix, while the vector that represents the ray contains all the information about both its temporal frequency and its position.

Manuscript received July 5, 1989; revised January 3, 1990. This work was supported in part by the Air Force Office of Scientific Research and by the Newport Corporation.

A. G. Kostenbauder is with the Edward L. Ginzton Laboratory, Stanford University, Stanford, CA 94305.

IEEE Log Number 9035232.

II. The Ray-Pulse Matrix Formalism

We begin by constructing an optic axis which corresponds to the path of a spatially transform-limited, pulsed, midband reference beam as it goes through the optical system. At each point along this reference beam, we erect transverse coordinates in the plane perpendicular to the reference ray. For convenience, we place the origin of these coordinates at the reference beam, as shown in Fig. 1. This beam is also to be thought of as being a temporally transform-limited pulse, so that it can simultaneously have a well-defined center frequency (the reference frequency or central frequency for the system) and can mark a well-defined time of arrival at each transverse plane. For convenience, we set the clocks in each transverse plane to zero at the time of arrival of the reference pulse.

We can now imagine firing another transform-limited pulse at a different starting time and with a different carrier frequency into the system at a slightly different position and slope. We will denote the changes in these four quantities as t_{in}, f_{in}, x_{in}, and θ_{in}, respectively. In order to simplify later results, we assume that each reference plane is surrounded by a slab of infinitesimal thickness of material of unit index of refraction. Equivalently, the θ's should be viewed as the slope normalized by the index of refraction. This normalization avoids the need to have matrices that describe flat dielectric interfaces. Also, we use hertzian frequency f rather than radian frequency ω as this reduces the number of π's that need to be carried along.

As this new pulse crosses each of the transverse planes, it defines a new arrival time, frequency, position, and slope relative to the reference pulse. (The time at each plane is really a time offset from the reference time at that plane.) We know that the coordinates at the output plane must be a function of the input parameters, i.e., that

$$\begin{bmatrix} x \\ \theta \\ t \\ f \end{bmatrix}_{out} = \mathfrak{F}\left\{ \begin{bmatrix} x \\ \theta \\ t \\ f \end{bmatrix}_{in} \right\}. \tag{1}$$

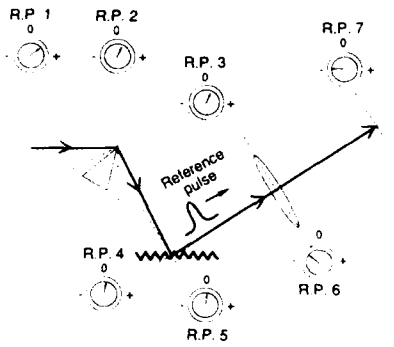

Fig. 1. Optical system with reference planes (R.P.1-R.P.7) and clocks constructed to measure path and time of flight of arbitrary pulse. Note that all clocks in R.P.1-R.P.5 show positive times, but those in R.P.6 and R.P.7 are negative and will reach zero when reference pulse arrives. Each R.P. is perpendicular to direction of propagation of reference pulse, and has its origin where reference pulse goes through R.P.

Also, by the definition of the reference ray, we know that $\mathfrak{F}\{0\} = 0$. For systems of interest the function $\mathfrak{F}$ is highly differentiable, so that it makes sense to replace (1) by the first nonzero term in its power series. This yields

$$\begin{bmatrix} x \\ \theta \\ t \\ f \end{bmatrix}_{\text{out}} = \begin{bmatrix} \frac{\partial x_{\text{out}}}{\partial x_{\text{in}}} & \frac{\partial x_{\text{out}}}{\partial \theta_{\text{in}}} & \frac{\partial x_{\text{out}}}{\partial t_{\text{in}}} & \frac{\partial x_{\text{out}}}{\partial f_{\text{in}}} \\ \frac{\partial \theta_{\text{out}}}{\partial x_{\text{in}}} & \frac{\partial \theta_{\text{out}}}{\partial \theta_{\text{in}}} & \frac{\partial \theta_{\text{out}}}{\partial t_{\text{in}}} & \frac{\partial \theta_{\text{out}}}{\partial f_{\text{in}}} \\ \frac{\partial t_{\text{out}}}{\partial x_{\text{in}}} & \frac{\partial t_{\text{out}}}{\partial \theta_{\text{in}}} & \frac{\partial t_{\text{out}}}{\partial t_{\text{in}}} & \frac{\partial t_{\text{out}}}{\partial f_{\text{in}}} \\ \frac{\partial f_{\text{out}}}{\partial x_{\text{in}}} & \frac{\partial f_{\text{out}}}{\partial \theta_{\text{in}}} & \frac{\partial f_{\text{out}}}{\partial t_{\text{in}}} & \frac{\partial f_{\text{out}}}{\partial f_{\text{in}}} \end{bmatrix} \begin{bmatrix} x \\ \theta \\ t \\ f \end{bmatrix}_{\text{in}}. \tag{2}$$

Most of these matrix elements can be put in simpler terms. Consider first the upper left 2 × 2 block in the matrix. These elements determine the changes in output position and slope caused by input changes in position and slope, with input frequency and time unchanged, and are thus just the conventional *ABCD* matrix elements for the system. (This is not entirely obvious, as the conventional *ABCD* matrix is defined in terms of the propagation of a monochromatic wave, while the elements of the generalized ray matrix are defined in terms of the propagation of a group. A rigorous proof of this equivalence will be given below at the end of the section on the generalized Huygens integral.)

Similarly, looking at the bottom row and knowing that in all cases $f_{\text{out}} = f_{\text{in}}$ for a time invariant linear system, we find that this row must be 0, 0, 0, 1. Finally, the third column, which determines how the output pulse depends on the input time must be 0, 0, 1, 0 due to the time invariance of the system. Putting all of these simplifications in place, we have

$$\begin{bmatrix} x \\ \theta \\ t \\ f \end{bmatrix}_{\text{out}} = \begin{bmatrix} A & B & 0 & \frac{\partial x_{\text{out}}}{\partial f_{\text{in}}} \\ C & D & 0 & \frac{\partial \theta_{\text{out}}}{\partial f_{\text{in}}} \\ \frac{\partial t_{\text{out}}}{\partial x_{\text{in}}} & \frac{\partial t_{\text{out}}}{\partial \theta_{\text{in}}} & 1 & \frac{\partial t_{\text{out}}}{\partial f_{\text{in}}} \\ 0 & 0 & 0 & 1 \end{bmatrix} \times \begin{bmatrix} x \\ \theta \\ t \\ f \end{bmatrix}_{\text{in}}. \tag{3}$$

For convenience, we name the remaining derivatives E thru I, so that a generalized 4 × 4 ray matrix or ray-pulse matrix has the form

$$\begin{bmatrix} x \\ \theta \\ t \\ f \end{bmatrix}_{\text{out}} = \begin{bmatrix} A & B & 0 & E \\ C & D & 0 & F \\ G & H & 1 & I \\ 0 & 0 & 0 & 1 \end{bmatrix} \begin{bmatrix} x \\ \theta \\ t \\ f \end{bmatrix}_{\text{in}}. \tag{4}$$

Each of the symbolic entries in this matrix can, in fact, take on any value, although the nine entries are not all independent. One of the relations among them is the familiar $AD - BC = 1$, while two other relations involve the dispersive elements and have no analog in *ABCD* matrices. The relations will be discussed in-depth in the section on the analog of the Huygens integral, where the form of the extra relations is easy to discover; however, it is easy to see why $AD - BC = 1$ without the use of the integral formalism. If we imagine placing blackbodies at the same temperature on both ends of the optical system, each emits a certain amount of energy per unit time per unit frequency per unit area into a unit angle. Because the matrix in (4) gives the output time, frequency, position, and slope as functions of the input, its determinant is the magnification of the phase space volume that the radiation is in. But by the second law of thermodynamics, there can be no net power transferred, and thus no change in radiation density, so that the determinant must be 1. Expanding out the determinant then yields $AD - BC = 1$.

III. Ray-Pulse Matrices for some Common Elements

As an example of this formalism, let us compute the ray-pulse matrix for a grating. The reference planes are taken perpendicular to the incident and outgoing parts of the reference ray, and are chosen for convenience to meet at the point of reflection, as shown in Fig. 2(a). Construc-

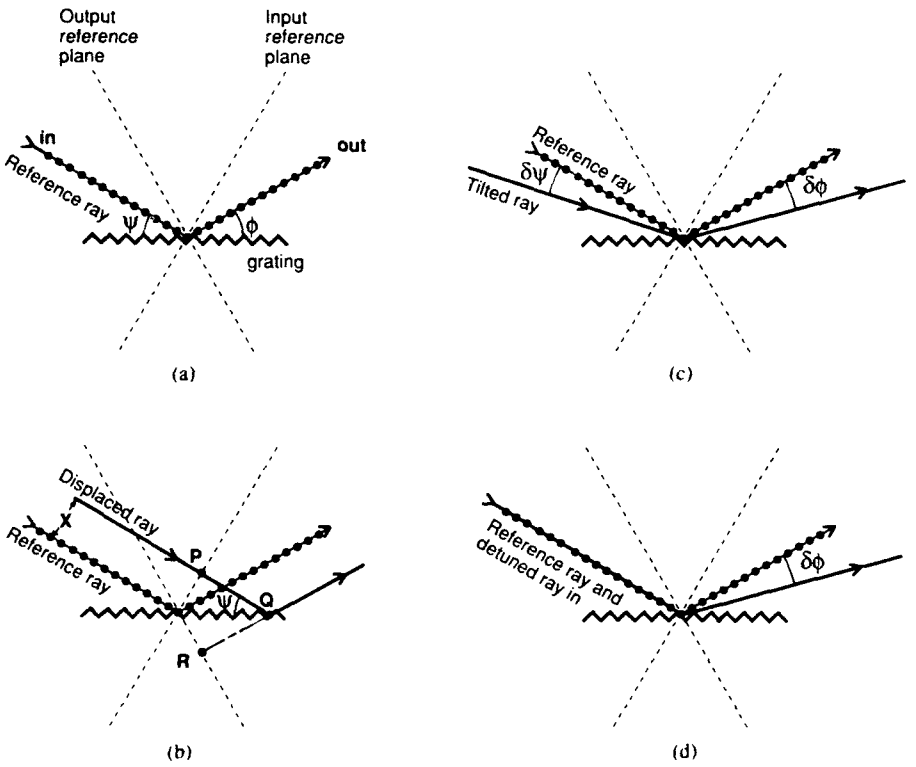

Fig. 2. Ray-pulse matrix for grating is computed from difference in behavior of reference ray (a), spatially offset ray (b), tilted ray (c), and detuned ray (d).

tion of the ray-pulse matrix begins by considering an incident wave parallel to the reference ray, but separated from it by x units as shown in Fig. 2(b). This new ray strikes the grating $x/\sin\psi$ units away from the reference, and the reflected ray can be extended backwards to the output plane where its height is $-x\sin\phi/\sin\psi$. Thus, $A = -\sin\phi/\sin\psi$. From the grating law, it is clear that the output is parallel to the reference from which we conclude that $C = 0$. Also, the extra distance traveled by the offset ray is just $\overline{PQ} - \overline{QR}$ so that the pulse will arrive $x(\cos\psi - \cos\phi)/(c\sin\psi)$ later, so that $G = (\cos\psi - \cos\phi)/(c\sin\psi)$.

We now consider a ray that meets the input plane at the same place as the reference ray, but that has a different slope as shown in Fig. 2(c). It is clear that the output position has not moved, and thus that $B = 0$. From differentiating the grating equation, $(f_0 + f)(\cos\phi - \cos\psi) = c/\lambda_{\text{grating}}$ where f_0 is the frequency of the reference ray, we can deduce that $-\sin\psi\delta\psi + \sin\phi\delta\phi = 0$ so that $D = -\sin\psi/\sin\phi$ because the input angle is $-\delta\psi$. We could also have obtained this element from the previously obtained values for A and B plus the relationship $AD - BC = 1$. Also, the delay of the tilted ray is seen to be zero so that $H = 0$.

Finally, consider a pulse that lies on top of the reference pulse, but has a different center frequency, as in Fig. 2(d). Just as in the case of the tilted input wave, it is clear that the output time and position are identical with the reference, and thus that $E = I = 0$. To obtain the last element, differentiate the grating equation with respect to

TABLE I
GENERALIZED RAY MATRICES FOR VARIOUS OPTICAL COMPONENTS

LENS OR MIRROR	DISPERSIVE SLAB
$\begin{bmatrix} 1 & 0 & 0 & 0 \\ -\frac{1}{f} & 1 & 0 & 0 \\ 0 & 0 & 1 & 0 \\ 0 & 0 & 0 & 1 \end{bmatrix}$	$\begin{bmatrix} 1 & \frac{L}{n} & 0 & 0 \\ 0 & 1 & 0 & 0 \\ 0 & 0 & 1 & \frac{\partial n_g}{\partial f}\frac{L}{\lambda_0} \\ 0 & 0 & 0 & 1 \end{bmatrix}$
f = focal length	L = thickness of slab
LITTROW PRISM	**PRISM**
$\begin{bmatrix} m & 0 & 0 & 0 \\ 0 & \frac{1}{m} & 0 & \frac{\partial n}{\partial f}\frac{\tan\psi}{m} \\ \frac{\partial n}{\partial f}\frac{\tan\psi}{\lambda_0} & 0 & 1 & 0 \\ 0 & 0 & 0 & 1 \end{bmatrix}$	$\begin{bmatrix} m & 0 & 0 & 0 \\ 0 & \frac{1}{m} & 0 & \frac{\partial n}{\partial f}\tan\psi \\ \frac{\partial n}{\partial f}\frac{m\tan\psi}{\lambda_0} & 0 & 1 & 0 \\ 0 & 0 & 0 & 1 \end{bmatrix}$
ψ = prism apex angle ray enters at normal incidence prism used at tip $m = \sqrt{1 - n^2\sin^2\psi}/\cos\psi$	ψ = prism apex angle ray exits at normal incidence prism used at tip $m = \cos\psi/\sqrt{1 - n^2\sin^2\psi}$
GRATING	**GENERAL PRISM**
$\begin{bmatrix} -\frac{\sin\phi}{\sin\psi} & 0 & 0 & 0 \\ 0 & \frac{\sin\psi}{\sin\phi} & 0 & \frac{\cos\phi - \cos\psi}{f_0\sin\phi} \\ \frac{\cos\psi - \cos\phi}{c\sin\psi} & 0 & 1 & 0 \\ 0 & 0 & 0 & 1 \end{bmatrix}$	$A = m_\phi m_\psi$ $B = Lm_\phi/nm_\psi$ $C = 0$ $D = 1/m_\phi m_\psi$ $E = (\partial n_g/\partial f)Lm_\phi\tan\psi/n$ $F = (\partial n_g/\partial f)(\tan\phi + \tan\psi)/m_\phi$ $G = (\partial n_g/\partial f)m_\psi\tan\psi + \tan\psi)\lambda_0$ $H = (\partial n_g/\partial f)L\tan\phi/m_\psi n\lambda_0$ $I = (\partial n_g/\partial f)^2 L\tan\phi\tan\psi/n\lambda_0$ $- (\partial n_g/\partial f)^2 L/n\lambda_0$
ψ = incident ray to grating surface angle ϕ = reflected ray to grating surface angle	ψ = internal ray to entrance face normal angle ϕ = internal ray to exit face normal angle L = path length in glass $m_\phi = \sqrt{1 - n^2\sin^2\phi}/\cos\phi$ $m_\psi = \cos\psi/\sqrt{1 - n^2\sin^2\psi}$

to obtain $f(\cos\psi - \cos\phi) - f_0 \sin\phi\delta\phi = 0$ from which we conclude that $F = (\cos\theta - \cos\phi)/(f_0 \sin\phi)$ where f_0 is the frequency of the reference ray.

Using the method of the preceding paragraphs, explicit values of the ray-pulse matrices for other common dispersive systems have also been calculated, as summarized in Table I. It is interesting to note that the matrices for a grating and for a prism used at its tip are formally identical and, in fact, the only difference (to the order of expansion treated here) is that the grating has much larger dispersive terms. Because of this, we will explicitly treat optical systems that are made with prisms, but the reader should remember that any of these prisms can be replaced with gratings. We consider now several uses of these 4 by 4 ray-pulse matrices.

IV. Multiple-Prism Systems

These ray-pulse matrices can be used to simplify the analysis of a variety of useful dispersive propagation systems. As a first example of a more complicated but useful system, let us consider a prism assembly similar to that used in femtosecond laser cavities, as discussed by Fork [4]. We assume that the reference beam passes through the apexes of all four prisms; that the input face of the first prism is parallel to the output face of the second prism; that all of the prism apex angles are the same; and that the second pair of prisms is a mirror image of the first pair, as indicated in Fig. 3(a). These specific conditions ensure that the rays at the input, output, and between the second and third prisms are parallel independent of the index of refraction and dispersion of the glass in the prisms. Under these conditions, the first prism has a generalized ray matrix given by

$$\begin{bmatrix} M & 0 & 0 & 0 \\ 0 & 1/M & 0 & D \\ MD/\lambda_0 & 0 & 1 & 0 \\ 0 & 0 & 0 & 1 \end{bmatrix} \tag{5}$$

while that of the second prism is

$$\begin{bmatrix} 1/M & 0 & 0 & 0 \\ 0 & M & 0 & -MD \\ -D/\lambda_0 & 0 & 1 & 0 \\ 0 & 0 & 0 & 1 \end{bmatrix}. \tag{6}$$

Explicit values of M and D in terms of the physical parameters of the prisms are of little importance here, but can be found in Table I. The matrices of the third and fourth prisms are respectively identical to (5) and (6) but with D replaced by $-D$. Assuming that the space between the first and second prisms is L, and that between the second and third is $\bar{L}$, the overall system matrix is found to be

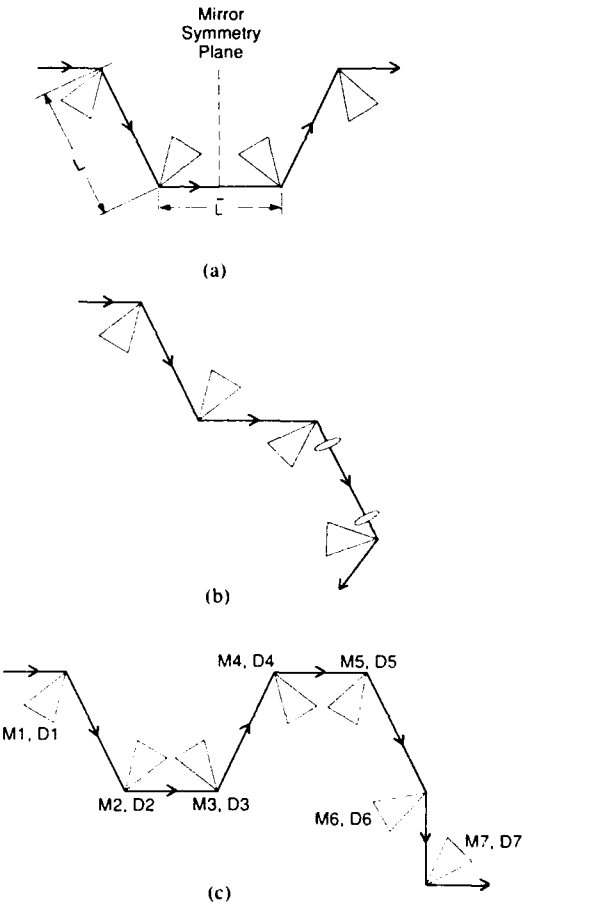

Fig. 3. Various systems that can be modeled with generalized ray matrices. (a) Multiple-prism system used to obtain positive group velocity dispersion in femtosecond laser cavities. (b) Variation on frequently used for short pulse amplification. (c) General prism beam expander whose ith prism has magnification M_i.

$$\begin{bmatrix} 1 & \bar{L} + 2L/M^2 & 0 & 0 \\ 0 & 1 & 0 & 0 \\ 0 & 0 & 1 & -2D^2L/\lambda_0 \\ 0 & 0 & 0 & 1 \end{bmatrix}. \tag{7}$$

This result says that rays of different wavelength that come into the system at the same position and slope will go out of the system at the same position and slope, but at different times. Indeed, this matrix is identical to that for a slab of material with a positive group velocity dispersion, independent of the sign of D, so that the cascaded prism assembly provides a method of achieving positive group velocity dispersion with no angular dispersion.

This approach has also been applied to the specific case discussed by Fork, in which the reference ray does not pass through the apexes of the second and third prisms, and the prisms have been cut so that they can be simultaneously used at Brewster's angle and $M = 1$. The result

obtained in this way for dt/df are in exact agreement with that found by Fork by a geometric construction.

As a simple variation, the second pair of prisms can be arranged as in Fig. 3(b), and a telescope of magnification -1 can be used to fill the space between the third and fourth prisms. This yields an overall system matrix of

$$\begin{bmatrix} -1 & \bar{L} & 0 & 0 \\ 0 & -1 & 0 & 0 \\ 0 & 0 & 1 & 0 \\ 0 & 0 & 0 & 1 \end{bmatrix} \tag{8}$$

which results in the beam being turned upside down and propagated backwards by a distance $\bar{L}$. Assemblies similar to this are in common use in ultrashort pulse amplification schemes. These systems are gratings instead of prisms, and are designed to temporally disperse the pulse before it passes through the gain medium (located between the second and third grating) and then reassemble the frequency components in the last two gratings.

As a final example, consider the design of an achromatic prism beam expander as shown in Fig. 3(c), where one wants to have the direction of the output beam not vary with the frequency of the input (i.e., $F = 0$). Since we are only interested in this one matrix element, it is clear that we can omit the matrices that correspond to the free space between the prisms, and that we may also assume that the beams go through the tips of the prisms. A straightforward induction shows that the overall matrix for k prisms is just

$$\begin{bmatrix} M_k & 0 & 0 & 0 \\ 0 & 1/M_k & 0 & D_k \\ M_k D_k/\lambda_0 & 0 & 1 & 0 \\ 0 & 0 & 0 & 1 \end{bmatrix} \cdots \begin{bmatrix} M_1 & 0 & 0 & 0 \\ 0 & 1/M_1 & 0 & D_1 \\ M_1 D_1/\lambda_0 & 0 & 1 & 0 \\ 0 & 0 & 0 & 1 \end{bmatrix}$$

$$= \begin{bmatrix} \prod_{l=1}^{k} M_l & 0 & 0 & 0 \\ 0 & 1/\prod_{l=1}^{k} M_l & 0 & \sum_{l=1}^{k} D_l \Big/ \prod_{m=l+1}^{k} M_m \\ 1/\lambda_0 \sum_{l=1}^{k} D_l \prod_{m=1}^{l} M_m & 0 & 1 & 0 \\ 0 & 0 & 0 & 1 \end{bmatrix} \tag{9}$$

where M_j is the magnification due to the jth prism, and D_j is the rate of change of output angle with input frequency in the jth prism. The overall angular dispersion is thus $\Sigma_{l=1}^{k} D_l / \Pi_{m=l+1}^{k} M_m$ in agreement with the result implied in Duarte and Piper [5] and given explicitly in Trebino [6]. This result implies that under common conditions the optimal design for an achromatic prism beam expander should have all but the last prism pointing in the same direction, as was pointed out by Trebino.

V. Generalized Huygens Integral

It is well known that optical systems characterized by an ordinary $ABCD$ matrix are equivalently represented by the monochromatic Huygens integral operator [3]

$$\sqrt{\frac{j}{\lambda_0 B}} \int dx_{\text{in}} U(x_{\text{in}}) \cdot \exp\left[-\frac{j\pi}{\lambda_0 B} (A x_{\text{in}}^2 - 2 x_{\text{in}} x_{\text{out}} + D x_{\text{out}}^2) \right] \tag{10}$$

where we have omitted a constant phase factor. This can be thought of as saying that the optical path length (eikonal) through an arbitrary $ABCD$ system from x_{in} to x_{out} is $(1/2B)(A x_{\text{in}}^2 - 2 x_{\text{in}} x_{\text{out}} + D x_{\text{out}}^2)$ plus a constant which we will ignore.

In this section, we will derive an analog to this result for the 4×4 ray-pulse matrices. We begin by specifying both the position and time that a pulse is to arrive at the

input and output planes. (This ability to use two-point boundary conditions is a result of the even number of coordinates, since a system with an odd number of coordinates will either be underdetermined or overdetermined when an even number of conditions are applied.) The specification of these four coordinates allows unique reconstruction of the other four coordinates, except in pathological cases such as imaging between the input and output planes.

The integral kernel is now expected to be of the form $\exp[-j2\pi L(x_{in}, x_{out}, t_{in}, t_{out})/\lambda_0]$ where the function L is real. Expanding L in a power series in all four coordinates yields first a constant length L_0 that is analogous to the overall phase factor in the Huygens integral formulation, which we will ignore just as we have done in (10). Next, there are linear terms that are zero because of the way we have constructed the reference planes. Again, this is analogous to the Huygens formulation where there are no linear terms in the exponential when treating systems in which all elements are on axis but, when elements are off axis, one must use *ABCDEF* matrices, and the kernel does indeed contain linear terms as given below in (20). The next term is a quadratic form in x_{in}, x_{out}, t_{in}, and t_{out} that can be reduced to a quadratic form in x_{in}, x_{out}, and $t_{in} - t_{out}$ by the time invariance of the system. As in the Huygens formulation, we stop with the quadratic terms, although there are in fact higher order terms that are of importance when rays are far off axis or are wildly detuned from the reference ray. Thus, we have the following ansatz for the space and time-varying analog of the Huygens integral:

$$\eta \iint dx_{in}\, dt_{in}\, U(x_{in}, t_{in}) \exp\left[-\frac{j\pi}{\lambda_0} \begin{pmatrix} x_{in} \\ x_{out} \\ t_{in} - t_{out} \end{pmatrix}^T \cdot \begin{pmatrix} \alpha & \beta & \gamma \\ \beta & \delta & \epsilon \\ \gamma & \epsilon & \zeta \end{pmatrix} \begin{pmatrix} x_{in} \\ x_{out} \\ t_{in} - t_{out} \end{pmatrix} \right] \tag{11}$$

where λ_0 is the wavelength of the reference ray.

A simple way to establish the correspondence between the elements of the generalized ray matrix and the unknown parameters $\alpha, \beta, \cdots, \eta$ is to take an incident wave which has its center at position $\bar{x}$, time $\bar{t}$, mean slope $\bar{\theta}$, and mean frequency $\bar{f}$ and perform the integration indicated in (11). Using the input wave

$$\exp\left[2\pi \left(-\frac{(x_{in} - \bar{x})^2}{\lambda_0^2} - \frac{(t_{in} - \bar{t})^2 c^2}{\lambda_0^2} - j\frac{\bar{\theta}}{\lambda_0}(x_{in} - \bar{x}) + j\bar{f}(t_{in} - \bar{t}) \right) \right] \tag{12}$$

yields an output wave which is a constant involving η times the exponential of a second-degree polynomial in x_{out} and t_{out} with coefficients that depend upon $\alpha, \beta, \cdots, \zeta$ and the coordinates of the input wave. In order to find the position, slope, frequency, and time of the output pulse, we must separate the wave into the product of an envelope and a phase. This is easily done as the polynomial in the exponential is easily split into real and imaginary parts, the exponential of the real part yielding the envelope, and the exponential of the imaginary part being the phase. The position and time of the output pulse can then be located by setting the derivatives with respect to x_{out} and t_{out} of the envelope to zero and solving for x_{out} and t_{out}.

Alternately, we could evaluate $\iint dx_{out}\, dt_{out}\, x_{out} |U_{out}|^2 / \iint dx_{out}\, dt_{out}\, |U_{out}|^2$ as the mean position of the output pulse, and use $\iint dx_{out}\, dt_{out}\, t_{out} |U_{out}|^2 / \iint dx_{out}\, dt_{out}\, |U_{out}|^2$ as the mean time for the output pulse. However, a basic theorem for Gaussian distributions tells us that these are identical to the position and time of the maximum amplitude of the pulse. Similarly, the frequency and slope of the output ray may be found by tedious integration, or by evaluating the derivative of the imaginary part of the polynomial at the position and time found just above. The result of this can be summarized as the generalized ray matrix

$$\begin{bmatrix} \dfrac{\gamma^2 - \alpha\zeta}{\beta\zeta - \gamma\epsilon} & \dfrac{-\zeta}{\beta\zeta - \gamma\epsilon} & 0 & \dfrac{-\gamma\lambda_0}{\beta\zeta - \gamma\epsilon} \\ \dfrac{\alpha\epsilon^2 + \zeta\beta^2 + \delta\gamma^2 - \alpha\delta\zeta - 2\beta\gamma\epsilon}{\beta\zeta - \gamma\epsilon} & \dfrac{\epsilon^2 - \delta\zeta}{\beta\zeta - \gamma\epsilon} & 0 & \dfrac{(\beta\epsilon - \gamma\delta)\lambda_0}{\beta\zeta - \gamma\epsilon} \\ \dfrac{\beta\gamma - \alpha\epsilon}{\beta\zeta - \gamma\epsilon} & \dfrac{-\epsilon}{\beta\zeta - \gamma\epsilon} & 1 & \dfrac{-\beta\lambda_0}{\beta\zeta - \gamma\epsilon} \\ 0 & 0 & 0 & 1 \end{bmatrix}. \tag{13}$$

Intermediate steps in the derivation of this result have been suppressed as they are exceedingly complicated, and required the use of MACSYMA. This result can be inverted to give $\alpha, \beta, \cdots, \zeta$ as functions of $A, B, \cdots, I$. The results are

$$\alpha = \frac{\lambda_0 A(EH - BI) + E^2}{\lambda_0 B(EH - BI)}$$

$$\beta = \frac{I}{EH - BI}$$

$$\gamma = \frac{E}{EH - BI}$$

$$\delta = \frac{D(EH - BI) + \lambda_0 H^2}{B(EH - BI)}$$

$$\epsilon = \frac{\lambda_0 H}{EH - BI}$$

$$\zeta = \frac{\lambda_0 B}{EH - BI}. \tag{14}$$

Finally, η can be determined up to a phase by insisting that energy is conserved. Doing so yields $\eta = j/\sqrt{\lambda_0(EH - BI)}$ where the phase of η has been chosen to make the output phase identical to the input in the limit of an identity ray-pulse matrix. With these identifications, (11) becomes a generalized time and space-varying Huygens kernel, analogous to the space-varying integral of (10), and dependent only on the A through I matrix elements.

In the expressions for $\alpha, \beta, \cdots, \eta$ we find that the expression $EH - BI$ occurs repeatedly in the denominator. Several of the systems that we have already discussed make this quantity zero, so we will describe how to handle this case. There are two distinct possibilities: if at least one of E, H, B, or I is nonzero, the kernel collapses into a one-dimensional delta function, which cancels one integral in (11) and the other integration remains nontrivial. If, on the other hand, all of E, H, B, and I are zero, we obtain two delta functions that renders both integrations trivial. Both of these cases are handled by making small perturbations in the matrix elements, and then letting these changes go to zero. For the case $EH - BI = 0$, but $B \neq 0$, we obtain the kernel $\sqrt{j/\lambda_0 B} \exp[(-j\pi/\lambda_0 B)(Ax_{in}^2 - 2x_{in}x_{out} + Dx_{out}^2)]\,\delta(t_{in} - t_{out} + Hx_{out}/B + Ex_{in}/\lambda_0 B)$. Formulas of a similar type exist for $E \neq 0$, $H \neq 0$, and $I \neq 0$. For the case where $B = E = H = I = 0$ the propagator is just $A^{-1/2} \exp[-j\pi C x_{out}^2/\lambda_0 A]\,\delta(x_{in} - x_{out}/A)\,\delta(t_{in} - t_{out} + Gx_{in})$.

Since the propagator has only six parameters that influence the output coordinates and the generalized ray matrix has nine variable elements, we know that there are three relations between these matrix elements. These relations may be taken to be

$$AD - BC = 1$$
$$BF - ED = \lambda_0 H$$
$$AF - EC = \lambda_0 G \tag{15}$$

or they may be taken to be

$$AD - BC = 1$$
$$\lambda_0(BG - AH) = E$$
$$\lambda_0(DG - CH) = F \tag{16}$$

depending upon whether one wants to think of H and G or E and F as being more fundamental. These constraints may also be written in the matrix form

$$\begin{bmatrix} A & B & 0 & E \\ C & D & 0 & F \\ G & H & 1 & I \\ 0 & 0 & 0 & 1 \end{bmatrix}^T \begin{bmatrix} 0 & 1 & 0 & 0 \\ -1 & 0 & 0 & 0 \\ 0 & 0 & 0 & -\lambda_0 \\ 0 & 0 & \lambda_0 & 0 \end{bmatrix} \times \begin{bmatrix} A & B & 0 & E \\ C & D & 0 & F \\ G & H & 1 & I \\ 0 & 0 & 0 & 1 \end{bmatrix} = \begin{bmatrix} 0 & 1 & 0 & 0 \\ -1 & 0 & 0 & 0 \\ 0 & 0 & 0 & -\lambda_0 \\ 0 & 0 & \lambda_0 & 0 \end{bmatrix}. \tag{17}$$

Quick inspection reveals that all of the matrices in Table I obey these relations. Also, it is easy to show that if a series of ray-pulse matrices satisfy (15), (16), or (17), then so does their product, from which we conclude that (15), (16), and (17) are in fact satisfied for any system made up of the components in Table I.

It was mentioned earlier that the A, B, C, and D elements of a generalized ray-pulse matrix are identical to the elements of a conventional ray matrix, despite the fact that the ray-pulse matrix is defined in terms of a temporal group while the conventional ray matrix is defined in terms of a monochromatic wave. There are two distinct arguments that can be made to establish this fact. First, an intuitive argument: note that a temporal group can be broken down into monochromatic waves, and that each of these can be propagated through the system by the use of a conventional $ABCDEF$ matrix. The matrix used for each frequency component will be slightly different if the system contains any dispersive elements, which means that the various monochromatic waves will emerge at locations and slopes centered around that of the monochromatic wave with the central frequency. Finally, noting that the energy per unit area per unit angle of the monochromatic waves is additive, we find that the temporal group emerges at the location and slope of its central fre-

uency component that implies the equivalence of the A, B, C, and D elements of the two types of matrix.

A second and more rigorous argument is based upon the Huygens integral formulation. We begin by taking an arbitrary generalized ray matrix and computing its generalized Huygens integral equivalent as given in (11) and (14). We then apply (11) to a wavefront $U(x_{in})$ with no time dependence, and perform the indicated time integral. The result is

$$\sqrt{\frac{j}{\lambda_0 B}} \int dx_{in}\, U(x_{in}) \cdot \exp\left[-\frac{j\pi}{\lambda_0 B} (Ax_{in}^2 - 2x_{in}x_{out} + Dx_{out}^2) \right] \quad (18)$$

which is identical to (10) except that the A, B, and D appearing now are elements of the generalized ray matrix. Thus, the generalized A, B, and D elements of the ray-pulse matrix are identical to those of the monochromatic ray matrix. Finally, the C elements of the two types of matrices are identical because both satisfy $AD - BC = 1$.

VI. Monochromatic Wave Propagation

Now that we have the analog of Huygens integral for ray-pulse matrices, we may obtain results for various special input wavefronts. We begin with a discussion of the case where the input wave is monochromatic at some frequency f. In this case, we will write the incident wave as $U(x_{in})\, e^{j2\pi ft}$ and perform the time integral. Doing so results in the output wave being given by

$$\exp\left[j2\pi ft + j\frac{\pi f^2}{B}(EH - BI) \right] \int dx_{in}\, U(x_{in}) \cdot \exp\left[-\frac{j\pi}{B\lambda_0} L(x_{in}x_{out}) \right] \quad (19a)$$

where the eikonal length $L(x_{in}, x_{out})$ is given by

$$L(x_{in}, x_{out}) = \begin{pmatrix} x_{in} \\ x_{out} \end{pmatrix}^T \begin{pmatrix} A & -1 \\ -1 & D \end{pmatrix} \begin{pmatrix} x_{in} \\ x_{out} \end{pmatrix} + 2 \begin{pmatrix} E \\ \lambda_0 H \end{pmatrix}^T \begin{pmatrix} x_{in} \\ x_{out} \end{pmatrix}. \quad (19b)$$

If the incident field is known in the form $U(x, f)$, the output field may be found in the same form by using (19) for each frequency component. The kernel

$$\exp\left[-\frac{j\pi}{\lambda B} \begin{pmatrix} x_{in} \\ x_{out} \end{pmatrix}^T \begin{pmatrix} A & -1 \\ -1 & D \end{pmatrix} \begin{pmatrix} x_{in} \\ x_{out} \end{pmatrix} - j\frac{2\pi}{\lambda B} \begin{pmatrix} E \\ BF - DE \end{pmatrix}^T \begin{pmatrix} x_{in} \\ x_{out} \end{pmatrix} \right] \quad (20)$$

corresponds to an *ABCDEF* matrix at wavelength λ so that the integral in (19) corresponds to the matrix

$$\begin{bmatrix} A & B & fE \\ C & D & fF \\ 0 & 0 & 1 \end{bmatrix} \quad (21)$$

plus terms that are quadratic and higher in the input variables. These higher order terms are not to be trusted as the entire theory can only predict accurately changes in position that are linear in the input variables. This result generalizes the argument made in the last section about the correspondence between the A through D elements of the conventional and generalized ray matrices, in that it also shows that the E and F elements of the ray-pulse matrix are closely related to the E and F elements of conventional monochromatic but misaligned *ABCDEF* matrices.

At this point, the problem with using only 3×3 *ABCDEF* matrices to model dispersive systems also becomes clear: the elements G, H, and I are missing from the 3×3 formulation. The loss of G and H causes no loss of information, as they are computable from the remaining elements via (15), but I, which contains information about the dispersion on axis is missing and is not recoverable. It is important to note that the reduction of a ray-pulse matrix to an *ABCDEF* matrix for each frequency ignores the phase factor in front of the integral in (19), and thus results in the inability of the reduced formalism to predict the relative phase of various frequency components.

A physical description of this loss of information may be obtained from the standard construction of the eikonal. For a single frequency, one can develop the phase of propagation through the system by considering rays that originate at a point some distance back from the optical system, and come to a focus downstream from the system. Since each of these rays must have the same total optical length, and the paths outside of the system are known, we can subtract to get the path in the system. Thus, the system path length involves the total length which may vary from one frequency to the next. If we were to treat the system with *ABCDEF* matrices, we would have to carry this extra path or phase as the auxiliary function Martinez calls ϕ_0. If we make a Taylor-series expansion of ϕ_0, the constant term is unimportant; the linear term is zero because of the way we have set up the clocks; and the quadratic term is given in (19). Thus, ϕ_0 is included in our theory, provided that we neglect cubic and higher terms.

VII. Generalized Gaussian Beam Propagation

Another special input wave that results in interesting output waves is a generalized Gaussian pulse. This can be

written as a wave of the form

$$\exp\left[-\frac{j\pi}{\lambda_0}\begin{pmatrix} x_{in} \\ -t_{in}\end{pmatrix}^T \tilde{Q}_{in}^{-1}\begin{pmatrix} x_{in} \\ t_{in}\end{pmatrix}\right] \tag{22}$$

which is a generalized form of the usual Gaussian beam with beam parameter $\tilde{q}$. The minus sign in the definition (22) is needed to make the $\tilde{Q}$ matrix have one covariant and one contravariant index, as is required by the formula below. The generalized Gaussian beam parameter $\tilde{Q}$ can be defined without the minus sign, but this results in several appearances of the metric tensor below. Also, since $\tilde{Q}^{-1}$ defines a quadratic form, we require that the xt and tx elements of $\tilde{Q}^{-1}$ are negatives of each other.

Several other points also need to be made about (22). First, the xx element of $\tilde{Q}$ does not give the beam width unless the xt element is zero. Similarly, the tt element does not determine the pulse width unless the cross term is zero. Finally, note that the intensity and phase fronts of (22) may be obtained by taking the imaginary and real parts of $\tilde{Q}^{-1}$, respectively. It is then not only possible for the two real quadratic forms that result to not have principal axes along x and t, but it is also possible for them to have different principle axes that result in pulses that have phase fronts and intensity fronts pointed in different directions.

If the pulse (22) is propagated through the system by the Huygens integral (11) above, we find that

$$\tilde{Q}_{out} = \left[\begin{pmatrix} A & 0 \\ G & 1\end{pmatrix}\tilde{Q}_{in} + \begin{pmatrix} B & E/\lambda_0 \\ H & I/\lambda_0\end{pmatrix}\right] \cdot \left[\begin{pmatrix} C & 0 \\ 0 & 0\end{pmatrix}\tilde{Q}_{in} + \begin{pmatrix} D & F/\lambda_0 \\ 0 & 1\end{pmatrix}\right]^{-1} \tag{23}$$

which is analogous to the result $\tilde{q}_{out} = (Aq_{in} + B)/(Cq_{in} + D)$ that holds for Gaussian beams. Of course, the analog is not quite exact, as the expressions previous are matrices and the order of the numerator and denominator matters, while in the conventional formula no such distinction needs to be made. The 2×2 blocks in the expression above can be written down by inspection by the following means: divide the variable elements in the last column by λ_0, and then reorder the rows and columns of the ray-pulse matrix so that the variables occur in the order x, t, θ, and f. The upper right 2×2 block is the coefficient of $\tilde{Q}_{in}$ in the numerator, the upper left 2×2 block is the constant in the numerator, and similarly the lower half of the rearranged matrix yields the denominator of the expression for $\tilde{Q}_{out}$.

We can now try to determine an eigen-$\tilde{Q}$ for the system. A quick computation shows that there is no input $\tilde{Q}$ that can yield the same $\tilde{Q}$ at the output except in degenerate cases, and then any value will do for $\tilde{Q}_{tt}$. The reason for this is that the time part of the problem behaves in a divergent fashion; the temporal width of any pulse expands without bound as it is repeatedly passed through a (time invariant) dispersive system, although it may narrow for the first few passes. This means that, except in the case of no dispersion, there cannot be any temporal eigenpulse, while in the case of zero dispersion, any temporal pulse shape will come through unaltered. Returning to the combined space and time treatment, it is reasonable to look for pulse shapes in which $\tilde{Q}_{xx}$ and $\tilde{Q}_{xt}$ do not change upon propagation through the system, while $\tilde{Q}_{tt}$ increases by Δ in each pass. Expanding out (23) under these assumptions yields

$$\begin{aligned}
\tilde{Q}_{xx} &= \frac{A\tilde{Q}_{xx} + B}{C\tilde{Q}_{xx} + D} \\
\tilde{Q}_{xt} &= \frac{\tilde{Q}_{xt} - G\tilde{Q}_{xx} - H/\lambda_0}{C\tilde{Q}_{xx} + D} \\
\Delta + \tilde{Q}_{tt} &= \frac{C\tilde{Q}_{xt} + F/\lambda_0}{C\tilde{Q}_{xx} + D}(G\tilde{Q}_{xx} - \tilde{Q}_{xt} + H) \\
&\quad - G\tilde{Q}_{xt} - I/\lambda_0 + \tilde{Q}_{tt}.
\end{aligned} \tag{24}$$

Letting $R = \sqrt{(A + D)^2 - 4}$, we obtain

$$\begin{aligned}
\tilde{Q}_{xx} &= \frac{A - D \pm R}{2C} \\
\tilde{Q}_{xt} &= \frac{AG - F/\lambda_0 + CH \pm R}{C(2 + A - D \pm R)} \\
\Delta &= -I/\lambda_0 - \frac{AG - F/\lambda_0 + CH \pm R}{C(2 + A - D \pm R)^2} \cdot \\
&\quad [AG - F/\lambda_0 + CH \pm R + (F/\lambda_0 + G) \\
&\quad \cdot (2 + A - D \pm R)]
\end{aligned} \tag{25}$$

as the parameters of the quasi-eigenpulse. Although the result in (25) for $\tilde{Q}_{xx}$ appears to be familiar from cavity mode theory, the beam waist is not $\sqrt{\lambda_0 \tilde{Q}_{xx}/\pi}$ unless $\tilde{Q}_{xt}$ is zero. When the optical system is designed to make propagation separable into space and time components, (25) reduces to

$$\begin{aligned}
\tilde{Q}_{xx} &= \frac{A - D \pm R}{2C} \\
\tilde{Q}_{xt} &= 0 \\
\Delta &= -I/\lambda_0
\end{aligned} \tag{26}$$

of which the first is truly familiar from standard cavity mode analysis while the last is from dispersive system theory.

The ray-pulse matrix theory as described here does not include active modelockers and other time-varying elements. It is clear that the theory can be expanded to cover time varying elements by allowing additional elements of the matrix to vary. Including time-varying modulation

elements should make it possible to determine the true combined temporal and spatial pulse shape of an actively mode-locked laser; but we are already in a position to see that the correct configuration for a passively modelocked system will have Δ near 0 as this means that the pulse does not spread much during its propagation around the cavity, and thus makes easy work for the nonlinear mechanisms that lead to pulse shortening.

VIII. Alternate Ray-Pulse Formulation

For compatibility with earlier forms of ray matrices, we defined the ray-pulse matrices in the form given in (4). An alternative approach would be to rearrange the variables with both coordinates first, both frequencies second in the form

$$\begin{bmatrix} x \\ t \\ \hline \theta \\ \lambda_0 f \end{bmatrix}_{\text{out}} = \left[\begin{array}{cc|cc} A & 0 & B & E/\lambda_0 \\ G & 1 & H & I/\lambda_0 \\ \hline C & 0 & D & F/\lambda_0 \\ 0 & 0 & 0 & 1 \end{array}\right] \begin{bmatrix} x \\ t \\ \hline \theta \\ \lambda_0 f \end{bmatrix}_{\text{in}}$$

$$= \left[\begin{array}{c|c} \mathbf{A} & \mathbf{B} \\ \hline \mathbf{C} & \mathbf{D} \end{array}\right] \begin{bmatrix} x \\ t \\ \hline \theta \\ \lambda_0 f \end{bmatrix}_{\text{in}}. \tag{27}$$

The 2×2 matrices $\mathbf{A}, \mathbf{B}, \mathbf{C}, \mathbf{D}$ are then obviously block-matrix analogs of the conventional elements A, B, C, D.

One advantage of this formulation is that the Gaussian beam transformation rule can be written in the simplified form

$$\tilde{\mathbf{Q}}_{\text{out}} = [\mathbf{A}\tilde{\mathbf{Q}}_{\text{in}} + \mathbf{B}][\mathbf{C}\tilde{\mathbf{Q}}_{\text{in}} + \mathbf{D}]^{-1} \tag{28}$$

which has an obvious similarity to the conventional rule that $\tilde{q}_{\text{out}} = (A\tilde{q}_{\text{in}} + B)/(C\tilde{q}_{\text{in}} + D)$.

IX. Conclusion

We have shown that time-invariant dispersive optical systems can be modeled in a very straightforward way by using 4×4 ray-pulse matrices, and that this formulation allows the construction of a Huygens type integral operator that describes the dispersive system up to quadratic phases in both spatial and temporal frequencies. The ability of 4×4 matrices to convert to this integral operator form relies upon the fact that the variables come in conjugate pairs. Several extensions of this work are possible. One extension would be to include elements such as Gaussian apertures whose ray-pulse matrices would have complex entries. Another would be the introduction of time-varying elements such as modelockers. By including these active elements it should be possible to find true eigenwaves for an arbitrary mode-locked system, with results similar to the Kuizenga-Siegman [7] theory of modelocking. The theory could also be extended to handle off-axis components, and finally, cubic and higher order theories might be developed in analogy with the higher order theories of monochromatic systems. For the dispersive problem, there is an interesting quadratic theory as there is no symmetry which rules out second-order terms as there is in the familiar case. Also, both transverse dimensions could be included by increasing the size of the matrix to 6×6, as it is only necessary to add the second slope and position as coordinates.

Acknowledgment

The author wishes to express appreciation for the opportunity to have seen [1] and [2] in manuscript form prior to their publication.

References

[1] O. E. Martínez, "Matrix formalism for pulse compressors," *IEEE J. Quantum Electron.*, vol. 24, pp. 2530-2536, 1988.
[2] ——, "Matrix formalism for dispersive laser cavities," *IEEE J. Quantum Electron.*, vol. 25, pp. 296-300, 1989.
[3] A. E. Siegman, *Lasers*. University Science, 1986, ch. 15, 16, 27.
[4] R. L. Fork, O. E. Martínez, and J. P. Gordon, "Negative dispersion using pairs of prisms," *Opt. Lett.*, vol. 9, pp. 150-152, 1984.
[5] F. J. Duarte and J. A. Piper, "Dispersion theory of multiple-prism beam expanders for pulsed dye lasers," *Opt. Commun.*, vol. 43, pp. 303-307, 1982.
[6] Rick Trebino, "Achromatic N-prism beam expanders: Optimal configurations," *Appl. Opt.*, vol. 24, pp. 1130-1138, 1985.
[7] D. J. Kuizenga, D. W. Phillion, T. Lund, and A. E. Seigman, "Simultaneous Q-switching and mode-locking in the cw Nd:YAG laser," *Opt. Commun.*, vol. 9, pp. 221-226, 1973.

A. G. Kostenbauder, photograph and biography not available at the time of publication.

The Stanford Resonator and Optics Programs

PARAXIA

B

What is PARAXIA?

PARAXIA is a family of Macintosh applications developed at Stanford University for the computation and analysis of laser resonator modes and laser beam propagation problems. Taking advantage of the fast processors and excellent graphics capabilities of modern personal computers, together with optimized algorithms including Fast Fourier and Fast Hankel transforms and the virtual source formalism, PARAXIA offers a set of powerful analysis and design tools that provide rapid and accurate results and are extremely easy to use.

PARAXIA can handle in general any separable paraxial optical system in cartesian or cylindrical coordinates, including complex-valued and misaligned ray matrices, with full diffraction effects between apertures. It includes the programs:

- **ABCD** provides complex-valued ray-matrix and Hermite-gaussian mode analyses for arbitrary paraxial resonators and optical systems, including astigmatism and misalignment in each element.
- **FRESNEL** uses FFT and FHT methods to propagate an arbitrary wavefront through any arbitrary paraxial optical system using Huygens' integral in rectangular or radial coordinates. The wavefront can be multiplied by an arbitrary mask or mirror profile before or after each successive propagation through the system; a scripting capability makes iterative Fox and Li resonator calculations easy to implement.
- **VSOURCE** implements the virtual source analysis to calculate accurate eigenvalues, eigenmodes, excess noise factors and cross-power coefficients for unstable resonators with both circular mirrors and rectangular hard-edged mirrors (including misaligned rectangular systems) over a full range of equivalent Fresnel numbers.
- **VRM** carries out mode calculations and design analyses for gaussian variable-reflectivity-mirror lasers.

Why use PARAXIA?

Because PARAXIA is general, fast, accurate, and easy to use.

- **Wide range of applications**
  PARAXIA can handle arbitrary paraxial optical systems with only a few restrictions, and can be used to solve a wide variety of problems, from resonator mode calculations to far-field beam patterns to misalignment sensitivity analysis.
- **Performance**
  PARAXIA uses optimized algorithms for fast and accurate results. (FRESNEL propagates a wavefront of 1024 points through the system in 3 seconds/iteration. VSOURCE computes 10 sets of lowest and higher-order unstable-resonator eigenvalues/second.)
- **User-friendly interface**
  All PARAXIA programs are highly interactive using an efficient user-friendly interface consistent with Macintosh User Interface guidelines. Menus, dialog boxes and help files make PARAXIA easy to use even for researchers not familiar with the Macintosh computer.
- **Compatibility**
  Each PARAXIA program can produce its own graphic output and exchange data files with other PARAXIA programs; but all the programs can also export data files to a variety of other Macintosh applications, including major graphics packages, for further analysis or enhanced display.

How to get PARAXIA?

PARAXIA is available from Stanford University at:

Software Distribution Center
857 Serra Street
Stanford, CA 94305–6225
(415) 723–0651

PARAXIA Stanford Resonator and Optics Programs

ABCD

Ray-matrix algebra made easy

ABCD is a highly interactive program that allows you to "build" an optical system as a succession of optical elements (lenses, mirrors, Brewster plates, etc.), and edit it in the same way you edit text on the Macintosh, using the Cut, Copy, Paste, Clear and Undo commands. The various parameters (focal length, thickness, etc.) specified independently for each element can be edited at any time, can be made variable, and each element can be made misaligned and/or astigmatic. ABCD will propagate an arbitrary gaussian beam (e.g., the eigenmode) through the system, and calculate the variation of the gaussian beam parameters (radius of curvature and width) at a given location when varying the parameters of the optical elements.

Examples of problems ABCD can easily solve include:

- the design/analysis of stable resonators (eigenmode calculation, astigmatism corrections, regions of stability, etc.)
- the design/analysis of coupling optics (e.g., coupling a laser beam into an optical fiber.)
- the calculation of an overall ABCD matrix to be used in FRESNEL.

In addition to being a powerful investigation tool, ABCD also proves very useful as a didactic software for teaching paraxial optics.

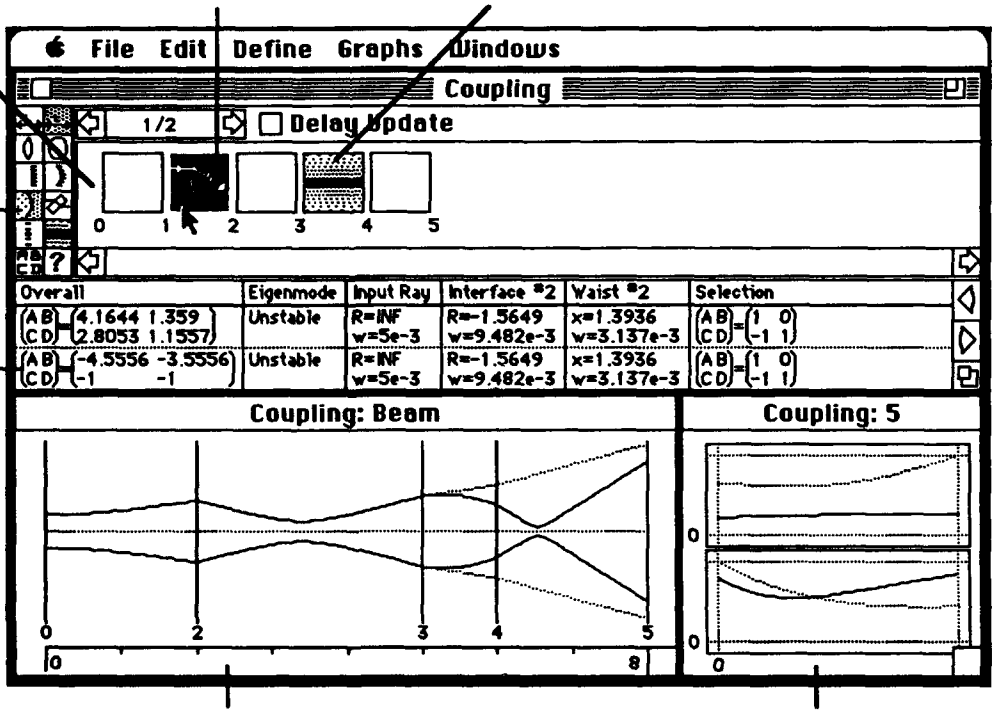

PARAXIA Stanford Resonator and Optics Programs

FRESNEL

General-purpose wavefront propagation

FRESNEL will propagate an arbitrary wavefront successively through a hard-edged aperture, an arbitrary mask, and an arbitray paraxial system described by a complex-valued ABCD-EF matrix. An iterative option allows for Fox & Li calculations of resonator eigenmodes.

FRESNEL uses Fast Fourier and Fast Hankel transform algorithms for fast, accurate results, even with large numbers of sampling points. FRESNEL has import and export capabilities, to exchange wavefront data file with other programs, and can be run either in interactive or batch mode using a script file to describe longer jobs.

Examples of problems FRESNEL can easily solve include:

- the propagation of a non-gaussian wavefront through an arbitrary paraxial system.
- finding the eigenmodes of any type of resonator (stable or unstable).

The hard-edged aperture and arbitrary mask in front of the system allow for modeling of such elements as:

- hard-edged mirrors
- hole coupling
- supergaussian variable-reflectivity-mirrors
- gain sheets

The input wavefront can either be a build-in analytic function or an imported user-defined data file.

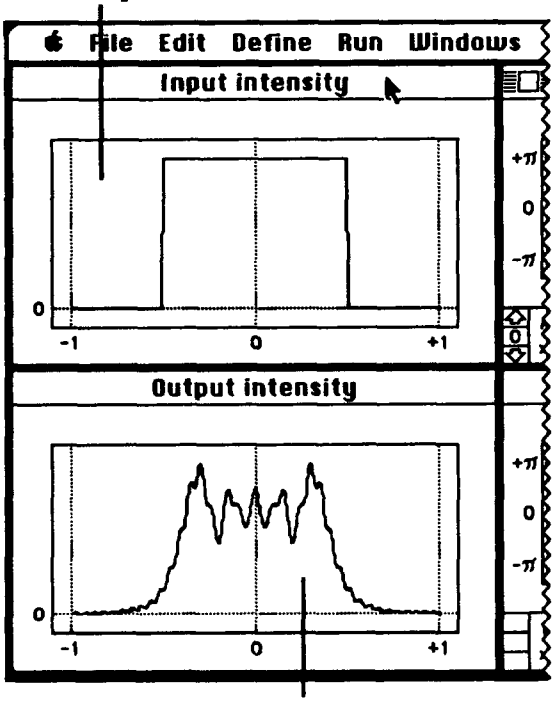

The output wavefront can be exported directly to graphics programs, such as Igor™.

Explicit dialog boxes allow for a highly interactive interface.

The output coordinate can be scaled within the calculation process.

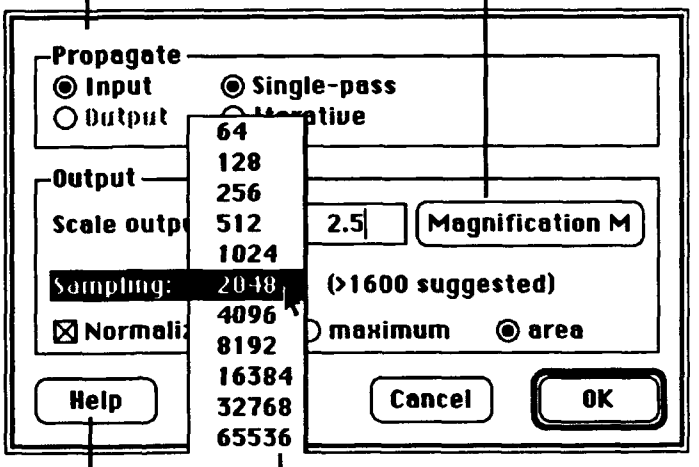

On-line help makes the programs even easier to use

The fast FFT and FHT algorithms allow for calculations with large numbers of sampling points in a fairly short time.
1024 points: 3 seconds/iteration
16384 points: 50 seconds/iteration

PARAXIA Stanford Resonator and Optics Programs

VSOURCE

All about unstable resonators

VSOURCE implements the virtual source formalism for the study of hard-edged strip or circular unstable resonators. VSOURCE will compute in real time multiple eigenvalues as a function of the effective Fresnel number and/or the magnification of the resonator, as well as the corresponding eigenwaves and associated overlap integrals (excess noise factor, cross-power, etc.).

The beam profile at other locations inside the resonator, as well as the far-field pattern outside the resonator, can be calculated by exporting the data to FRESNEL. In cartesian coordinates, VSOURCE can handle asymmetric (or misaligned) resonators, allowing the study of one-sided unstable resonators.

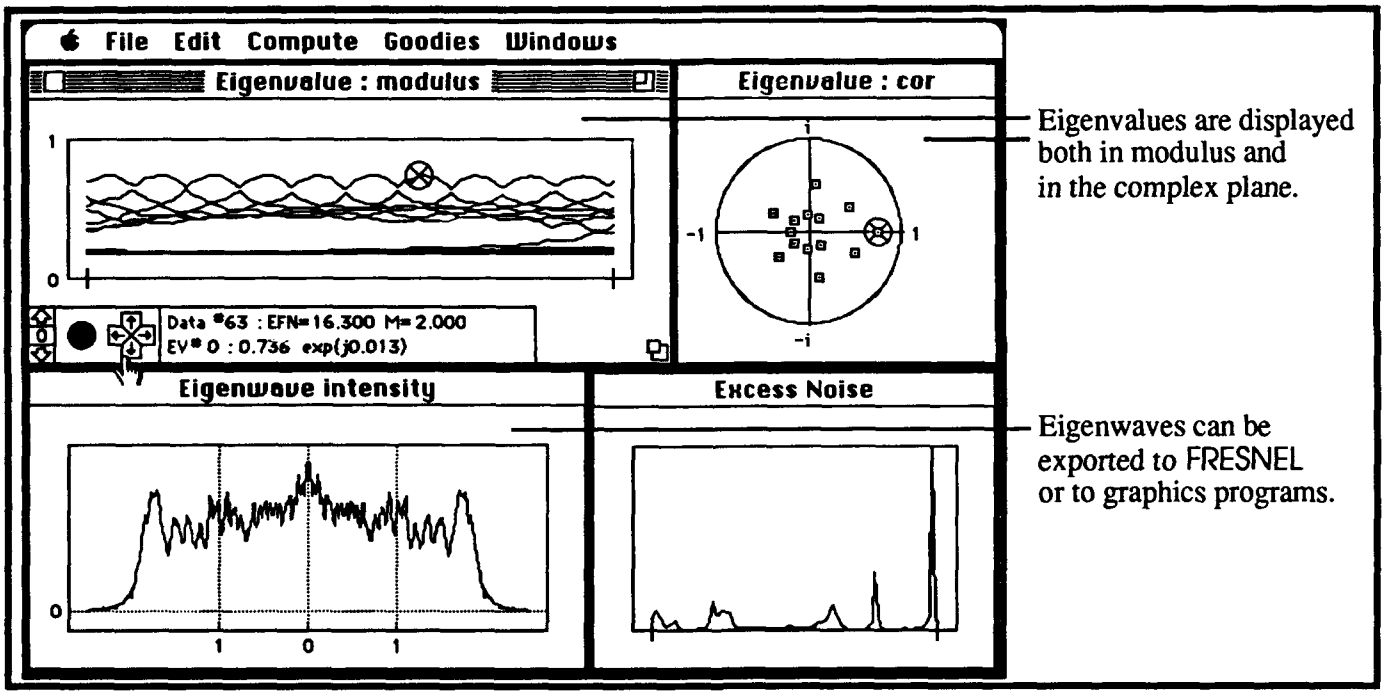

PARAXIA Stanford Resonator and Optics Programs

VRM

Gaussian variable-reflectivity-mirror resonators

VRM is a numerical implementation of complicated analytical results obtained for the gaussian variable-reflectivity-mirror resonators (both stable and unstable). VRM will compute the variation of the eigenvalues as a function of the equivalent (gaussian aperture) Fresnel number and/or the magnification of the resonator. For selected eigenvalues, VRM will compute the corresponding eigenwaves at the output mirror plane, and associated overlap integrals (excess noise factor, cross-power, etc.).

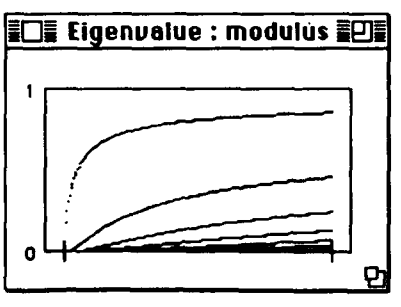

LASER BEAM AND RESONATOR CALCULATIONS ON DESKTOP COMPUTERS

A DISSERTATION
SUBMITTED TO THE DEPARTMENT OF APPLIED PHYSICS
AND THE COMMITTEE ON GRADUATE STUDIES
OF STANFORD UNIVERSITY
IN PARTIAL FULFILLMENT OF THE REQUIREMENTS
FOR THE DEGREE OF
DOCTOR OF PHILOSOPHY

By

Jean-luc Doumont

June 1991

ABSTRACT

There is a continuing interest in the design and calculation of laser resonators and optical beam propagation. In particular, recently, interest has increased in developing concepts such as one-sided unstable resonators, supergaussian reflectivity profiles, diode laser modes, beam quality concepts, mode competition, excess noise factors, and nonlinear Kerr lenses.

To meet these calculation needs, I developed a general-purpose software package named PARAXIA™, aimed at providing optical scientists and engineers with a set of powerful design and analysis tools that provide rapid and accurate results and are extremely easy to use. PARAXIA can handle separable paraxial optical systems in cartesian or cylindrical coordinates, including complex-valued and misaligned ray matrices, with full diffraction effects between apertures. It includes the following programs:

ABCD provides complex-valued ray-matrix and gaussian-mode analyses for arbitrary paraxial resonators and optical systems, including astigmatism and misalignment in each element. This program required that I generalize the theory of gaussian beam propagation through real-valued ray matrices to the case of an off-axis gaussian beam propagating through a misaligned, complex-valued ray matrix.

FRESNEL uses FFT and FHT methods to propagate an arbitrary wavefront through an arbitrary paraxial optical system using Huygens' integral in rectangular or radial coordinates. The wavefront can be multiplied by an arbitrary mirror profile and/or saturable gain sheet on each successive propagation through the system. Among other calculations, I used FRESNEL to design a one-sided negative-branch unstable resonator for a free-electron laser, and to show how a variable internal aperture influences the mode competition and beam quality in a stable cavity.

VSOURCE implements the virtual source analysis to calculate accurate eigenvalues, eigenmodes, excess noise factors and cross-power coefficients for unstable resonators with both circular and rectangular hard-edged mirrors (including misaligned rectangular systems). I used VSOURCE to show the validity of the virtual source approach (by comparing its results to those of FRESNEL), to study the properties of hard-edged unstable resonators, and to obtain numerical values of the excess noise factors in such resonators.

VRM carries out mode calculations and design analyses for gaussian variable-reflectivity-mirror lasers. It implements complicated analytical results that I derived to point out the large numerical value of the excess noise factor in geometrically unstable resonators.

Accepted by
~~Submitted to~~ *Optics Commun.*
Revised version of 7/25/1991

PERFORMANCE LIMITATIONS OF THE SELF-FILTERING UNSTABLE RESONATOR*

A. E. Siegman
Edward L. Ginzton Laboratory
Stanford University
Stanford, California 94305, USA

The self-filtering unstable resonator (SFUR) can provide excellent mode properties for high-gain lasers having active-medium Fresnel numbers up to a few times unity or perhaps a few tens. This note is merely to point out that the SFUR design is generally not suitable for much larger Fresnel number devices, because the output coupling that results for single-mode operation with full energy extraction then becomes unacceptably large.

Subject Index: 8,1.

Received November 29, 1990; in revised form,

*Work supported by the U. S. Air Force Office of Scientific Research.

The self-filtering unstable resonator (SFUR) design shown in Figure 1 has been proposed and experimentally demonstrated by Gobbi and Reali [1–5] and a number of other workers [6–11] in recent years. In essence the SFUR is a negative-branch confocal unstable resonator in which a small aperture through the scraper mirror also provides an internal spatial filter at the common focal point of the two mirrors. As this earlier work has well demonstrated, the SFUR cavity is a simple and practical design which can provide excellent mode properties, including very good beam quality and good energy extraction, for a wide variety of moderate to high-gain lasers. It is therefore a very practical and useful design for many laser systems.

The one additional point that I would like to make in this comment is that despite its many advantages there are some limitations to the use of the SFUR. This type of resonator is associated with the class of "unstable" resonators and might therefore seem potentially suitable for large Fresnel numbers as pointed out by Anan'ev [12]. What I wish to establish in this comment is that the SFUR is inherently limited to laser systems with at best moderate values of the laser Fresnel number, that is to Fresnel numbers on the order of a few times unity, up to a few multiples of ten at the most. The SFUR design, at least in its basic form, is not suitable for laser devices in which the inherent Fresnel numbers are much larger than a few multiples of ten because the output coupling that results for single-mode operation with full energy extraction then becomes unacceptably large.

This point can be demonstrated as follows. Figure 1 shows the basic parameters of the SFUR design (the notation and formulas are taken from the paper of Boffa *et al* [9]). This and earlier references have demonstrated that if the self-filtering

aperture in the output coupling mirror has an optimum diameter given by

$$d \equiv 2a \approx 2 \times (0.61 f_2 \lambda)^{1/2} \tag{1}$$

then this resonator will produce a very clean near-gaussian lowest-order mode with a gaussian spot size $w \approx Ma$, where $M = f_1/f_2$ is the geometric magnification of the unstable resonator. The magnitude of the eigenvalue $\tilde{\gamma}$ for the lowest-order mode and thus the power loss per round trip $1 - |\tilde{\gamma}|^2$ will then be given to a good approximation by

$$1 - |\tilde{\gamma}|^2 \equiv 1 - R \approx 1 - \left(\frac{1.968}{M^2}\right)\left[1 - \frac{0.6084}{M^2}\right] . \tag{2}$$

The reflectivity value $R \equiv |\tilde{\gamma}|^2$ can be viewed as the effective power reflectivity of the output mirror or output coupler in this cavity.

An additional parameter that is of large practical importance in high-power or high-energy laser designs is the Fresnel number [12] which characterizes the laser medium from which the laser mode is to extract power or energy. In particular, if $2A$ is the diameter and L the length of the laser gain medium, then it is convenient to define a Fresnel number N_T given by

$$N_T \equiv \frac{A^2}{L\lambda} . \tag{3}$$

This is sometimes called the "tube Fresnel number" because it characterizes the laser tube or laser rod from which the laser energy is to be extracted. If one is to obtain significant energy extraction from a laser gain medium of diameter $2A$ using a gaussian beam profile with mode spot size w, while avoiding significant clipping of the gaussian mode by the tube edges, the mode size and the tube diameter need to be related by a ratio on the order of

$$2A \approx \pi w \tag{4}$$

For the particular case of a SFUR cavity, the tube Fresnel number N_T and the magnification M will then be related by

$$N_T \approx \left(\frac{\pi}{2}\right)^2 \frac{w^2}{L\lambda} \approx 1.5 \times (f_1/L) \times M \tag{5}$$

Since N_T is determined by the laser medium, and M is more or less constrained by the allowable output coupling through Eq. (2), the only adjustable parameter is the ratio of the mirror focal length f_1 (which is also to a first approximation the overall resonator length) to the length L of the gain medium.

The most difficult situations for laser resonator design arise in high-power lasers having large-diameter gain media and therefore values of N_T that are sometimes very much greater than unity. A laser tube with bore diameter $2A = 1$ cm and length $L = 1$ m at a visible wavelength $\lambda = 500$ nm, for example, has $N_T \approx 50$. Equation (5) indicates that efficient single-mode energy extraction from such large-N_T laser media can only be accomplished with an SFUR design either by using a very large magnification M, which means very large output coupling and hence requires very high laser gain, or by using a mirror focal length f_1 very much longer than the gain medium length L, or possibly by using a folded multipath arrangment through the laser medium. The latter arrangments tend to be both mechanically and optically inconvenient.

To demonstrate this requirement in a graphic fashion, Figure 2 plots the relationship between the tube Fresnel number N_T and the effective output mirror reflectivity $R \equiv |\tilde{\gamma}|^2$ for three different ratios of the mirror focal length f_1 to the length L of the active laser medium, assuming a SFUR design which satisfies both the single-mode condition of Eq. (1) and the full power extraction condition of Eq. (4). (Note that the magnification M is a variable parameter along each of these

curves.) Note that in each case the effective reflectivity of the output mirror drops rapidly to values below 10% as the value of N_T increases; and that only a few lasers operate well with output reflectivities of $R = 10\%$ or lower. Most of the high-power and high-energy lasers of practical interest operate best with output couplings of 20% to 50% or larger (though there are of course some exceptions to this).

The general observation from this figure is that the SFUR can provide reasonable output coupling values or mirror reflectivities for laser gain media characterized by values of the Fresnel number N_T ranging from a few times unity up to perhaps $N_T = 10$ or 20. The SFUR approach cannot, however, provide a solution for single-mode operation with good energy extraction in the more difficult case of gain media with much larger tube Fresnel numbers, because the required values of magnification needed to fill the gain medium will make the effective output coupling from the cavity larger than can be tolerated. Lasers with larger values of N_T will require the use of some combination of either the original hard-edged unstable resonator approach [13] or some form of variable-reflectivity-mirror (VRM) resonator design [5,14] or possible some form of injection locking or seeding [7], along with possible folding or multipass operation of the laser cavity.

REFERENCES

[1] P. G. Gobbi and G. C. Reali, "A novel unstable resonator configuration with a self filtering aperture," Opt. Commun. 52 (1984) 195.

[2] P. G. Gobbi, S. Morosi, G. C. Reali, and Amin S. Zarkasi, "Novel unstable resonator configuration with a self filtering aperture: Experimental characterization of the Nd:YAG loaded cavity," Appl. Optics 24 (1985) 26.

[3] P. G. Gobbi, G. C. Reali, and C. Malvicini, "Numerical optimization study of a self-filtering unstable resonator for high power solid state and gas lasers," presented at CLEO '85, Baltimore, Md. (May 1985).

[4] P. G. Gobbi and G. C. Reali, "Numerical study of a self filtering unstable resonator," in Southwest Conference on Optics, Proc. SPIE 540,(1985) 119.

[5] P. G. Gobbi and G. C. Reali, "Mode analysis of a self-filtering unstable resonator with gaussian transmission aperture," Opt. Commun. 57 (1986) 355.

[6] A. Bianchi, A. Ferrario, P. G. Gobbi, C. Malvicini, and G. C. Reali, "Characterization of a modified SFUR Nd:YAG oscillator in various pulsed regimes," ECOOSA 1986, Proc. SPIE 701 (1987) 132.

[7] R Barbini, et al, "Injection locked single mode high power low divergence TEA CO2 laser using SFUR configuration," Opt. Commun. 60 (1986) 239.

[8] P. Di Lazzaro, T. Hermsen, T. Letardi, and Chengen Zheng, "Self-filtering unstable resonator: An approximate analytical model with comparison to computed and XeCl laser experimental results," Opt. Commun. 61, 393–396 (March 1987).

[9] V. Boffa, P. Di Lazzaro, G. P. Gallerano, G. Giordano, T. Hermsen, T. Letardi,

and C. E. Zheng, "Self-filtering unstable resonator operation of XeCl excimer laser," IEEE J. Quantum Electron. QE–23 (1987) 1241.

[10] P. Di Lazzaro, T. W. P. M. Hermsen, and Chengen Zheng, "A generalization of the self-filtering unstable resonator," IEEE J. Quantum Electron. QE–24 (1988) 1543.

[11] P. Di Lazzaro, V. Nassisi, and M. R. Perrone, "Experimental study of a generalized self-filtering unstable resonator applied to an XeCl laser", IEEE J. Quantum Electron. QE–24 (1988) 2284.

[12] Yu. A. Anan'ev, "Selection of the resonator type," Sov. J. Quantum Electron. 19 (1989) 1357.

[13] A. E. Siegman, "Unstable optical resonators," Appl. Opt. 13 (1974) 353.

[14] S. De Silvestri, V. Magni, O. Svelto, and G. Valentini, "Lasers with supergaussian mirrors," IEEE J. Quantum Electron. QE–26 (1990) 1500.

FIGURE CAPTIONS

Fig. 1. Basic self-filtering unstable resonator (SFUR) design. The gain medium is assumed to have an outer diameter 2A and to extend over a length $L \leq f_1$.

Fig. 2. Effective power reflectivity $R \equiv |\tilde{\gamma}|^2$ of the output coupling element versus Fresnel number $N_T \equiv A^2/L\lambda$ for SFUR designs with three different values of mirror focal length f_1 to active gain medium length L. (The magnification M is a variable parameter along each of these curves.)

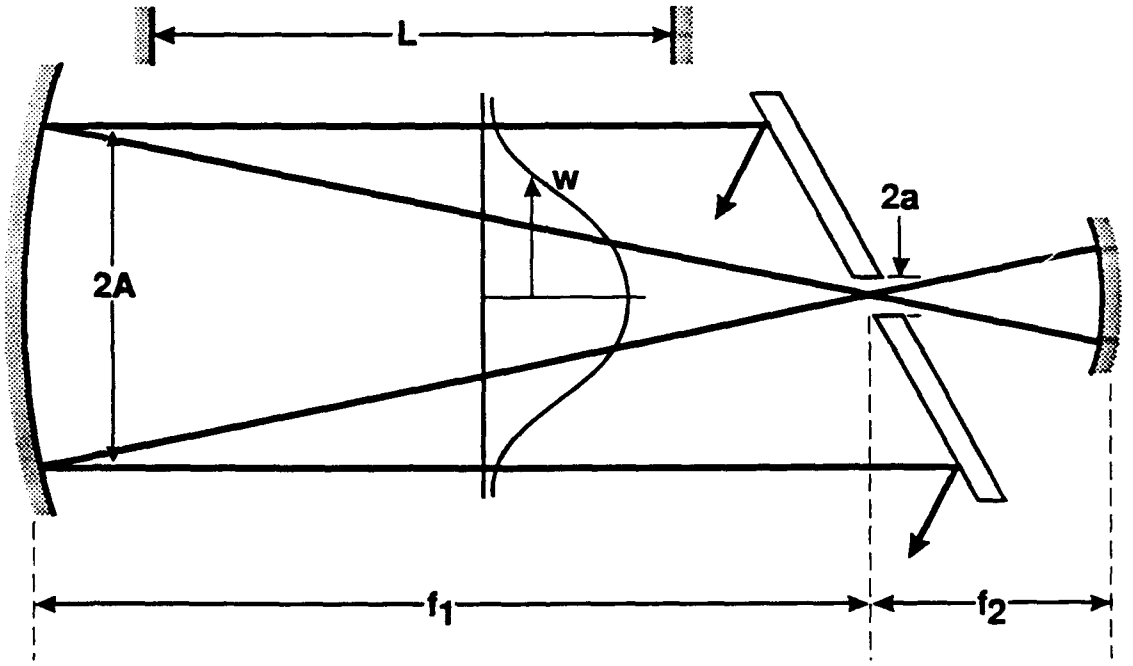

Fig. 1

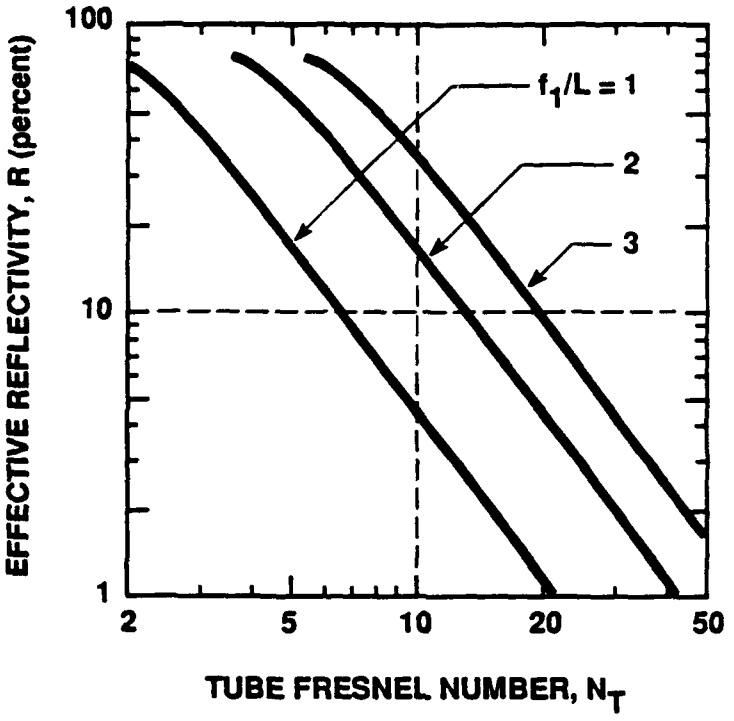
100
10
1
2
5
10
20
50
EFFECTIVE REFLECTIVITY, R (percent)
TUBE FRESNEL NUMBER, N_T
$f_1/L = 1$
2
3

Fig. 2

E

Laser Resonators: Retrospective and Prospective

R. V. Pole Memorial Lecture
1990 Joint CLEO/IQEC Meeting
Anaheim, California
May 1990

A. E. Siegman
Edward L. Ginzton Laboratory
Stanford University

With special thanks to

- CLEO/IQEC organizers
- Jacques Arnaud
- AFOSR
- Many students and colleagues

Laser Resonators: Retrospective and Prospective
(R. V. Pole Memorial Lecture, CLEO/IQEC 90)

Professor A. E. Siegman
Edward L. Ginzton Laboratory
Stanford University, Stanford CA 94305
(415) 723-0222

In the retrospective part of this talk I'd like to take a look backward at the many important and interesting concepts in optical resonators that have evolved since lasers were first developed some three decades ago.

Then in the prospective part I'll take a look forward at some of newer ideas that are now emerging, or that have recently been revitalized, and that are likely to play an important role in the coming decades.

Except in few cases I will not try to identify the people who made all these contributions. Let me apologize in advance to those whom I do not mention, and also to those whose favorite ideas I may have overlooked.

But I would particularly like to Jacques Arnaud who, along with several others, made helpful suggestions for this talk; the Air Force Office of Scientific Research which has supported nearly all of my research in this area over the years; and the many students and other colleagues with whom it has been such a pleasure to work on these resonator ideas over the past several decades.

An overall list of the most important ideas that have been developed in optical resonator theory and practice would surely include all of the following areas:

LASER RESONATORS: RETROSPECTIVE

- **The existence of modes in open-sided resonators**
- **Ray matrices and gaussian beams**
- **Gaussian resonator modes**
- **Generalized paraxial wave optics**
- **Unstable optical resonators**
- **Biorthogonality properties of optical resonators**
- **Frequency-selective and tunable laser cavities**
- **Other beam and resonator ideas**

We'll try to take a more detailed look at some, though not all, of these topics. Let's walk through them quickly, one by one.

Some of the important basic ideas that emerged in the first days of the laser era included the following:

Existence of "Modes" in Open-Sided Resonators

- **The Fabry-Perot laser cavity concept (Schawlow and Townes)**
- **The first Fox and Li recirculating-pulse calculations**
- **Gobau's beam waveguide ideas**
- **The equivalent periodic lensguide viewpoint**
- **Existence of unique resonator eigenmodes and eigenvalues**
- **Existence of low-loss curved-mirror resonators**
- **Importance of the resonator Fresnel number**
- **Transverse modes and transverse mode beats**

The ideas of ray matrices or ABCD matrices, and of gaussian beams and resonators, and of the interconnections between them, have been evolving in tandem ever since:

Ray Matrices and Gaussian Beams

- **Ray matrices (ABCD matrices)**
- **Periodic focusing systems and periodic lensguides**
- **Ray matrix eigenvalues and eigenrays**
- **Stable and unstable periodic focusing systems**
- **Hermite-gaussian optical beams**
- **Gaussian beam propagation rules**
- **The complex radius of curvature or gaussian $\tilde{q}$ parameter**
- **Imaginary source points, the confocal parameter, and the Rayleigh range**
- **Focal phase shifts and the Gouy effect**
- **Gaussian ducts and graded-index (GRIN) rods and lenses**
- **Gaussian mode matching and the Collins chart**
- **Ray matrices and Huygens' integral**

Developing the analytical and experimental understanding of gaussian cavity modes and their application in lasers has been an important part of this subject—and also one of the many areas in which R. V. Pole made fundamental contributions:

Gaussian Resonator Modes

- **Stable and unstable paraxial optical resonators**
- **Hermite-gaussian and Laguerre-gaussian resonator modes**
- **Relationship to periodic focusing systems**
- **The resonator stability diagram**
- **The confocal cavity concept**
  - **Wieder and Pole's conjugate-concentric laser cavity**
  - **Scanning Fabry-Perot interferometers**

In fact, we've now come to understand that not just geomerical optics but essentially all of diffraction optics in the paraxial approximation can be incorporated into a generalized complex-valued ray matrix and paraxial optical formulation of optical beams and resonators:

Generalized Paraxial Wave Optics

- **Gaussian apertures as lenses of imaginary focal length**
- **Complex-valued optical elements and ABCD matrices**
- **Complex-valued paraxial optical systems**
- **Hermite-gaussian functions of complex argument**
- **Complex spot sizes as well as complex $\tilde{q}$ parameters**
- **Generalized paraxial resonator analysis**
  - **Confined and unconfined gaussian modes**
  - **Geometrically stable and unstable gaussian modes**
  - **Perturbation-stable and unstable gaussian modes**
  - **Huygens integral and complex-valued ABCD matrices**

The unstable resonator of course represented a different, complicated, challenging, and very useful area of resonator theory and practice:

Unstable Optical Resonators

- **Stable modes in "unstable" systems...?**
- **Geometrical mode solutions for unstable resonators**
- **Magnifying and demagnifying spherical wave solutions**
- **Positive-branch and negative-branch resonators**
- **Real unstable resonator eigenmodes and eigenvalues**
- **FFT, FHT and Prony computational methods**
- **Mode crossings and the equivalent Fresnel number**
- **Confocal unstable resonators**
- **Self-imaging unstable resonators**
- **Edge waves, and the *Poisson Spot* or *Spot of Arago***
- **The asymptotic approach, or "virtual source" analysis**
- **Self-focusing (SFUR) unstable resonators**

Some of the most interesting aspects of optical resonators arise from the fact that, unlike most physical systems with which we are familiar, laser cavities are generally *not* described by a Hermitian operator, and therefore their resonant modes are *not* orthogonal—especially the modes in unstable optical resonators:

Biorthogonality Properties of Optical Resonators

- **Optical resonator modes are NOT in general power orthogonal**
- **More power in one mode than total power in all modes...?**
- **Matched coupling and adjoint coupling methods**
- **Excess quantum noise in unstable resonator modes**

There are many other intriguing and ingenious ideas related to laser resonators that have also been developed over the years, in order to solve one or another of the practical problems facing the laser designer:

Frequency-Selective and Tunable Laser Cavities

- **Multi-mirror cavities**
- **Michelson, Fox-Smith, and vernier interferometer cavities**
- **Tunable birefringent filters**
- **Prism beam expanders**
- **Etalon mirrors**
- **Sagnac interferometers and antiresonant ring cavities**
- **"Twisted-ribbon" laser cavities**

And still more clever ideas, inventions and concepts that have been applied to less conventional sorts of laser resonators and laser beams:

Other Important Beam and Resonator Ideas

- **Ring laser cavities and optical diodes and isolators**
- **Optical diodes and isolators**
- **Distributed-feedback (DFB) cavity concepts**
- **Distributed Bragg reflector(DBR) cavity mirrors**
- **Waveguide lasers and waveguide laser cavities**
- **Heterojunction diode laser structures**
- **Corner-cube and rooftop resonators**
- **Axicons, waxicons, reflaxicons, HSURIAs, and so-ons**
- **Whispering gallery modes and "droplet" resonators**
- **Pulse compressors, grating and prism dispersive systems**
- **Image relay systems and supergaussian beam profiles**

Just making up the preceding lists of topics, without examining them in detail, shows how far we've come, and how many new and interesting ideas have emerged in the resonator field. And yet the topics mentioned so far do not even include all of the complex aspects of laser oscillation and laser mode dynamics, such as are illustrated by the following topics:

Laser Oscillation and Laser Dynamics

- **Laser gain saturation effects**
- **Mode build-up and mode competition**
- **Spiking and relaxation oscillations**
- **Laser Q-switching**
- **Axial mode coupling and mode-locking**
- **Instabilities and chaotic behavior of laser oscillators**

Nor do these lists include the even more complex world of *nonlinear* optical propagation effects and optical mode behavior, as briefly summarized in the following list:

Nonlinear optical propagation effects

- **Concept of phase matching in nonlinear optics**
- **Self-focusing and trapping**
- **Self-phase-modulation**
- **Optical bistability**
- **Optical phase conjugation**
- **Optical chaos in passive beams and resonators**
- **Solitons**

But now, in the remaining time, let's turn to the "prospective" portion of this talk, and take a look forward at some newer ideas now emerging that will play an important role in coming decades.

Of course, some of these "new" ideas are in fact older ideas that are only now becoming really important in practical laser designs, while others represent ingenious new ideas, developed to solve new problems.

In any event, I believe a broad overview of the ideas now emerging in the laser resonator field would surely include emerging developments in each of the following three areas:

LASER RESONATORS: PROSPECTIVE

- **New kinds of resonators for new kinds of lasers**
- **New developments in diode laser resonators**
- **New design tools and beam diagnostic methods**

Again, let's take a look at each of these topics in more detail.

There are several new kinds of resonators that are now emerging for use in new kinds of laser devices that have great promise for the future. A list of these new resonator concepts might include the following, and I'll try to say a few words about each:

New Kinds of Resonators for New Kinds of Lasers

- **Tapered reflectivity and VRM laser cavities**
  - **Advances in tapered-reflectivity mirror fabrication**
  - **Supergaussian mirrors and mode profiles**
- **Fiber-optic resonators**
  - **Couplers, rings, interferometers, fiber gyros**
- **Miniature and monolithic laser cavities**
  - **Diode-pumped solid-state lasers**
  - **Integrated-optical resonator structures**
  - **"Platelet" laser structures**
- **Nonplanar ring resonators**
  - **Monolithic diode-pumped NPR lasers**
  - **"UR-90" single-sided unstable resonators**
- **Advances in high-power slab laser designs**
- **Coupled lasers and laser oscillator arrays**
- **Advances in FEL resonator designs**

Of course one of the most important and active areas of current laser research is in the burgeoning world of semiconductor diode lasers, where many fascinating new resonator concepts are emerging to meet the special needs and constraints of this class of lasers:

New Developments in Diode Laser Resonators

- **Coupled-stripe diode laser arrays**
- **Antiguidinge (ROW) diode laser stripe arrays**
- **Talbot-plane and Talbot-mirror resonator concepts**
- **Grating-coupled surface-emitting diode lasers**
- **Active on-chip waveguide structures and MOPA chains**
- **Stable-unstable resonator concepts for diode lasers**
- **Vertical-cavity surface-emitting diode laser structures**
- **Etched-facet diode laser mirrors**

Some of the ideas listed above will turn out to be of great practical importance in the future, and I expect some of them will be only of historical interest a few years from now. We'll just have to wait and see, however, which of these ideas fall into which of these categories!

Finally, I'd like to say a few words about three current developments in design tools and diagnostic methods related to laser resonators and beams in which I've been fortunate to have had some involvement:

New Design Tools and Diagnostic Methods

- **New measures for specifying and determining laser beam quality**
- **Resonator analysis and design using personal computers**
- **Ray-pulse matrices for dispersive optical systems**

First of all, after talking for several decades about "laser beam quality" we are finally getting around to developing real instruments that will really measure real laser beam quality. In fact an instrument that does just this in real time will be on display for the first time at this meeting. (It's been developed by Coherent, Inc., if I may be allowed mention of a commercial product.)

At the same time we're developing new ways of defining the quality of an arbitrary laser beam, and making theoretical use of this definition. Part of this is based on still another extension of ABCD matrix theory: new understanding of how the moments of an arbitrary (nongaussian) beam can be propagated through an arbitrary paraxial system, using only the ABCD matrix elements.

I'd also like to mention briefly the development by my students and myself of resonator and optical beam analysis and design programs that can be implemented on desktop personal computers rather than mainframes. We've developed a set of four useful programs for doing laser beam propagation and Fox-and-Li type resonator calculations, unstable resonator design and analysis, and the analysis of complex ABCD matrix systems.

These programs will become available from Stanford University some time later this summer. They run on Macintosh computers, and can do nearly everything that used to be done a decade or more ago on mainframe supercomputers.

Finally I'd like to mention a very general and powerful "ray-pulse matrix" formulation recently developed by one of my students, Ad Kostenbauder. This formulation extends the familiar ray-matrix formalism to include both spatial *and* temporal (or spectral) variations, making it possible to handle both the time and the space dependence of optical beams and pulses in one calculation.

This requires 4×4 rather than just 2×2 matrices, of course, but this approach has already proven extremely valuable for calculations like the propagation of femtosecond pulses in dispersive optical systems and the behavior of dispersive prism and grating beam expanders.

In conclusion, I think one can only be impressed first by the large number of clever and innovative ideas that have been developed in this field over the years, and second by the often remarkable simplicity and elegance of the basic underlying principles that have emerged. It really seems that the most important ideas are often the simple ones, and that nature rewards us with elegance in the most basic ideas.

I think R. V. Pole recognized these principles, and practiced them in his own work, and I'm honored to speak today in his memory.

Looking at the present and the future, one can also still find great vitality in this field, with a set of challenging new problems and, one hopes, still more interesting and elegant ideas yet to come.

I'd like to thank once again the CLEO/IQEC organizers for inviting me to speak, especially Steve Guch who suggested the title for this talk; and the many students and colleagues who've stimulated me and contributed to my work over the years.

And, I'd also like to acknowledge once again the research support from the General Physics division of the Air Force Office of Scientific Research (AFOSR), which has made possible almost all of my own work and that of many others in this field.

F

Defining the Effective Radius of Curvature for a Nonideal Optical Beam

A. E. Siegman

***Abstract*—A simple expression is given for evaluating the effective or average radius of curvature $R(z)$ of an arbitrarily wrinkled, distorted, or nondiffraction-limited optical beam. This real-beam radius of curvature obeys the same free-space propagation equation as does the wavefront curvature of an ideal Gaussian beam; and extracting this "correctable curvature" from the beam at any plane simultaneously collimates the beam, makes that location a waist for the real beam, and minimizes the far-field beam divergence starting from that position.**

CONSIDER a monochromatic optic beam propagating within the paraxial approximation, but suppose that this beam is, in general, neither spherical nor collimated nor diffraction-limited. To say this in another way, the wavefront of the beam across any transverse plane may be wrinkled as well as curved, and the transverse amplitude profile may have complicated and irregular variations as well. What, then, is an appropriate definition for the effective or averaged or "removable" radius of curvature $R(z)$ of this real-beam wavefront at that transverse plane? The purpose of this note is to show how to define an effective radius of curvature $R(z)$ for such a real or nonideal laser beam.

By way of analytical background, let the complex phasor amplitude profile $\tilde{E}(x, z)$ of this beam be specified at a plane $z = z_1$ which is not necessarily coincident with the waist location $z = z_0$ of the beam, as illustrated in Fig. 1. The phasor amplitude $\tilde{E}(x, z)$ of the beam at any plane z can then be related to a complex phasor amplitude $\tilde{P}(s, z)$ which describes the beam in the angular or spatial-frequency domain through the Fourier transform relation

$$\tilde{E}(x, z) = \int_{-\infty}^{\infty} \tilde{P}(s, z) e^{-j2\pi sx}\, ds \tag{1}$$

with $\tilde{P}(s, z)$ given by the reverse transform

$$\tilde{P}(s, z) = \int_{-\infty}^{\infty} \tilde{E}(x, z) e^{+j2\pi sx}\, dx. \tag{2}$$

The spatial frequency variable s is related to the angular direction θ of a corresponding plane-wave component of the beam by $s \equiv \lambda^{-1} \sin\theta$, which becomes $\theta \approx \lambda s$ in the paraxial approximation. The spatial-frequency distribution $\tilde{P}(s, z)$ then propagates in free space according to

$$\tilde{P}(s, z) = \tilde{P}(s, z_1) e^{+j\pi\lambda s^2 (z - z_1)} \tag{3}$$

Manuscript received November 20, 1990. This work was supported by the U.S. Air Force Office of Scientific Research.

The author is with the Edward L. Ginzton Laboratory, Stanford University, Stanford, CA 94305.

IEEE Log Number 9144633.

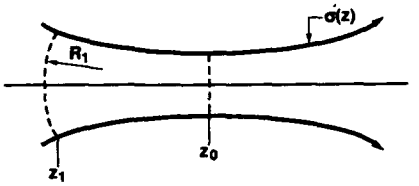

Fig. 1. An arbitrary nondiffraction-limited optical beam propagating outward from an input plane $z = z_1$ towards a waist at $z = z_0$.

which shows that individual components of $\tilde{P}(s, z)$ rotate in phase, but do not change in magnitude with distance z. We also assume for simplicity that $\tilde{E}(x, z)$ is normalized so that $\int_{-\infty}^{\infty} |\tilde{E}(x, z)|^2\, dx = \int_{-\infty}^{\infty} |\tilde{P}(s, z)|^2\, ds = 1$.

It can then be shown that the variance $\sigma^2(z)$ of this real-beam profile in the transverse direction, evaluated using the intensity distribution $|\tilde{E}(x, z)|^2$, will have an axial variation given by

$$\sigma^2(z) = \sigma^2(z_1) - A_1 \times (z - z_1) + \lambda^2 \sigma_s^2 \times (z - z_1)^2 \tag{4}$$

where $\sigma^2(z_1)$ is the spatial variance at the input plane $z = z_1$; σ_s^2 is the variance of the beam in the angular or spatial-frequency domain, evaluated using the spatial-frequency intensity distribution $|\tilde{P}(s, z)|^2$; and A_1 is the value of the function

$$A(z) \equiv -j \frac{\lambda}{2\pi} \int_{-\infty}^{\infty} s \left[\tilde{P}(s, z) \frac{\partial \tilde{P}^*(s, z)}{\partial s} - \tilde{P}^*(s, z) \frac{\partial \tilde{P}(s, z)}{\partial s} \right] ds \tag{5}$$

evaluated at $z = z_1$. The Fourier transform relations between $\tilde{E}(x, z)$ and $\tilde{P}(s, z)$ imply that there will be corresponding Fourier transform relations between the quantities $\partial\tilde{E}(x, z)/\partial x$ and $-j2\pi s\tilde{P}(s, z)$, and also between the quantities $xE(x, z)$ and $-(j/2\pi)\, \partial P(s, z)/\partial s$. If these Fourier transform relations are substituted into (5), the function $A(z)$ can also be written as

$$A(z) = +j \frac{\lambda}{2\pi} \int_{-\infty}^{\infty} x \left[\tilde{E}(x, z) \frac{\partial \tilde{E}^*(x, z)}{\partial x} - \tilde{E}^*(x, z) \frac{\partial \tilde{E}(x, z)}{\partial x} \right] dx \tag{6}$$

with A_1 again being this function evaluated at $z = z_1$.

The axial variation of $\sigma^2(z)$ in (4) can be rewritten as an expansion about a waist location $z = z_0$ in the form [1], [2]

0018-9197/91/0500-1146$01.00 © 1991 IEEE

$$\sigma^2(z) = \sigma_0^2 \times \left[1 + \left(\frac{z - z_0}{z_R}\right)^2\right] \tag{7}$$

where σ_0^2 is the minimum value of the spatial variance at the real-beam waist, given by $\sigma_0^2 = \sigma^2(z_1) - A_1^2/4\lambda^2\sigma_s^2$, and z_0 is the waist location which is related to z_1 by $z_0 = z_1 + A_1/2\lambda^2\sigma_s^2$. It is also convenient to introduce a beam quality factor [2], [3] which is related to the space-beam-width product $\sigma_0\sigma_s$ for the real beam by $M^2 = 4\pi\sigma_0\sigma_s$. This quality factor has the property that $M^2 \geq 1$ for any real beam, reducing to the limiting value $M^2 \equiv 1$ only for an ideal TEM_{00} Gaussian beam. Equating the quadratic terms in (3) and (7) then gives a formula for the Rayleigh range z_R of the real beam, namely,

$$z_R = \frac{4\pi\sigma_0^2}{M^2\lambda}. \tag{8}$$

This is the same as the formula for the Rayleigh range of an ideal TEM_{00} Gaussian beam with waist variance σ_0, which is $z_R = \pi w_0^2/\lambda = 4\pi\sigma_0^2/\lambda$, except that the Rayleigh range z_R for a real nonideal beam is reduced by the factor $M^2 \geq 1$. Equation (7) confirms that any arbitrary real beam always has a waist, with a spot size or variance which varies quadratically on either side of the waist just like an ideal Gaussian beam, except that the Rayleigh range for the real beam is reduced by the beam quality factor M^2.

A general expression for the effective radius of curvature $R(z)$ of any real-beam wavefront at any arbitrary plane z can then be written as

$$\frac{1}{R(z)} \equiv \frac{-A(z)}{2\sigma^2(z)} \tag{9}$$

where $A(z)$ can be evaluated using either (5) or (6). This expression may not be entirely new. Essentially this same formula was used on an empirical basis as a way of extracting the macroscopic wavefront curvature in early numerical beam propagation calculations [4], and the same formula has also arisen in recent work by Belanger [5]. The primary objective of this note, in light of current discussions of laser beam quality and laser beam laser beam propagation, is to reiterate the usefulness of (9) as the basic definition of effective wavefront curvature, and to point out three or four different ways in which this definition is physically meaningful as an effective radius of curvature.

The physical significance of the definition of $R(z)$ given in (9) can be demonstrated first of all by noting that this definition, together with the other equations above, leads to the free-space propagation law

$$R(z) = (z - z_0) + \frac{z_R^2}{(z - z_0)} \tag{10}$$

where z_R is the same real-beam Rayleigh range as in (9). In other words, with the use of the real-beam Rayleigh range, both the real-beam variance $\sigma^2(z)$ from (7) and the real-beam effective radius $R(z)$ from (9) obey exactly the same free-space propagation rules as do the corresponding quantities for an ideal Gaussian beam.

Another way of arriving at the curvature definition in (9) is to ask what is the radius of curvature $R(z)$ for a real-beam wavefront at any plane z which, when extracted from the input phasor amplitude $\tilde{E}(x, z)$ at this plane, will make the modified wavefront at this plane be a waist, which means, in turn, that the modified value of $A(z)$ after this extraction should be zero. This would seem to be a meaningful way of defining an effective radius of curvature for the real beam since it determines what radius of curvature has to be extracted from the real wave using an appropriate thin lens to convert it into a collimated beam waist. To determine this removable curvature, we can suppose that the input wave $\tilde{E}(x, z)$ at plane z is passed through a thin lens of focal length f so that the beam wavefront is transformed to

$$\tilde{E}'(x, z) = \tilde{E}(x, z) \times \exp\left[+j\frac{\pi x^2}{f\lambda}\right] \tag{11}$$

where $\tilde{E}'(x, z)$ is the collimated (although potentially still wrinkled) phasor amplitude for the wave that will be left after the effective curvature has been removed using the lens of focal length f. This is sometimes referred to as removing the "correctable divergence" of the beam at the plane z. The modified value of the integral $A(z)$ after this curvature-extraction process will be given by

$$A'(z) = -j\frac{\lambda}{2\pi}\int_{-\infty}^{\infty} x\left[\tilde{E}'\frac{\partial\tilde{E}'^*}{\partial x} - \tilde{E}'^*\frac{\partial\tilde{E}'}{\partial x}\right]dx$$

$$= A(z) + \frac{2\sigma^2(z)}{f}. \tag{12}$$

Requiring that $A'(z) = 0$ after the lens then gives

$$\frac{1}{f} = \frac{1}{R(z)} = \frac{-A(z)}{2\sigma^2(z)} \tag{13}$$

exactly as expected.

As another approach to the definition of effective curvature, we can note from (4) that the far-field angular spread of an arbitrary beam is directly proportional to the spatial-frequency standard deviation σ_s. The effective radius of curvature for an arbitrary wavefront would then seem to be that radius which, if extracted from the wavefront using a thin lens as above, will minimize the resulting value of σ_s^2. From standard Fourier transform identities, the value of σ_s^2 can be calculated using either of the expressions

$$\sigma_s^2 = \int_{-\infty}^{\infty} s^2|\tilde{P}(s, z)|^2\,ds = \left(\frac{1}{2\pi}\right)^2\int_{-\infty}^{\infty}\left|\frac{\partial\tilde{E}(x, z)}{\partial x}\right|^2 dx. \tag{14}$$

Let the complex wavefront $\tilde{E}(x, z)$ at plane z again be passed through a lens of focal length f so that the wavefront is modified as in (11). Putting this modified wavefront into the last integral in (14) shows that σ_s^2 after the

lens is modified to

$$\sigma_s'^2 = \sigma_s^2 + \frac{A(z)}{f\lambda^2} + \frac{\sigma^2(z)}{f^2\lambda^2}. \quad (15)$$

The value of f which minimizes σ_s' is then exactly the same as in (13).

Finally, we can note that if the complex phasor amplitude of the beam is separated into amplitude and phase functions in the form

$$\tilde{E}(x, z) \equiv |\tilde{E}(x, z)| \exp[-j\phi(x, z)] \quad (16)$$

then the general definition of (9) can be written as

$$\frac{1}{R(z)} = \frac{-\lambda}{2\pi\sigma^2(z)} \int_{-\infty}^{\infty} \left(x \frac{\partial\phi(x, z)}{\partial x} \right) |\tilde{E}(x, z)|^2 \, dx. \quad (17)$$

This says that $1/R(z)$ represents a weighted average of the wavefront curvature term $[x\, \partial\phi(x, z)/\partial x]$ across the wavefront, which is physically reasonable. Inserting the purely spherical form $\phi(x, z) = \pi x^2/R(z)\lambda$ will confirm that the integral in (17) converges to the expected value $R(z)$.

To recapitulate, we have shown that any real or nonideal laser beam with a wrinkled or nonspherical wavefront will have an effective radius of curvature $R(z)$ given at any arbitrary plane z by the expression in (9). The axial variation of this effective radius $R(z)$ is then given rigorously by the Gaussian-beam-like formula of (10). Extracting this curvature from the wavefront at any plane both converts the beam profile to a waist at that plane and minimizes the far-field spread of the beam starting from that plane. The close identification between the propagation formulas for the real-beam values of $\sigma^2(z)$ and $R(z)$ given in (7) and (10) and the corresponding formulas for an ideal TEM_{00} Gaussian beam is both remarkable and useful.

As a final note, we can observe from (15) above that once the average phase curvature $R(z)$ has been extracted from the wavefront at any plane z, the resulting value of σ_s^2 after the lens becomes the minimum value for that plane given by

$$\sigma_{s,\min}^2(z) = \sigma_s^2(z) - \left(\frac{\sigma(z)}{R(z)\lambda} \right)^2. \quad (18)$$

But this says that the total far-field divergence of the beam before the curvature is extracted can be written as

$$\sigma_s^2(z) = \sigma_{s,\min}^2(z) + \left(\frac{\sigma(z)}{R(z)\lambda} \right)^2. \quad (19)$$

In other words, the far-field angular beam spread σ_s of an arbitrary beam at any plane z can be viewed as the rms combination of a correctable or removable portion $\sigma(z)/\lambda R(z)$, which is proportional to the average wavefront curvature $1/R(z)$, plus an irreducible portion $\sigma_{s,\min}(z)$ which cannot be removed with any simple focusing element. A direct analog to this far-field expression which applies instead to the time duration and the spectral bandwidth of chirped pulse signals in time was pointed out some time ago by Pohlig [6].

References

[1] M. R. Teague, "Irradiance moments: Their propagation and use for unique retrieval of phase," *J. Opt. Soc. Amer.*, vol. 72, pp. 1199-1209, 1982.

[2] A. E. Siegman, "New developments in laser resonators," in *Laser Resonators*, D. A. Holmes, Ed., *Proc. SPIE*, vol. 1224, pp. 2-14, 1990.

[3] A. E. Siegman, M. W. Sasnett, and T. F. Johnston, Jr., "Defining and measuring laser beam quality: The M^2 factor," in preparation.

[4] E. A. Sziklas, United Technol. Res. Lab., East Hartford, CT, and K. E. Oughstun, Univ. Vermont, Burlington, private communications.

[5] P. A. Belanger, "Beam propagation and the ABCD ray matrices," *Opt. Lett.*, to be published.

[6] S. C. Pohlig, "Signal duration and the Fourier transform," *Proc. IEEE*, vol. 68, pp. 629-630, 1980.

Choice of Clip Levels for Beam Width Measurements Using Knife-Edge Techniques

Anthony E. Siegman, *Fellow, IEEE*, M. W. Sasnett, and T. F. Johnston, Jr.

***Abstract*—The scanning knife-edge technique provides one of the better methods for measuring the width of an optical beam having an arbitrary or irregular transverse profile. To implement this method, however, one must select both a clip level and a scale factor for converting the measured clip width into an effective width of the laser beam. We show that the preferred clip level for beam width measurements using this technique should be chosen in the range between $\epsilon \approx 8.5\%$ and $\epsilon \approx 11.6\%$. With a suitably matched clip level and scale factor within this range, the conversion from measured clip width to standard deviation can be made exactly accurate for TEM_{00} Gaussian beams, and the conversion factor will become only slightly inaccurate for a wide range of other higher-order or poorer-quality beam profiles.**

I. Introduction

DETERMINING the spot size of a laser beam, whether in the near- or far-field region is a fundamental problem in laser diagnostics. The transverse profiles of real laser beams are sometimes very irregular in shape, displaying multiple peaks and lacking clearly defined edges. Even defining the width of a laser beam in a meaningful way can be difficult for an aberrated or multimode laser beam with an irregular intensity profile, let alone measuring this width experimentally.

One precisely defined width parameter that is of fundamental significance for any laser beam is the standard deviation σ_x evaluated in the x transverse direction over the beam intensity profile. The variances σ_x^2 and σ_y^2 evaluated in two transverse directions across an optical beam profile play a particularly significant role in theoretical beam propagation analysis and in definitions of laser beam quality. Making a direct measurement of the standard deviations σ_x and σ_y for a real beam profile can be difficult in practice, however, since this requires first an accurate measurement of the two-dimensional intensity profile $I(x, y)$ and then accurate calculation of the first and second moments of this profile.

A much simpler and more widely used measurement technique is the scanning knife-edge method. In this method, one scans an opaque knife edge transversely across the beam profile in, say, the x transverse direction while detecting the transmitted intensity reaching a large-area photodetector as the knife edge opens up the beam. The first derivative of this detected intensity versus scan position x gives an indication of the beam intensity profile in the x direction, integrated over the y direction.

Although the complete knife-edge profile contains useful information, in many cases one wants only a single number to characterize the effective size of the beam in each of the x and y directions. In this case, one can use the "clip width" of the beam measured in each of the two transverse dimensions. The clip width D_c for the beam in either direction is defined as the width between points in the scan where the transmitted intensity passing the knife edge rises from a lower clip level ϵP_0 to an upper clip level $(1 - \epsilon)P_0$ where P_0 is the total power in the beam. Clip levels in the range around 10% and 90% are often used.

Selecting an optimum clip width and an associated scale factor for such knife-edge measurements is the primary topic of this paper. We show that 1) there is an unavoidable error or uncertainty in converting such clip width measurements into more theoretically significant measures such as the standard deviation of the beam in the same direction; and 2) any clip level ϵ in the range between about 8.5% and 11.6%, together with a scale factor based on an ideal TEM_{00} Gaussian beam, can be about equally valid as a standard definition for knife-edge measurements on a wide variety of real laser beams.

II. Clip Level and Scale Factor Selection

A. Scale Factor Errors in Clip Level Measurements

The clip width D_c for any specific beam, measured using a specified clip level ϵ, is of course a definite and fairly easily measured quantity. The standard deviation σ_x of the beam in the knife-edge scanning direction, which is a quantity of more theoretical significance, can then be estimated from the measured clip width using a suitable scaling factor S such that $\sigma_x = D_c/S$. There is, however, an unavoidable uncertainty in going from measured clip width to the more fundamental standard deviation in this fashion. The exact scale factor or the exact value of the ratio D_c/σ_x for an arbitrary beam will depend not only on the clip level employed but also to a certain extent on the exact shape of the laser beam.

Manuscript received September 10, 1990. The work of A. E. Siegman was supported by the Air Force Office of Scientific Research.

A. E. Siegman is with Stanford University, Stanford, CA 94305.
M. W. Sasnett is with Coherent, Inc., Palo Alto, CA.
T. F. Johnston, Jr., is with Coherent, Inc., Auburn, CA.

IEEE Log Number 9144338.

To put this in another way, different beams having the same standard deviation σ_x will give slightly different measured clip widths D_c depending on the exact profile and modal content of the beam, which is assumed to be unknown. Hence, there will always be some uncertainty in the scale factor S that should be used to transform from the measured clip width D_c to the more theoretically interesting value σ_x. In practice, one selects the scaling factor S to match the calculated value D_c/σ_x for some standard beam profile, preferably a TEM_{00} Gaussian profile. This scale factor will then, in general, exhibit some error when applied to other beam profiles. Our primary objective in this paper is to show how to estimate and minimize these errors for a wide range of real beam profiles, by examining the theoretical clip level versus clip width curves for a representative sample of different beam profiles.

B. Low-Order Gaussian Beams

Fig. 1 shows by way of example the fractional power falling outside a given clip width D_c on one side of the beam only (which is the same thing as the clip level ϵ) for several different Hermite-Gaussian (HG) or Laguerre-Gaussian (LG) optical beam profiles. The fractional power in each case is plotted versus the clip width D_c normalized to the standard deviation σ_x for that specific beam. The four mode profiles considered in this figure are: 1) the lowest-order or $n = 0$ Hermite-Gaussian mode, which corresponds also to a TEM_{00} mode in two transverse dimensions; 2) the first antisymmetric or $n = 1$ HG mode, which would correspond to a TEM_{10} but not an TEM_{01} HG mode in two transverse dimensions; 3) the "donut" mode, or Laguerre-Gaussian TEM_{01}^{*} mode, which often appears as a perturbation in stable-resonator laser oscillators, and which corresponds also to an incoherent superposition of TEM_{10} and TEM_{01} HG modes; and finally 4) an annular ring mode which represents an asymptotic approximation for a very high-order HG mode, as discussed below. Note again that the horizontal axis in each case is scaled to the standard deviation σ_x of each given mode, and not to a common Gaussian spot size w characterizing the family of modes.

The dashed lines on this plot show that if one selects, for example, a clip level $\epsilon = 11.59\%$ and a scale factor $S = 2.392$, knife-edge measurements using these parameters will yield exactly accurate values of σ_x for beams consisting of either pure TEM_{00} or pure HG $n = 1$ (although not, in general, for mixtures of these two modes). Using this same clip level and scale factor for the other modes shown will slightly underestimate the scale factor or overestimate the value of σ_x, with an error in the range of 5–10%, because the scale factor S will be slightly different than the exact D_c/σ_x values for these modes at this selected clip level. (Note again that in a simple automated knife-edge measurement, only the clip level ϵ and clip width D_c will be directly determined, and one will in general have no direct knowledge of the exact beam profile being measured.)

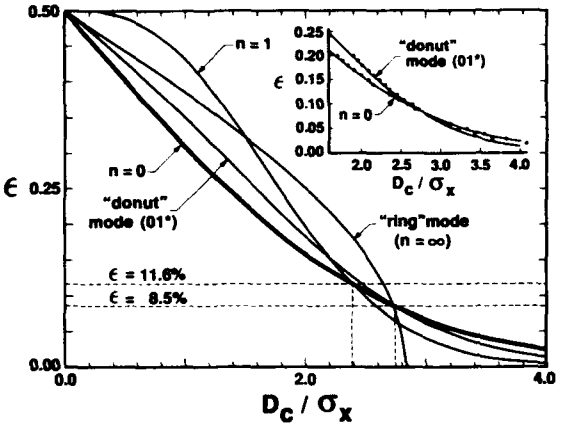

Fig. 1. Fractional power falling outside a given clip width D_c on one side plotted versus D_c/σ_x for several low-order Hermite-Gaussian modes. Shown in this figure are the two lower-order Hermite-Gaussian modes $n = 0$ and $n = 1$; the donut mode (incoherent mixture of TEM_{10} and TEM_{01}); a ring mode which corresponds to the asymptotic Hermite-Gaussian case with $n \to \infty$; and two suggested clip levels at $\epsilon = 8.5\%$ and $\epsilon = 11.6\%$. The insert shows experimental data for the TEM_{00} and donut modes measured on the same argon-ion laser using a knife-edge system with an adjustable clip level.

From this figure it appears that a useful alternative choice could be to select a clip level $\epsilon = 8.485\%$ and a scale factor $S = 2.746$. This choice would give exact results for both the TEM_{00} mode and the donut mode, with scale-factor errors of plus or minus a few percent for the other modes shown. As an experimental confirmation of this point, the smaller plot in Fig. 1 displays clip widths measured on the same argon-ion laser beam under two different operating conditions, using a scanning knife-edge system with an electronically adjustable clip level. In one case, the laser was operated in a TEM_{00} mode as determined by a suitable intracavity mode-control aperture. In the other case, a Brewster plate with a small defect burned into one spot on the plate was positioned within the ion laser cavity so as to force oscillation in the donut mode within the same cavity mirrors. Single-transverse-mode operation was confirmed in each case by the absence of any transverse mode beats. The measured clip widths in the two cases were then scaled to the appropriate standard deviations σ_x assuming a common Gaussian spot size parameter w for the two modes in the same resonator, with w being measured on the TEM_{00} mode. The measured clip level curves intersect at almost exactly 8.5% as predicted, and this intersection occurs at a D_c/σ_x ratio of 2.75 as also predicted by the theory.

Either of the two clip levels $\epsilon = 8.5\%$ or $\epsilon = 11.65\%$ might be regarded as "natural" choices, at least for beams made up of HG mode mixtures. We will show more generally, however, that any choice of clip level between these two extremes will give a very similar range of errors for a very wide range of optical beam profiles, whether Hermite-Gaussian in character or not.

C. Higher-Order Hermite-Gaussian Beams

Fig. 2 shows curves of the same structure as Fig. 1 with the donut mode removed for simplicity and with higher-

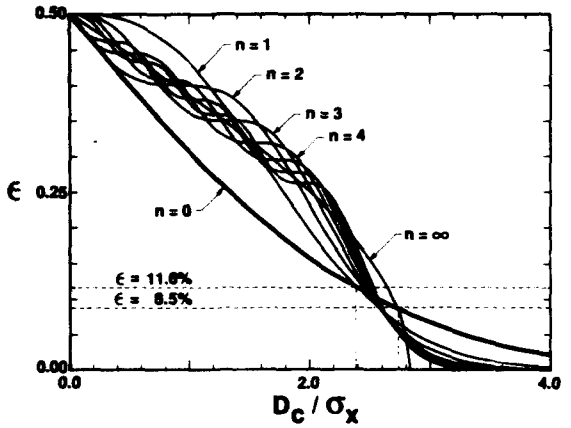

Fig. 2. Clip level plot similar to Fig. 1 with the donut mode removed and higher-order HG modes from $n = 2$ to $n = 7$ added.

order Hermite-Gaussian modes with indexes from $n = 2$ up to $n = 7$ added. From this figure it is evident from the curves for the higher-order HG modes oscillate in a regular fashion about the "ring mode" or asymptotic HG $n \rightarrow \infty$ curve introduced in Fig. 1. This behavior can be understood as follows.

The one-dimensional intensity profiles for higher-order Hermite-Gaussian beams have the general form $I_n(x) = H_n^2(\sqrt{2}x/w) \exp(-2x^2/w^2)$, with standard deviation $\sigma_x = \sqrt{2n+1}\,w/2$. The Hermite-Gaussian intensity profile for the specific case $n = 10$ is shown by the solid line in Fig. 3. But this mode profile is also the well-known quantum probability distribution for a one-dimensional quantum harmonic oscillator. As many quantum theory texts point out, when the mode index n becomes large, these Hermite-Gaussian profiles with the high-frequency periodic variation averaged out approach the one-dimensional probability distribution for a classical particle executing sinusoidal harmonic motion in one dimension. The latter distribution has the normalized form

$$\lim_{n\to\infty} I_n(x) \approx I_\infty(x) = \frac{1}{\pi}\sqrt{\frac{1}{x_\infty^2 - x^2}}, \qquad -x_\infty \le x \le x_\infty \tag{1}$$

with the outer width and the standard deviation being related by $x_\infty = \sqrt{2}\,\sigma_x$. This limiting profile is indicated by the dashed line in Fig. 4.

But a classical particle oscillating sinusoidally in one transverse dimension has the same probability distribution with respect to that dimension as does a particle traveling at constant velocity around a circular orbit in two transverse dimensions. As a result, the asymptotic one-dimensional intensity distribution for HG modes as $n \rightarrow \infty$ also represents equally well the one-dimensional distribution for an infinitely thin annular "ring" beam with equal intensity around the annulus.

D. Other Elementary Beam Profiles

The focus on Hermite-Gaussian modes in Figs. 1 and 2 may merit further discussion. The mode patterns for real

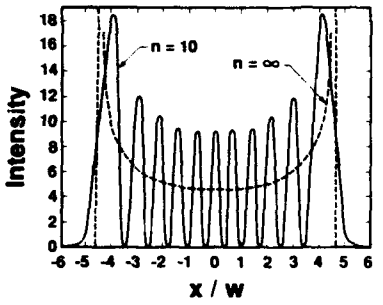

Fig. 3. Intensity profile $I_n(x)$ for the Hermite-Gaussian mode with $n = 10$ (solid line), and the asymptotic form of this profile for $n \rightarrow \infty$ (dashed line).

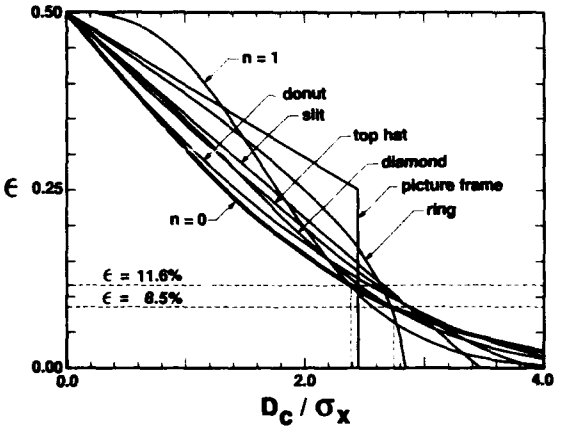

Fig. 4. Clip level plot similar to Fig. 1 with various other simple beam profiles added.

laser beams will in many cases not be single Hermite-Gaussian or Laguerre-Gaussian modes, but rather may have a variety of more complex forms. These more complex profiles can nonetheless be viewed, if one wishes, as either coherent or incoherent superpositions of Hermite-Gaussian modes (other basis sets could of course be used equally as well). Our assumption is that if one uses a measurement procedure that is demonstrably accurate for the limiting case of an $n = 0$ Hermite-Gaussian beam, and that has a small and bounded error for all higher-order Hermite-Gaussian modes, then this procedure 1) will be most accurate for the most important case, namely, low-order and thus high-quality beam profiles; and 2) it may have only small and well-understood inaccuracies for arbitrary beams, which can always be described as mixtures of higher-order Hermite-Gaussian modes. The latter assumption is, unfortunately, not entirely correct, as we will demonstrate in the following.

To supplement the HG and LG examples of Figs. 1 and 2, several other elementary beam profiles including uniform top hat and uniform rectangular beams, and diamond-shaped and "picture-frame" beam profiles, have been plotted in Fig. 4 along with the same low-order Gaussian beams as in Fig. 1. The picture-frame mode, representing a beam profile in the form of a very thin square annulus, is something of an "odd man out" in this plot, with a clip level that jumps instantaneously from 0

to 25% at the point where the knife edge encounters the flat edge of the picture frame.

Fig. 5 shows an expanded view of the clip level region between $\epsilon = 7\%$ and $\epsilon = 13\%$ with all the curves shown in Figs 1–4 included. Three potential clip levels and scale factors are also indicated, namely, the clip level at 11.6% where the TEM_{00} and HG $n = 1$ modes will have equal D_c/σ_x values; the clip level at 8.5% where the TEM_{00} and the donut modes will have equal D_c/σ_x values; and a compromise value arbitrarily located at the 10% clip level. The sum total of the results in Figs. 1–5 give a reasonable (although unfortunately not complete) indication of the spread in scale factors that might be encountered for real laser beams in practice. The middle choice $\epsilon = 10\%$ might represent a reasonable compromise between the two outer values, with a range of scale factors which remains small for low-order Hermite-Gaussians and is distributed more or less symmetrically about the TEM_{00} scale factor.

In all of these cases, we chose a scale factor S which will be exactly correct for a TEM_{00} Gaussian beam. This is done for two reasons. First, in real lasers using stable resonators and having good beam quality, the output mode will often be very close to a TEM_{00} beam; to get the most accurate results in this case, one should select a scale factor which applies to that beam. Second, in the more general case of more irregular beam profiles, the "beam quality" for an arbitrary beam is most often defined in a manner which uses the TEM_{00} beam as a reference standard. Beam quality measurements using the TEM_{00} scale factor will therefore become most accurate in the important limit of good quality beams, and the unavoidable uncertainty in the scale factor will only show up in the less important case of poorer quality beams.

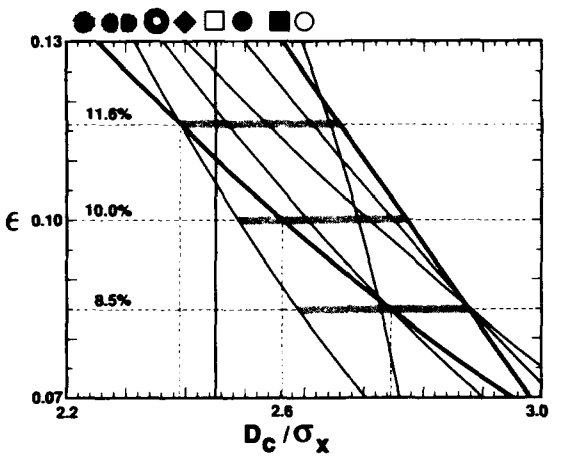

(a)

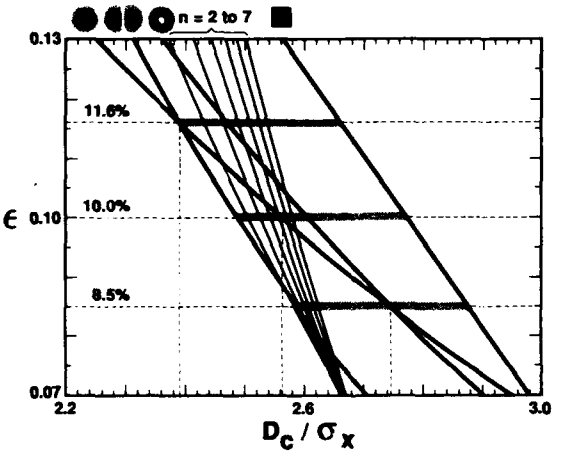

(b)

Fig. 5. Expanded views of selected clip level curves from Figs. 1–5 over the range $\epsilon = 7\%$ to $\epsilon = 13\%$. Three suggested clip levels and the associated scale factors for the TEM_{00} mode are indicated.

E. Pedestal Beams

Despite the reasonable range of error values indicated by Figs. 1–5, one should be aware that there can always be extreme beam profiles having very different values of D_c/σ_x, both higher and lower, than the ranges indicated for a given choice of clip level in Figs. 1–5. Consider, for example, a beam profile consisting of two outer spikes or delta functions located at $x = \pm Ma$ with $M > 1$, each containing just under ϵ of the total beam power, and two spikes at $x = \pm a$ each containing $0.5 - \epsilon$ of the beam power. The normalized clip width for chip level ϵ in this case will be $D_c/\sigma_x = 2/\sqrt{1 + 2(M^2 - 1)\epsilon}$, which can be made as small as desired for $M >> 1$. Alternatively, consider a beam profile with two outer spikes at $x = \pm a$ containing just over ϵ of the total power each, with all the remaining energy in a narrow spike at $x = 0$. The normalized clip width in this case will be given by $D_c/\sigma_x \approx 1/\epsilon$, which will be much larger than any of the values shown in Figs. 1–5.

Another bothersome case is the simple example of the far-field pattern of a single slit, which has the general form (at least in the elementary paraxial approximation) of $I(x) = \sin^2 x/x^2$. The problem in this case is that, because of the very slow $1/x^2$ falloff of this profile at large x, the value of σ_x actually diverges logarithmically. Hence, the value of D_c/σ_x cannot even be defined without putting in some truncation of the $\sin^2 x/x^2$ function at some large but finite value of X.

Still another not uncommon example would be a "pedestal beam," which might be modeled as consisting of a TEM_{00} Gaussian primary beam with a Gaussian spot size w_1 containing a fraction $1 - \alpha$ of the total power, superimposed on a "pedestal" modeled as a second TEM_{00} beam with a spot size w_2 containing the remaining α of the total beam power. High-power laser oscillators will sometimes produce beams of this general character, with a central beam lobe of rather good quality containing some fraction of the total beam power, surrounded by a broad low pedestal containing the remaining power. (Such beams are in fact of quite poor beam quality, despite their well-formed central lobe.)

Figs. 6 and 7 show clip level plots for a series of such pedestal beams: first for a fixed pedestal width ratio $M \equiv w_2/w_1$ and varying fractional power α, and then for fixed

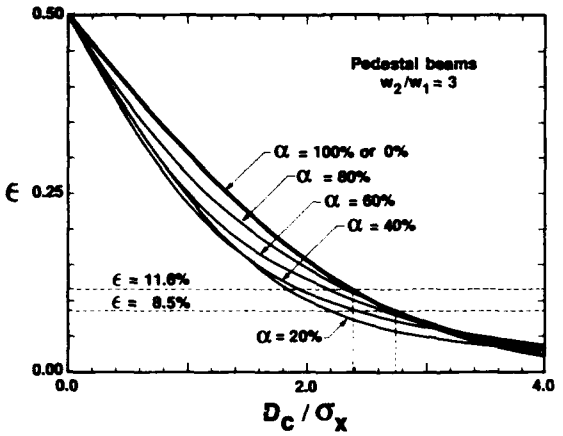

Fig. 6. Clip level plot similar to Figs. 1, 2, and 4 for a "pedestal" beam in which the pedestal Gaussian is $M = 3$ times wider than the central Gaussian, with varying fractions $\alpha = 20$, 40, 60, and 80% of the total beam power in the pedestal.

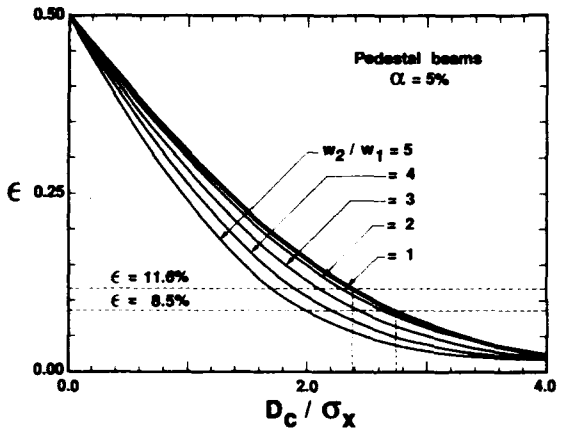

Fig. 7. Clip level curves for pedestal beams with 5% of the total beam power in the pedestal, with the pedestal Gaussian being a varying factor $M = 2$, 3, 4, and 5 times wider than the central Gaussian.

pedestal power α and varying width ratio M. The general conclusion is that over most of the clip level range, these beams have a D_c/σ_x ratio that falls below the TEM_{00} value; and the scale factor errors in measuring these beams can become quite sizable for wide pedestals or pedestals that contain any significant fraction of the total power. There is probably no simple way around this difficulty, except the practical answer of using a spatial filter in the real laser beam to eliminate most of the pedestal, and then measuring the remaining output beam after the spatial filter. In any event, the scale factor error for a pedestal beam becomes sizable only for rather poor quality beams.

F. Mixed-Mode Gaussian Beams

Finally, one might guess that if a clip level is chosen at which two different HG modes have the same scale factors (as at $\epsilon = 11.6$ or 8.5%), then an incoherent mixture of these two modes might have the same D_c/σ_x value also. This turns out to be nearly but not exactly true. If one

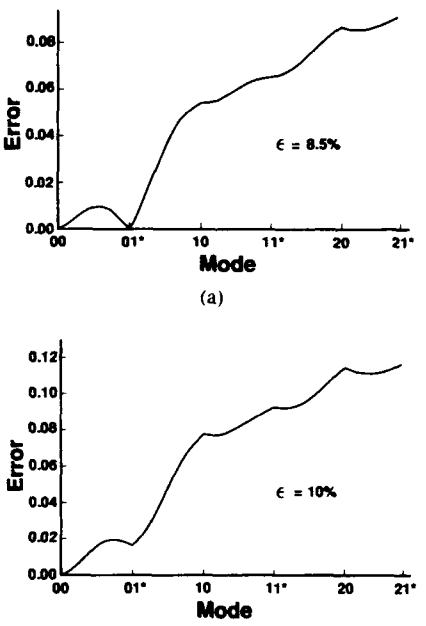

Fig. 8. Fractional changes in the clip width to standard deviation ratio D_c/σ_x versus fractional mode mixture for incoherent superpositions of Laguerre-Gaussian modes. Results are shown for clip levels (a) $\epsilon = 8.5\%$ (where the 00 and 01* modes have the same scale factor) and (b) $\epsilon = 10.0\%$. In each segment of the plots, the beam profile is an incoherent mixture of the two adjacent Laguerre-Gaussian mode profiles, with the fractional percentage varying linearly along the horizontal axis as one moves from one mode pattern to the next.

considers a beam profile consisting of an incoherent mixture of two modes with varying fractions of each mode, the clip width and the standard deviation for the mixed mode will both change in a slightly different manner as the mixture ratio is changed; and the D_c/σ_x ratio will also change slightly even if it returns to the same value at both end points. To illustrate this point, Fig. 8(a) and (b) shows the fractional change in the D_c/σ_x ratio, relative to the TEM_{00} Gaussian mode, for various incoherent binary mixtures of modes at the two different clip levels $\epsilon = 11.6\%$ and $\epsilon = 10\%$. In each segment of these plots, the beam profile is assumed to be an incoherent mixture of the two adjacent HG mode profiles, with the fractional percentage of each mode varying linearly as one moves from one intersection point to the next. The general conclusion is that there is a small variation of the D_c/σ_x ratio with mode mixture ratio, even when the endpoints have the same limiting value. This variation is in general so small, however, that it will have negligible importance in affecting the accuracy of any practical measurement.

III. Summary

The curves in Figs. 1–8 should give a good indication of the variation in D_c/σ_x likely to be encountered with real laser beams, and thus provide guidance in selecting a clip level for standardized knife-edge measurements. The primary conclusion of this paper is that any clip level in the range between $\epsilon \approx 8.5\%$ and $\epsilon \approx 11.6\%$ could be

about equally useful as a standard value for knife-edge beam-width measurements. The exact clip level can be chosen based on other considerations such as numerical simplicity or experimental convenience. Smaller clip levels are probably less convenient experimentally, from considerations of noise and detector sensitivity. Hence, either $\epsilon = 10\%$ with a scale factor = 2.563, or $\epsilon = 11.6\%$ with a scale factor $D_c/\sigma_x = 2.39$ might be equally useful.

The scale factor D_c/σ_x to be used for converting measured clip widths D_c into (approximate) values of σ_x for real laser beams should, in any case, be the value appropriate a TEM_{00} Gaussian beam. Proposals have been made by some standards groups to define the half-width W_x in the x-direction for a real laser beam to be $W_x \equiv 2\sigma_x$. This half-width quantity for real laser beams would then match up directly with the $1/e^2$ half-width parameter or Gaussian spot size parameter $w_x \equiv 2\sigma_x$ that is widely used for TEM_{00} Gaussian beams. If this proposal were adopted, and if the 10–90% choice were also adopted as a standard for the clip level ϵ, then the measured full width $D \equiv 2W$ for a laser beam would be related to the measured clip width by

$$D = 2W = \frac{4D_c}{2.563} = 1.561D_c.$$

We note again that in making a measurement, one will usually not know the modal content of the beam, so that one can only measure the clip width at a predetermined clip level and then apply the predetermined scale factor to obtain an estimated value of the standard deviation or other selected beam size parameter. Since at least some real lasers approach pure TEM_{00} behavior, often with small amounts of TEM_{01} or TEM_{10} mixed in, this approach will become exactly correct in the TEM_{00} limit. Measurements using this approach will then become gradually less accurate for higher-order or poorer-quality beams, depending upon the exact beam profile.

There will always be extreme beam profiles for which the error in converting from clip width to standard deviation can become rather large. There appears to be no easy way around this problem. One can, of course, gain a substantial amount of additional information by using the knife-edge technique to record the complete profile of transmitted intensity versus position, and then using this information to determine the character of the mode profile more accurately. But this requires considerably more data handling and recording than the simple procedure of recording a single clip width D_c at a single standardized clip level ϵ.

Appendix A
Clip Level Forumulas

The analytical clip level formulas for the modes discussed in this paper are summarized in this Appendix.

Given an arbitrary transverse intensity profile $I(x, y)$, the total beam profile P_0 and the standard deviation σ_x in the x-direction for an optical beam are given by

$$P_0 = \int_{-\infty}^{\infty}\int_{\infty} I(x, y)\, dx\, dy \quad \text{and}$$

$$\sigma_x^2 = \int_{-\infty}^{\infty}\int_{\infty} x^2 I(x, y)\, dx\, dy. \tag{2}$$

The clip width in the x-direction for a given clip level ϵ will then be given by $D_c = a_2 - a_1$, where a_1 and a_2 are the points at which

$$\int_{-\infty}^{a_1} dx \int_{\infty}^{\infty} dy\, I(x, y) = \epsilon P_0 \quad \text{and}$$

$$\int_{-\infty}^{a_2} dx \int_{\infty}^{\infty} dy\, I(x, y) = (1 - \epsilon)P_0. \tag{3}$$

If we consider only symmetric beam profiles for simplicity, then $a_1 = a_2 = D_c/2$ and the clip level ϵ can be related to the clip width D_c by

$$\epsilon = \tfrac{1}{2}\left[1 - \int_{-D_c/2}^{D_c/2} dx \int_{\infty}^{\infty} dy\, I(x, y)\right]. \tag{4}$$

The knife-edge method of course automatically integrates over the y variation when the knife moves in the x-direction, and we can drop the y variation for any cases where $I(x, y)$ is separable in the form $I(x, y) = I_x(x) \times I_y(y)$. Clip level formulas for the beams considered in this paper are then given by the following formulas.

1) Lowest-Order Hermite-Gaussian Mode: The clip level for the lowest-order HG_0 mode profile $I_0(x) = \exp(-2x^2/w^2)$, or for the corresponding TEM_{00} or TEM_{00} HG modes, is given by

$$\epsilon = \frac{1}{2}\left[1 - \operatorname{erf}\left(\frac{D}{2\sqrt{2}\sigma_x}\right)\right]. \tag{5}$$

2) Next Higher-Order Hermite-Gaussian Mode: The clip level for the HG $n = 1$ mode or for the corresponding TEM_{10}, but not TEM_{01}, mode is given by

$$\epsilon = \frac{1}{2}\left[1 - \operatorname{erf}\left(\frac{\sqrt{3}D}{2\sqrt{2}\sigma_x}\right) + \frac{2}{\sqrt{\pi}}\frac{\sqrt{3}D}{2\sqrt{2}\sigma_x} \cdot \exp\left(-\left(\frac{\sqrt{3}D}{2\sqrt{2}\sigma_x}\right)^2\right)\right]. \tag{6}$$

3) The "Donut" Mode: This mode, which is often seen in stable-resonator lasers in which the mode-controlling aperture is made slightly too large, can be viewed either as a Laguerre-Gaussian TEM_{01}^* mode with profile given by $I(r, \theta) = r^2 \exp[-2r^2/w^2]$, or as the incoherent superposition of equal amounts of the TEM_{10} and TEM_{01} HG modes with profiles given by $I_{10} = x^2 \exp[-2(x^2 + y^2)/w^2]$ and $I_{01} = y^2 \exp[-2(x^2 + y^2)/w^2]$.

In either case, the clip level is given by

$$\epsilon = \frac{1}{2}\left|1 - \operatorname{erf}\left(\frac{D}{2\sigma_x}\right) + \frac{1}{\sqrt{\pi}}\frac{D}{2\sigma_x}\exp\left(-\left(\frac{D}{2\sigma_x}\right)^2\right)\right|. \tag{7}$$

4) "Ring" Mode (Asymptotic Hermite-Gaussian Mode): As discussed in the text, the asymptotic limit for an HG mode as $n \to \infty$ has the same properties in one transverse dimension as does a narrow ring annulus beam in two dimensions. The D/σ_x ratio as a function of clip level for either case is given by

$$\epsilon = \frac{1}{2}\left|1 - \frac{2}{\pi}\sin^{-1}\left(\frac{D}{2\sqrt{2}\sigma_x}\right)\right|. \tag{8}$$

5) "Top hat" Mode: A circular uniform-amplitude top hat beam has clip level and clip width related by

$$\epsilon = \frac{1}{2}\left|1 - \frac{2}{\pi}(\theta + \sin\theta\cos\theta)\right| \tag{9}$$

where $\theta \equiv \sin^{-1}(D/2\sigma_x)$.

6) Uniform Slit or Rectangular Mode: A uniformly illuminated slit, or any form of equivalent rectangular beam scanned across either of its principal axes, will have the form

$$\epsilon = \frac{1}{2}\left|1 - \frac{D}{\sqrt{6}\sigma_x}\right|. \tag{10}$$

7) "Diamond" Mode: A "diamond" profile (a uniformly illustrated square beam rotated by 45°) obeys the formula

$$\epsilon = \frac{1}{2}\left(1 - \frac{D}{2\sqrt{6}\sigma_x}\right)^2. \tag{11}$$

8) "Picture Frame" Mode: A very thin square annulus (the square analog of the ring mode) obeys the formula

$$\frac{D}{\sigma_x} = \begin{cases} \sqrt{6} \times (2 - 4\epsilon), & 0.25 \le \epsilon \le 0.5 \\ \sqrt{6}, & \epsilon \le 0.25. \end{cases} \tag{12}$$

9) Higher-Order Hermite-Gaussian Modes: Analytic formulas can be developed if necessary for higher-order HG modes with $n \ge 2$, but in most cases it proves simpler to evaluate the properties of these modes by numerical evaluation using a computer package such as Mathematica, and this was done to calculate the results in Figs. 2 and 5.

10) Pedestal Beams: Consider a beam consisting of a central TEM_{00} Gaussian with spot size w_1 containing $1 - \alpha$ of the total power, and a pedestal with spot size w_2 containing the remaining fraction α of the total power. The clip level is then given by

$$\epsilon = \frac{1}{2}\left|1 - (1 - \alpha)\operatorname{erf}\left(\frac{\sqrt{2}a}{w_1}\right) - \alpha\operatorname{erf}\left(\frac{\sqrt{2}a}{w_2}\right)\right| \tag{13}$$

where

$$\frac{\sqrt{2}a}{w_1} = \sqrt{\frac{1 - \alpha + M^2\alpha}{2}}\,\frac{D_c}{2\sigma_x} \tag{14}$$

and $M \equiv w_2/w_1$.

Anthony E. Siegman (S'54–M'57–F'66) was born in Detroit, MI, on November 23, 1931. He received the A.B. degree from Harvard University, Cambridge, MA, in 1952, the M.S. degree in applied physics from the University of California, Los Angeles, in 1954 under the Hughes Aircraft Cooperative Plan, and the Ph.D. degree in electrical engineering from Stanford University, Stanford, CA, in 1957.

Since then he has been on the faculty at Stanford where he directs an active research program in lasers and their applications. He currently holds the Burton J. and Ann M. McMurtry Professorship of Engineering in the Departments of Electrical Engineering and (by courtesy) of Applied Physics and is presently with the Edward L. Ginzton Laboratory at Stanford. He has made many contributions to the fields of microwave electronics, traveling-wave tubes, laser devices, and lasers applications, and has written a highly regarded textbook, *Lasers* (University Science Books, 1986). He has been a consultant to numerous industrial and government laboratories, and served for six years on the Air Force Scientific Advisory Board.

Dr. Siegman is a Fellow of the Optical Society of America and the American Physical Society, and a member of the National Academies of Engineering (1973) and of Science (1988). In 1980 he received the R. W. Wood Prize of the Optical Society of America for the invention of the unstable optical resonator, and in 1987 was awarded the Frederic Ives Medal of the Optical Society of America for overall distinction in optics.

M. W. Sasnett, photograph and biography not available at the time of publication.

T. F. Johnston, Jr., photograph and biography not available at the time of publication.

Accepted for publication
Appl. Optics. Oct. 91

H1

Single Pulse Laser Beam Quality Measurements Using a CCD Camera System

J. A. Ruff and A. E. Siegman

Stanford University, Edward L. Ginzton Laboratory, Stanford, California 94305-4085

We have assembled a CCD-camera-based system that is capable of measuring laser beam quality on a single-shot pulsed basis. The system has been tested using a pulsed HeNe laser beam with added spatial distortion.

The concept of beam quality as a measure of the multi-mode or "times-diffraction-limited" character of a laser beam has been of interest since the early days of the laser field.[1] Only recently, however, has there begun to be convergence on standard methods for defining and measuring laser beam quality.[2] In the past few years commercial instruments for measuring laser beam quality on a CW basis have become available and have been found to yield useful new information on laser physics.[3] Our device enables similar investigations of pulsed lasers.

We have developed a CCD-camera-based system that makes single-shot beam quality measurements on pulsed laser sources. The system employs three CCD cameras, a Macintosh computer and three video frame grabber boards, as shown in Fig. 1. The cameras monitor the transverse beam profile as the beam propagates through a small beam waist formed by a high quality lens. The frame grabber boards convert, or digitize, the video images of the laser beam into arrays of numbers that the computer uses to calculate beam widths at each plane. The combination of the beam waist size and the far-field divergence of the laser beam provides a measure of the beam quality.

To ensure an accurate measurement of beam quality the samples of the transverse beam profile must be taken near the beam waist and several Rayleigh ranges away from the waist. Use of a short Rayleigh range enables measurement in a confined laboratory. In our experiments a high quality 10 cm focal length lens produces a very small waist with a typical Rayleigh

range of a few centimeters.

The transverse profiles are measured with standard Sony SSC-D5 CCD cameras. The frame grabber boards quantize the continuous video information from the cameras into a finite number of light intensity samples (pixels on the computer screen). They also quantize the intensity at each sample into a finite number of levels. To reduce quantization error, each transverse beam image should fill as much of the area of its camera's CCD array as possible without overflow. Also, the intensity should be as great as possible without saturating the camera. If only 10% of the maximum range of intensity levels is used, the measured beam width can be in error by as much as 5%. Below that, the measured width falls quickly with intensity.

One CCD camera coupled with a microscope objective monitors the transverse profile of the laser beam at the small waist formed by the focusing lens (Fig. 1). The microscope objective allows measurement of waists as small as a few microns. The distance between the camera and the microscope objective is fixed so that objectives can be easily interchanged and the magnification simply read off the objective in use. As mentioned above, the power of the objective must be chosen to project the beam waist onto the largest possible area of the CCD detector. For example, with 256 intensity levels and a near-gaussian laser beam, the gaussian spot size should be roughly 30% of the short edge of the camera's CCD array. At this size, with the intensity at the center of the beam just below saturation, the intensity at the edge of the camera will be below the lowest quantization level.

The exact position of the beam waist is located by moving the camera and microscope objective as a unit, as in a video microscope[4], and making measurements on repeated shots of the pulsed laser, looking for a minimum spot size. In the case of an astigmatic beam, the two transverse axes must be measured separately. During positioning of the microscope assembly, the computer calculates a continuous rough estimate of beam width using a rapid width

measurement technique , such as a simulated knife scan. A more accurate width measurement algorithm is used during data collection.

The two other cameras monitor the transverse beam profile at varying distances beyond the waist (Fig. 1). As the laser beam spreads, one of the cameras is moved to a position where the laser beam just fills the entire CCD array, as mentioned before. The third camera is placed somewhat closer, to obtain a measurement at a different distance from the beam waist. The beam profile on this camera will not quite fill the array.

Any imperfect optical components in the optical path will, of course, change the beam quality we are attempting to measure. Our design reduces the number of these components in the measuring device to a 10 cm focal length lens, a microscope objective and two high-quality beamsplitters (Fig. 1). The CCD cameras were used without lenses. In general, a variable neutral density filter will also be required to provide control of the over-all intensity. In our testing of this system, however, we are able to control the average intensity of the beam by changing the pulse length. Separate neutral density filters are not required for each camera if the beamsplitters are selected so that the maximum (spatial) intensity is just below saturation on each camera. In our set-up the first beamsplitter reflects roughly 33% and the second beamsplitter reflects roughly 50% (Fig. 1). Slight adjustments of a camera's location can be used to fine-tune peak intensity since maximum intensity drops as the laser beam diverges.

The integration/storage capacity of CCD arrays combined with the ability to simultaneously capture a video frame from three independent cameras allows a measurement to be made from a single pulse of laser light, once the waist location has been found. The Sony SSC-D5 cameras are locked in synch and run continuously. A pulse of light from the laser triggers the Data Translation QuickCapture video frame grabber boards to capture the next frame in the video sequence from each camera. Those frames, which each of the three boards

converts into an image, contain the transverse laser beam profiles at the cameras. Each image is composed of 640 x 480 pixels using 256 grey levels. Laser pulses of interest will in general be short compared to the single frame integration time of the CCD cameras (17 ms).

The effective beam widths can then be determined in software in any of several different ways, such as simulation of a knife edge scan (for any clip level), which is very fast, or direct computation of variances, which is more theoretically correct. Fast assembly language routines are used for all computations, including determination of principal axes, to provide immediate feedback on beam quality. The beam quality is determined from the product of the standard deviation of the transverse beam profile at the beam waist σ_0, and the standard deviation σ_z, of the beam profile at a known distance away, z, in the form[2]

$$M^2 = \frac{4\pi\sigma_0\sigma_z}{z\lambda}$$

The two far-field cameras provide two measurements of the M^2 value.

It would also be possible to measure beam quality by finding the best-fit parabola through the beam widths of all three transverse profiles. However, this method is very sensitive to small errors in the size of the beam waist. Thus, it is much better to find the beam waist independently and calculate the best-fit parabola while holding the beam waist constant. In our case, this would amount to little more than averaging the two values of M^2 as obtained by the two cameras as outlined above.

We have tested the operation of this system using single pulses from a HeNe laser with various artificial distortions added, and are now beginning a series of measurements on other pulsed laser sources. To simulate a distorted pulsed laser source, a CW HeNe laser beam was sent through an acousto-optic modulator and a prism pair. The AO modulator produces 62 μs square-wave pulses, and the prism pair elongates and slightly distorts the beam along one axis. Figure 2 shows the three transverse profiles taken during a single pulse. The principal axes and

beam widths as measured by the computer have been added to the figure. The lengths of the ellipse semiaxes are equal to the laser beam image variances. The principal axes, as calculated by the computer, differ from each other by about one degree. We assume that this is due to small alignment errors and not to the laser beam being nonorthogonal[5]. The fringes seen in the transverse profiles do not greatly effect the value of M^2 if the power in the fringes is relatively small. The astigmatism of the measured laser beam was negligable.

The distance from the beam waist to camera B in this case was $z_b = 124 \pm 1$ mm (Fig. 1). The distance from the beam waist to camera C was $z_c = 173 \pm 1$ mm. A single pixel measures 13.4 μm on a side. At the beam waist the pixels of camera A are the same, but a 40x microscope objective makes the effective length 0.335 μm on a side. Repeated measurements on different pulses from the same laser give variances which differ by roughly one pixel.

The measured beam widths were:

Camera A (waist):	σ_{0x} = 75 pixels (25.1 μm)	σ_{0y} = 21 pixels (7.04 μm)
Camera B:	σ_{cx} = 23 pixels (308 μm)	σ_{cy} = 67 pixels (898 μm)
Camera C:	σ_{bx} = 32 pixels (429 μm)	σ_{by} = 97 pixels (1300 μm)

From this data, using the previous equation, the calculated M^2 values are:

camera A (waist) and camera B:	$M_x^2 = 1.24$	$M_y^2 = 1.01$
camera A (waist) and camera C:	$M_x^2 = 1.24$	$M_y^2 = 1.05$

The two cameras agree to within about 5% of each other.

We expect to extend these measurements to other pulsed laser sources, such as pulsed semiconductor diode lasers and Q-switched diode-pumped lasers. Given the interesting phenomena already found when examining the beam quality of cw laser sources for different ranges of operation,[3] we expect to find similarly interesting results in the modal and beam-development properties of pulsed laser sources.

References:

1. See for example J. A. Arnaud, W. M. Hubbard, G. D. Mandeville, B. de la Claviere, E. A. Franke, and J. M. Franke, "Technique for fast measurement of Gaussian laser beam parameters," Appl. Opt. **10**, 2775-2776 (1971); C. B. Hogge, R. R. Butts, and M. Burlakoff, "Characteristics of phase-aberrated nondiffraction-limited laser beams," Appl. Opt. **13**, 1065 (1974); A. E. Siegman, "Effects of small-scale phase perturbations on laser oscillator beam quality," IEEE J. Quantum Electron. **QE-13**, 334-337 (1977).
2. See for example J. M. Fleischer, John M. and James M. Darchuk, "Standardizing the measurement of spatial characteristics of optical beams," Proc. SPIE, **888**, *Laser Beam Radiometry* (1988); A.E.Siegman, "New Developments in Laser Resonators," Proc. SPIE, **1224**, 2-14 (1990).
3. T. F. Johnston, Jr., and M. W. Sasnett, "Modeling multimode CW laser beams with the beam quality meter," Paper OSM2.4, LEOS '90 Conference Digest, IEEE LEOS 1990 Annual Meeting, Boston MA, November 1990.
4. See for example Shinya Inoué, *Video Microscopy* (Plenum Press, New York, 1986) or *Optics Guide* **4**, (Melles Griot,1988), Chap 16.
5. J. A. Arnaud and H. Kogelnik, "Gaussian Light Beams with General Astigmatism," Appl. Opt. **8**, 1687-1692 (1969).

Figure Captions

Fig. 1. Laboratory setup for measuring Beam Quality of Pulsed lasers.

Fig. 2. Transverse beam profiles of a single laser pulse.

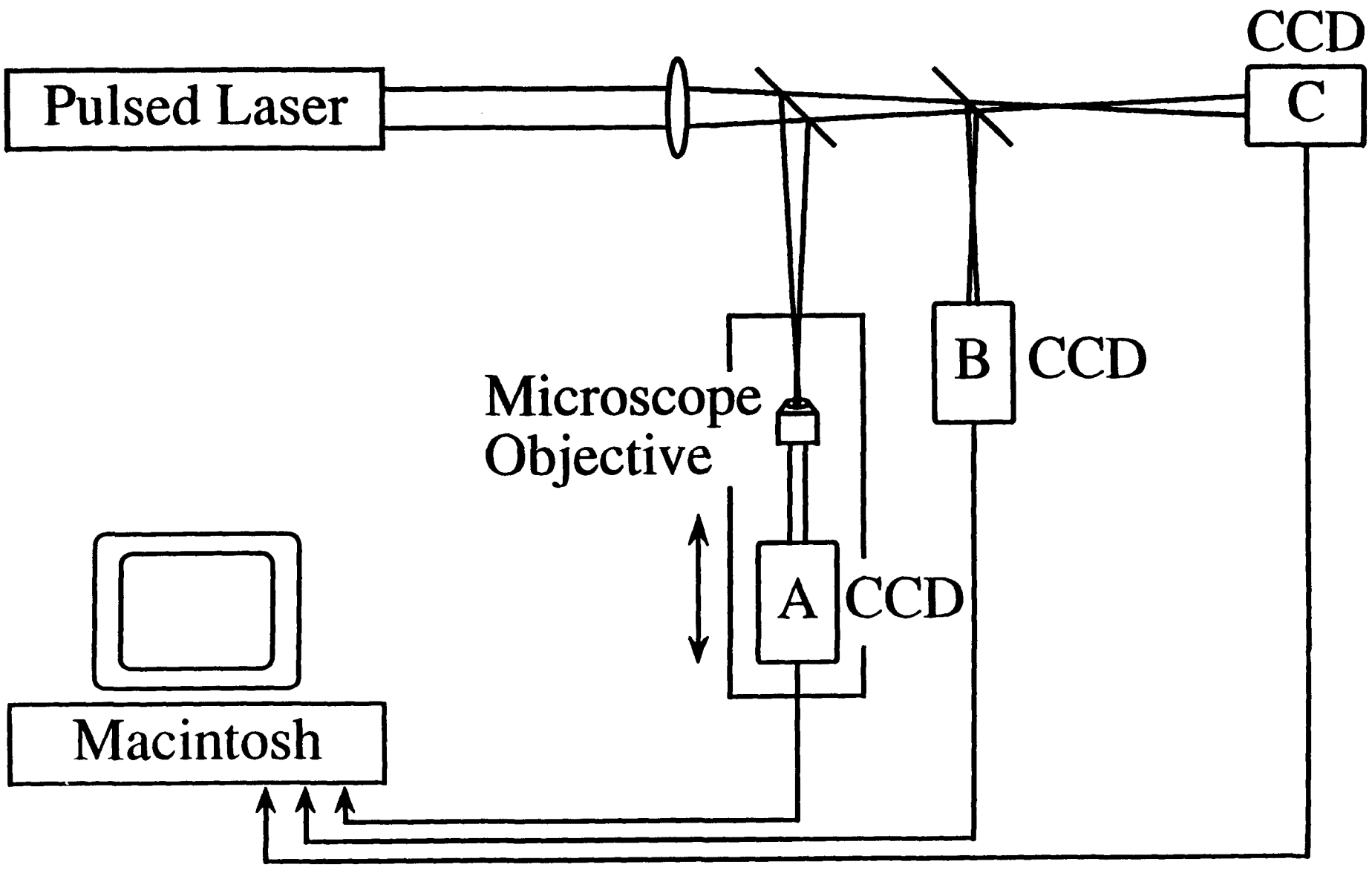
CCD
Pulsed Laser
C
B
CCD
Microscope
Objective
A
CCD
Macintosh

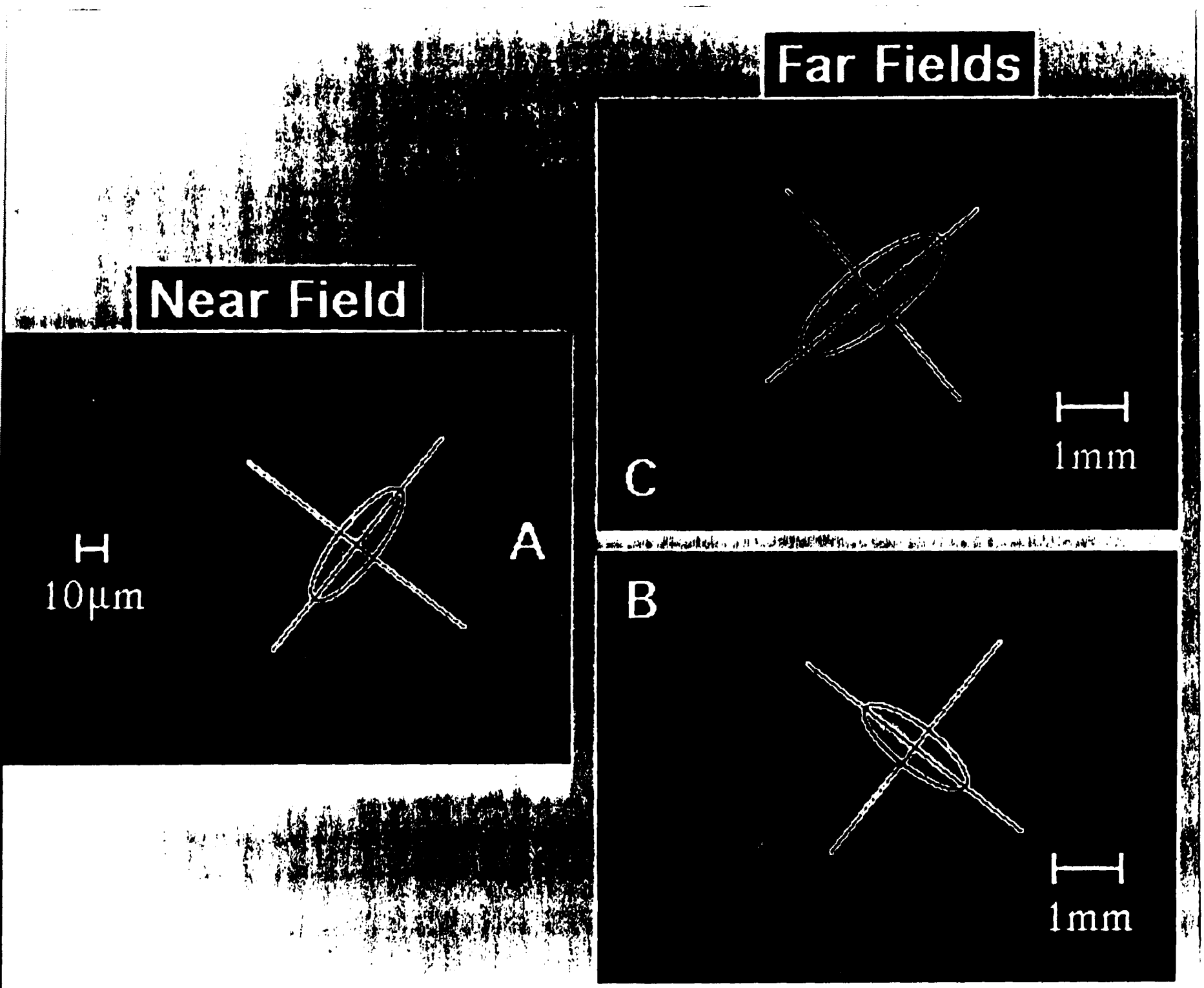
Far Fields
Near Field
C
1mm
H
10µm
A
B
1mm

I

Enhanced Schawlow-Townes linewidth in lasers with nonorthogonal transverse eigenmodes

Paul L. Mussche and A. E. Siegman

Edward L. Ginzton Laboratory, Stanford University
Stanford, California 94305-4085

ABSTRACT

A recent reformulation of the laser field equations, using the true modes of the laser cavity and including a noise polarization term to account for spontaneous emission, shows that conventional understanding of amplifier noise figure, oscillator linewidth, and oscillator build-up time needs to be modified for laser amplifiers or oscillators with nonorthogonal transverse eigenmodes. Gain-guided lasers and unstable-resonator lasers in particular have nonorthogonal transverse modes, and hence exhibit unconventional noise behavior. One important consequence of this theory is the appearance of an excess spontaneous emission factor (the "Petermann factor") which multiplies the well-known Schawlow-Townes formula for the laser linewidth. This factor can be substantially greater than unity for unstable resonators with large magnification or Fresnel number. We discuss our investigations of the consequences of the nonorthogonality of the transverse eigenmodes, especially on laser linewidth in unstable-resonator lasers. We believe that the results of these investigations are important where the temporal coherence properties of the laser are of interest, namely in coherent optical communications, spectroscopy, optical wavelength standards, and also in the injection seeding of pulsed high-power unstable resonator lasers. Extensive calculations of the excess noise factor in real hard-edged unstable resonators have been carried out using a virtual-source approach to calculate the exact unstable-resonator eigenmodes. An experiment is also being carried out to demonstrate the linewidth enhancement in a small diode-pumped geometrically unstable laser oscillator.

1. INTRODUCTION

In many applications, understanding laser linewidth is an important consideration for example for the design of coherent optical communication schemes, for spectroscopy (when investigating fundamental properties of materials), and for the use of lasers in gravity wave detection using interferometers. The fundamental source of laser linewidth is spontaneous emission noise which is the unavoidable process accompanying stimulated emission. It is this contribution to laser linewidth we are interested in as opposed to external noise contributions which depend on the environment in which the ideal laser with spontaneous emission noise is imbedded.

Let us now turn our attention to laser resonators. It is well known that unstable resonator lasers have several advantages over stable resonator lasers, in particular good transverse mode discrimination and large gain volume. Two examples of practical lasers built with unstable resonators are CO_2 lasers and some Q-switched Nd:YAG lasers. The property that we are particularly interested in is that the modes of unstable resonators are nonorthogonal and, as we shall describe in this paper, this has direct bearing on the fundamental linewidth of the laser.

Note that for most lasers, the environmental or external noise sources typically dominate the contribution due to spontaneous emission. An important exception is the semiconductor laser whose

linewidth is dominated by spontaneous emission noise. We can therefore anticipate that by building semiconductor lasers with unstable resonators or, if more generally these semiconductor lasers have nonorthogonal eigenmodes, they will exhibit excess spontaneous emission noise properties which bear directly on their fundamental linewidth.

Note that when we say "quantum linewidth" or "Schawlow-Townes linewidth" or "fundamental linewidth" of a laser we mean the spontaneous emission noise linewidth.

We shall first review the orthogonality properties of modes in lasers, then outline the theory of excess quantum noise, and give some numerical results for the excess quantum noise for two types of lasers, and follow by a discussion of experimental issues involved in trying to measure the excess quantum noise.

2. MODES IN RESONATORS

We wish to give some details concerning resonator modes and their properties in order to avoid referring the reader to a large collection of papers discussing one or another aspect of the topic. (See reference 1 for background.)

Consider the unstable optical resonator in Fig. 1. We define a reference plane in the resonator which, for convenience, will be taken as the plane transverse to the optic axis just before the output coupling mirror. Note that in the paraxial approximation, the output mirror is considered to be of negligible width. We mean by "mode" or "eigenmode" of this resonator any field distribution which will reproduce after one round trip through the resonator. In order to make the picture clearer, it is useful to consider the following lensguide equivalent where the resonator is unfolded and the mirrors are replaced by lenses. Also, coupling to the outside is denoted by the presence of an absorbing wall (representing radiation going out to infinity) as shown in Fig. 2. A field distribution u at plane z_1 is an eigenmode if when propagated to plane z_2 (one round-trip through the resonator) it reproduces its shape both in amplitude and phase, so that

$$v(\overline{s}, z_2) = \gamma\, u(\overline{s}, z_1)$$

where $\overline{s}$ is the transverse dimension. Note that u is the slowly varying part of a field $ue^{i(kz-\omega t)}$. The constant γ is the eigenvalue associated with the eigenmode u. The mode u obeys the paraxial wave equation with appropriate boundary conditions

In order to understand the orthogonality property of modes it is more instructive to consider the *integral equation* obeyed by u. This is nothing else but the Fresnel diffraction integral

$$v_2(\overline{s}_2) = \int_A K(\overline{s}_2, \overline{s}_1) u_1(\overline{s}_1)\, d\overline{s}_1$$

where A is the aperture area, and where the kernel K depends on the optical elements between the reference planes at z_1 and z_2 and the integral is taken over the aperture in the equivalent lensguide. We write $u_1(\overline{s}_1)$ as a shorthand for $u_1(\overline{s}_1, z_1)$, and likewise for v_2. For simplicity of argument, we will consider the one-dimensional case where $\overline{s} = x$ and $\overline{s}_2 = y$. This choice is by no means restrictive, but it makes the notation easier and also, for the two-dimensional case, it suffices to

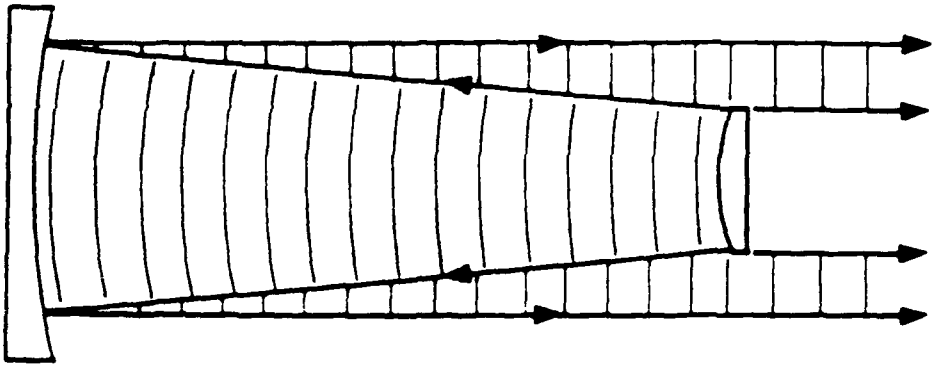

Fig. 1. Positive branch hard-edge unstable resonator with diffractive output coupling

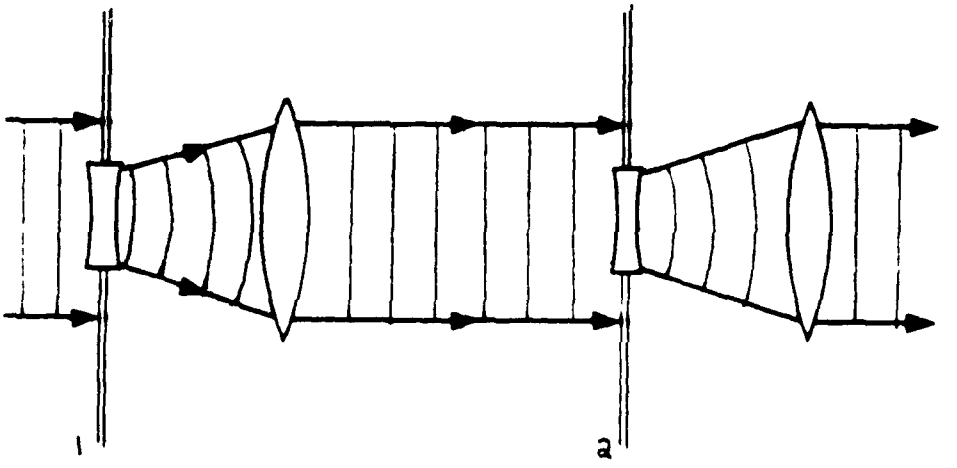

Fig. 2. Lensguide equivalent of the resonator shown in Fig. 1. The arrows represent the toward propagating eigenwave. The reference planes 1 and 2 are located just before the absorbing walls.

view x as the vector (x_1, x_2) and y as the vector (y_1, y_2). So we write the integral equation for the mode as

$$v(y) = \int K(y,x)u(x)\,dx$$

A mode of the resonator is the self-reproducing field u such that

$$v(y) = \gamma u(y)$$

or

$$\gamma u(y) = \int K(y,x)u(x)\,dx$$

so that u is an *eigenmode* of the integral operator which transforms $u(x)$ into $\int K(y,x)u(x)\,dx$ with its corresponding eigenvalue γ.

Let us suppose that $\{u_n\}, \{\gamma_n\}$ is the collection of eigenmodes and corresponding eigenvalues. We define the scalar product $\langle u_m, u_n \rangle$ by

$$\langle u_m, u_n \rangle \equiv \int u_m^*(x)u_n(x)\,dx$$

where the integral is taken over the aperture. In many cases in physics the eigenmodes are orthogonal, i.e.

$$\langle u_m, u_n \rangle = \delta_{mn} = \begin{cases} 1 & n = m \\ 0 & n \neq m \end{cases}$$

but in the case of unstable resonators this is *not* the case.

$$\langle u_m, u_n \rangle \neq \delta_{mn} \quad \text{for unstable resonators}$$

It is possible however to define a set of modes $\{v_m\}$ which is orthogonal to the set of modes $\{u_m\}$

$$\langle v_m, u_n \rangle = \delta_{nm}$$

It turns out that these modes are the eigenmodes of the integral equation

$$\gamma_m^* v_m(y) = \int K^*(x,y)v_m(x)\,dx$$

Note that the arguments of K are switched and it is complex conjugated. The field v_m is called an adjoint mode of u_m. In laser resonators another definition is used: we define the mode ϕ_m as the solution to

$$\gamma_m \phi_m = \int K(x,y)\phi_m(x)\,dx \qquad \text{(no complex conjugate)}$$

So that $\phi_m = v_m^*$ and it obeys the biorthogonality property

$$\langle \phi_m, u_n \rangle \equiv \int \phi_m(x)u_n(x)\,dx = \delta_{mn}$$

The reason for using this definition is that ϕ_m can be interpreted as the eigenmode of the resonator propagating in the *opposite direction* (with the optical axis reversed).

It turns out that for optical resonators in the paraxial approximation we have

$$\phi_m(x) = \beta_m \, u_m(x) e^{-i\alpha x^2}$$

where the constant α is given for a given resonator. If the reference plane is a symmetry plane of the resonator we have $\alpha = 0$, and then the biorthogonality relation becomes

$$\int u_m(x) u_n(x)\, dx = 0 \qquad m \neq n \qquad \text{(no complex conjugation)}$$

It is necessary also to define a normalization of the modes. We will choose

$$\int_{-\infty}^{\infty} |u_m(x)|^2 \, dx = 1$$

and

$$\int_A \phi_m(x) u_m(x)\, dx = 1$$

But from the previous equation we have that

$$\int_A \beta_m u_m(x) e^{-i\alpha x^2} u_m(x)\, dx = 1$$

so

$$\beta_m = \frac{1}{\int_A u_m^2(x) e^{-i\alpha x^2}\, dx}$$

It is easy to show that

$$\int_{-\infty}^{\infty} |u_m(x)|^2 dx = |\gamma_m|^{-2} \int_A |u_m(x)|^2 dx$$

so we have finally a set of eigenmodes $\{u_m\}$ with corresponding eigenvalues $\{\gamma_m\}$ such that

$$\gamma_m u_m(y) = \int_A K(y,x) u_m(x)\, dx$$

with the normalization

$$\int_A |u_m(x)|^2 dx = |\gamma_m|^2$$

and ϕ_m such that

$$\phi_m(x) = \frac{u_m(x) e^{-i\alpha x^2}}{\int_A u_m^2(x') e^{-i\alpha x'^2} dx'}$$

The quantity we are ultimately interested in is the excess noise factor K_{mm} defined by

$$K_{mm} = \int_A \phi_m^*(x)\phi_m(x)\,dx$$

And from the above relations we have

$$K_{mm} = \frac{\int_A u_m^*(x)u_m(x)dx}{\left|\int_A u_m^2(x)e^{-i\alpha x^2}dx\right|^2}$$

which at a symmetry plane simplifies to

$$K_{mm} = \frac{\int_A |u_m(x)|^2 dx}{\left|\int_A u_m^2(x)dx\right|^2} \qquad \text{(symmetry plane)}$$

3. EXCESS NOISE FACTOR THEORY

We shall describe in words the derivation leading to the excess noise factor. For the full theory we refer the reader to reference 2.

The gist of the theory is to go from Maxwell's equations for the electric field to the equation for the photon number in a single lasing mode by an expansion of the field in the *true* resonator eigenmodes (longitudinal and transverse). Conventional theories assume an orthogonal mode decomposition using the modes of a closed cavity with no losses. The laser resonator is inherently an open resonator and cannot be correctly approximated by a closed resonator especially for lasers with diffractive output coupling such as provided by unstable resonators.

The central result we are interested in is the equation of motion for the photon number in a single lasing mode

$$\frac{dn}{dt} = \kappa N_2(n + K) - \kappa N_1 n - \gamma_c n$$

We recognise the familiar stimulated emission term $\kappa N_2 n$ (κ is a coupling constant), the stimulated absorption $-\kappa N_1 n$, and the photon loss $\gamma_c n$. The spontaneous emission is given by $\kappa N_2 K$ which is different from the conventional result κN_2 (K replaced by 1). The factor K depends directly on the orthogonality property of the modes. It is composed of a "longitudinal" part

$$K_L \equiv \frac{1}{|\gamma_o|^2}\left(\frac{1-|\gamma_o|^2}{\ln(1/|\gamma_o|^2)}\right)^2$$

and a "transverse" part

$$K_T = \int \phi_o^*(x)\phi_o(x)\,dx$$

where ϕ_o is the backward-propagating mode associated with the lasing mode u_o.

The factor K_L is close to unity except for resonators with very large output coupling. It is based on the nonorthogonality of the longitudinal modes of the laser. The factor K_T is close to unity

for stable resonator lasers and can be much larger than unity (as we shall see later) for unstable resonator lasers which have strongly nonorthogonal eigenmodes.

4. QUANTUM LINEWIDTH

The Schawlow-Townes linewidth or quantum linewidth of the laser is determined by the amount of spontaneous emission into the lasing mode. If the laser has nonorthogonal eigenmodes we conclude that the amount of spontaneous emission in the lasing mode is larger by a factor K than predicted by a conventional laser theory based on an orthogonal mode expansion. We therefore expect that the quantum linewidth of the laser will be increased by the same factor. The expression for the laser linewidth is then

$$\Delta\nu_L = \frac{2\pi\hbar\omega}{P}\Delta\nu_c^2 \cdot K$$

The first two terms represent the conventional laser linewidth depending on the cold cavity linewidth $\Delta\nu_c$ and the output power P. We should note that in general, two more factors may appear in the above expression, namely the incomplete inversion factor $N_2/(N_2 - N_1)$ (important for 3-level lasers) and the linewidth enhancement factor $(1+\alpha^2)$ for lasers exhibiting AM to FM noise coupling such as semiconductor lasers.[3] The excess spontaneous emission factor K is then the product of the longitudinal factor K_L and the transverse factor K_T.

The longitudinal (K_L) factor has been investigated experimentally by Hamel and Woerdman,[4] and is important for lasers with very large output couplings. We are particularly interested in the transverse (K_T) factor because it is greater than unity for unstable resonator lasers.

5. EXCESS NOISE FACTOR: NUMERICAL PREDICTIONS

5.1. Variable reflectivity mirror laser

We have investigated the case of variable reflectivity mirror (VRM) lasers partly because such lasers are increasingly popular. Also, in the case of a gaussian reflectivity profile, the eigenmodes and eigenvalues can be computed analytically. Detailed computations can be found in reference 5, but we shall summarize the essential features here. Figure 3 shows a plot of the excess noise factor of the lowest loss mode in a VRM resonator laser as a function of the geometrical stability parameter m (the half-trace of the round-trip ABCD matrix representing the resonator). In the stable resonator region ($|m| < 1$) the excess noise factor is essentially unity so that there is no excess noise. For a flat-flat resonator ($m = 1$), the excess noise factor is equal to 2, and in the unstable resonator region the excess noise factor increases very rapidly and reaches a value of 100 at a magnification M ($M = m + \sqrt{m^2 - 1}$) of 1.6 for this particular case. We conclude that VRM unstable resonator lasers can exhibit very large excess noise factors.

5.2. Hard-edged unstable resonator laser

In this case, the eigenmode problem cannot be solved analytically, but we have computed the excess noise factor using an efficient algorithm called the virtual source method which allows generation of plots of the excess noise factor without having to rely on standard algorithms (the Fox-Li method or Prony method) which would be much more time-consuming.

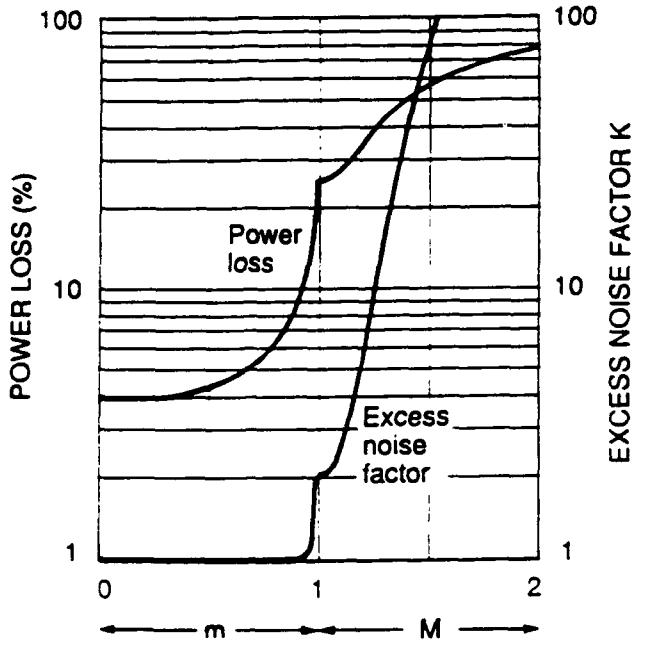

Fig. 3. Power loss $1 - |\gamma|^2$ in percent per round trip and excess noise factor K plotted versus geometrical magnification for the lowest-order Hermite-gaussian mode in a VRM cavity with a ratio of gaussian aperture to confocal spot size of $w_{ga}/w_{cf} = 5$ or gaussian Fresnel number $N_{ga} \approx 8$. The horizontal scale variable in the half-trace parameter m for $0 < m < 1$, and the geometrical magnification $M = m + \sqrt{m^2 - 1}$ for $m > 1$.

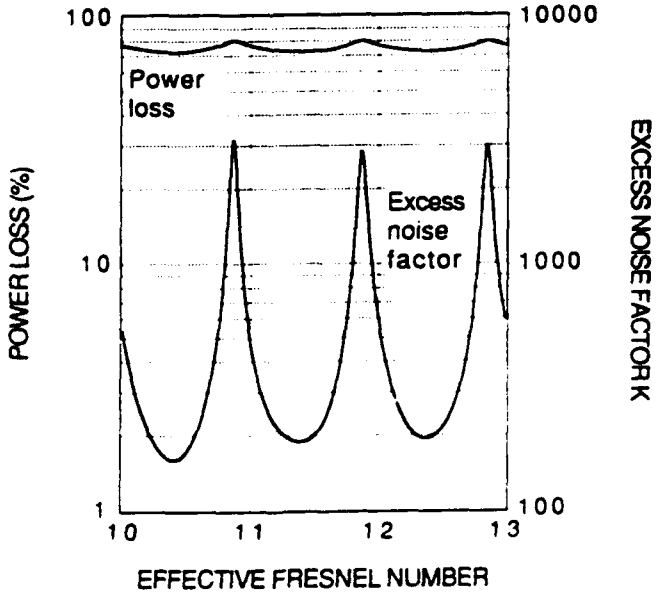

Fig. 4. Power loss and excess noise factor versus effective Fresnel number for a hard-edged strip unstable resonator with a magnification of 4.

We plot here power losses and the excess noise factor as a function of the effective Fresnel number in the resonator (i.e., as a function of output coupling mirror diameter, all other parameters being kept constant). Figure 4 shows how the excess noise factor is "resonant" with the Fresnel number in the same way as are the losses. This fact is typical of hard-edged mirror resonators. Again, we see that the excess noise factor can reach very large values.

6. EXPERIMENTAL CONSIDERATIONS

We are currently setting up an experiment to measure the excess noise factor using a diode-pumped monolithic Nd:YAG laser system (Fig. 5). The rod has a flat mirror on one end and a negative curvature mirror on the other. It is thus inherently geometrically unstable. The rod is end-pumped by a single mode high-power diode laser which induces a lasing mode in the rod by the mechanism of gain-guiding. Although the theory presented above makes the assumption that the gain is uniform throughout the laser, we anticipate an effect on the excess of noise from the mirror curvature.

For the noise measurement we are setting up a Pound-Drever-type noise measurement scheme[6] where a Fabry-Perot cavity is locked to the laser and frequency noise is observed at frequencies beyond the locking bandwidth, i.e., where the laser is free-running and where external noise sources have become negligible, leaving the spontaneous emission noise.

We have observed lasing action in our diode-pumped rod system at a rod temperature of 80K when the gain is high enough to go above threshold and to avoid multi-longitudinal mode oscillation by narrowing of the gain curve (hence avoiding spatial-hole burning).

We wish to stress that this laser scheme is interesting in itself because it has good transverse mode discrimination in a large gain volume, so that it is not limited by the problem of stable rod designs where all the pump power has to be mode matched into the fundamental mode of the rod laser. Figure 6 shows the near-field beam emanating from the rod.

7. CONCLUSIONS

Unstable resonator lasers can exhibit large deviations from standard predictions for the fundamental laser linewidth due to eigenmode nonorthogonality. Indeed, the standard expression for the laser linewidth due to spontaneous emission noise needs to be multiplied by a so-called "excess spontaneous factor." We have performed analytic and numerical computations for the excess noise factor, and conclude that it can be very much larger than unity for unstable resonators. Note that the excess noise factor theory was first studied in the context of gain-guided semiconductor lasers by Petermann.[7] Therefore, it is also called the Petermann factor.

We are currently investigating the excess noise factor experimentally, and have demonstrated what is to our knowledge the first diode-pumped monolithic unstable resonator Nd:YAG laser system.

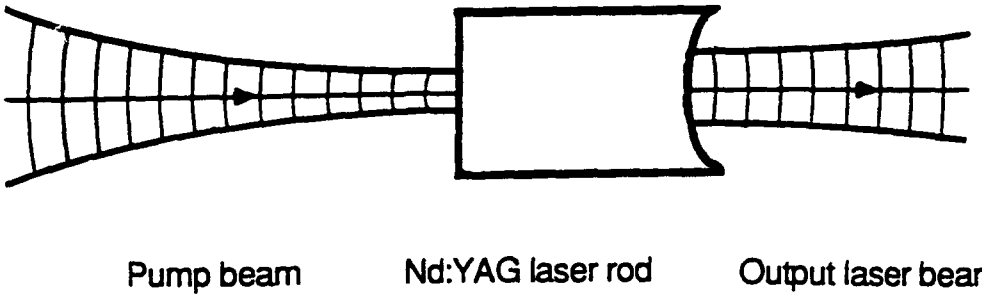

Fig. 5. Optical set-up of the diode-pumped monolithic unstable resonator Nd:YAG rod laser. The rod is 3 mm long with a flat mirror at one end (HR at 1064 nm and HT at 809 nm) and a -10 cm radius mirror at the other end (95% reflector at 1064 nm). The material is 1% doping Nd:YAG.

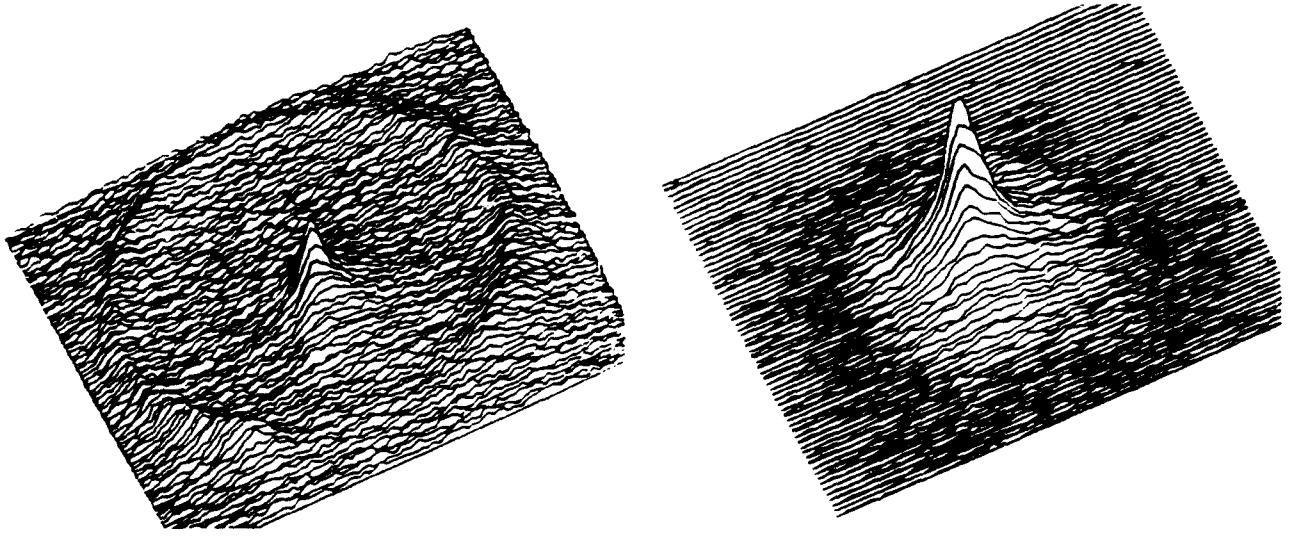

Fig. 6. Near field of the beam emanating from the rod. On the left the laser is below threshold and on the right the laser is above threshold. Notice a change in vertical scale by a factor of 1000 and a change in horizontal scale by a factor of 3/4. The ring of light in the left pattern is the glow from the edge of the laser rod.

8. ACKNOWLEDGEMENTS

We would like to acknowledge the support of the Air Force Office of Scientific Research under contract F49620-89-K-0004.

9. REFERENCES

1. A. E. Siegman, *Lasers* (Unversity Science Books, Mill Valley, CA, 1986).

2. A. E. Siegman, "Excess Spontaneous Emission in Non-Hermitian Optical Systems. I: Laser Amplifiers," *Phys. Rev. A*, vol. 39, pp. 1253–1263, Feb. 1, 1989; A. E. Siegman, "Excess Spontaneous Emission in Non-Hermitian Optical Systems. II: Laser Oscillators," *Phys. Rev. A*, vol. 39, pp. 1264–1268, Feb. 1, 1989.

3. M. Osinski and J. Buus, "Linewidth Broadening Factor in Semiconductor Lasers—An Overview," *IEEE J. Quantum Electron.* vol. QE–23, pp. 9–29, Jan. 1987.

4. W. A. Hamel and J. P. Woerdman, "Observation of Enhanced Fundamental Linewidth of a Laser Due to Nonorthogonality of Its Longitudinal Eigenmodes," *Phys. Rev. Lett.* vol. 64, pp. 1506–1509, March 26, 1990.

5. J-L. Doumont, P. L. Mussche, and A. E. Siegman, "Excess Spontaneous Emission in Variable-Reflectivity-Mirror Lasers," *IEEE J. Quantum Electron.* vol. QE–25, pp. 1960–1967, August 1989.

6. K. Petermann, "Calculated Spontaneous Emission Factor for Double-Heterostructure Injection Lasers with Gain-Induced Waveguiding," *IEEE J. Quantum Electron.* vol. QE–15, pp. 566–570, July 1979.

7. R. W. P. Drever, J. L. Hall, F. V. Kowalski, J. Hough, G. M. Ford, A. J. Munley, and H. Ward, "Laser Phase and Frequency Stabilization Using an Optical Resonator," *Appl. Phys. B.* vol. 31, pp. 97–105, 1983.